Journal Of Applied Chemistry

Vol. 24 No. 4

THE ABSORPTION COEFFICIENT OF HORIZONTAL MECHANICAL SCRUBBERS AT LOW RPM*

L. I. Agarev

The references in the literature to the use of absorption equipment in industry in which contact is renewed mechanically are extremely few. We possess descriptions of the design of individual mechanical scrubbers, but we have no quantitative data on their operation.

It has been the objective of the present research to derive the values of the adsorption coefficient in a large-scale laboratory model of a horizontal mechanical scrubber. The absorption coefficients were measured as functions of the shaft rpm, the gas flow rate, and the liquid flow rate. Most of the experiments on the effect of these factors involved the absorption of carbon dioxide, a slightly soluble gas, by water, only a few experiments having been performed on the absorption of ammonia, a freely soluble gas, by water.

The coefficient of absorption as determined in the model have been compared with the coefficients measured for the same systems in apparatus of different design. This comparison has yielded conclusions regarding the absorption efficiency of mechanical scrubbers with a horizontal axis of rotation.

In most absorption apparatus (bubblers, sprayers, checkerwork towers), the intermixing and development of the surface of contact between the liquid and gaseous phases are effected by means of specially designed stationary devices for distributing and impelling these phases through the apparatus.

In mechanical scrubbers, the contact is renewed by mixing the liquid and gas together in rotating mechanical equipment.

The mechanical scrubbers described in the literature may be divided into two groups:

1) Scrubbers with a vertical rotating shaft: the Field scrubber; the MacLauren centrifugal scrubber [1]; etc.

2) Scrubbers with a horizontal rotating shaft: scrubbers with screen discs [2]; standard scrubbers [1]; etc.

All vertical mechanical scrubbers, as well as some of the horizontal ones, have rpms of 100 and more. The various types of atomizing devices mounted on the shaft (paddles, discs, bundles of rods, etc.) spray the liquid in the current of gas. This entails an extremely high growth of the area of the absorption surface, ensuring the efficient operation of the apparatus. In these scrubbers, the conditions governing the absorption of the gas are closest to those prevailing in tubular absorption towers with liquid sprayers.

A mechanical scrubber whose shaft is horizontal [2] operates on a different

principle. The shaft rotates rather slowly. Once per revolution, the screen or lattice discs pick up liquid at the bottom of the scrubber and carry it as a thin film to the upper zone, where it is saturated with the gas to be absorbed, after which the film is again plunged into the bulk of the liquid and renewed, again being lifted out of the liquid into the gas, etc., etc.

In this case, the absorption process most closely resembles the process occurring in checkerwork scrubbers, with the liquid film flowing down the checkerwork being replaced by the transference of the film via the rotating discs.

As we have said, there are no numerical data in the literature on the efficiency of these mechanical scrubbers. On the basis of considerations of a general nature and the available descriptions, we may, however, make the following assertions: the resistance offered to the passage of the gas should be negligible; the gas can be absorbed by an extremely small amount of absorbent; the continuous replenishing of the liquid film should yield high efficiency in the absorption of slightly soluble gases. Horizontal scrubbers are particularly useful for absorption processes in which the liquid is contaminated with a precipitate or when a precipitate is formed during absorption itself as the result of the reactions that take place.

A disadvantage common to all mechanical scrubbers is the additional energy required to turn the shaft. This consumption of energy, which is especially high in scrubbers with a high rpm, is what has made the latter uneconomical in the past; that is why we have chosen to investigate the type of scrubber in which the horizontal shaft runs at a low rpm.

EXPERIMENTAL

The dimensions and the capacity of our experimental model were those of a large-scale laboratory installation (Fig. 1).

The housing of the model scrubber, 150 mm in diameter and 400 mm long, consisted of two semicylindrical parts. The lower half, or trough, was divided into 4 sections by partitions to ensure systematic overflow of the absorbent liquid. The upper half, or cover, was made of plexiglass. This enabled us to observe everything taking place within the apparatus during the runs. To ensure airtightness, a hydraulic seal was installed between the upper and lower semicylinders.

Six outlets were soldered to the bottom of the trough: two as inlet and outlet for the absorbent, and the others as drains and samplers for the individual sections. The shaft passed through the axis of the cover, with the discs attached to it. The latter were made of 0.5 mm sheet iron. Each disc was perforated with 60 holes, 10 mm in diameter, arranged evenly over its entire surface, the center-to center distance being 15 mm (Fig. 2). We first tried out discs with smaller holes (4, 6, and 8 mm), but found that the holes were often closed up by the liquid film after they emerged from the liquid, thus interfering with the passage of the gas through the scrubber. Holes 10 mm in diameter were no longer plugged up by the film, so that we adopted this size for the discs of the tested model. The discs were 150 mm in diameter. The clearance between the edges of the discs and the inner surface of the housing did not exceed 1.0-1.5 mm. The discs numbered 20 in all. The discs were spaced 20 mm apart on the shaft.

All the discs were carefully degreased before being set on the shaft. This ensured complete wetting of the surface. The speed of the shaft could be varied from 2 to 55 rpm.

The overall layout of the apparatus is shown in Fig. 1. The air required for producing the gas mixture was supplied by a blower. The gas to be absorbed (carbon dioxide or ammonia) was supplied from a tank (1), passing through a

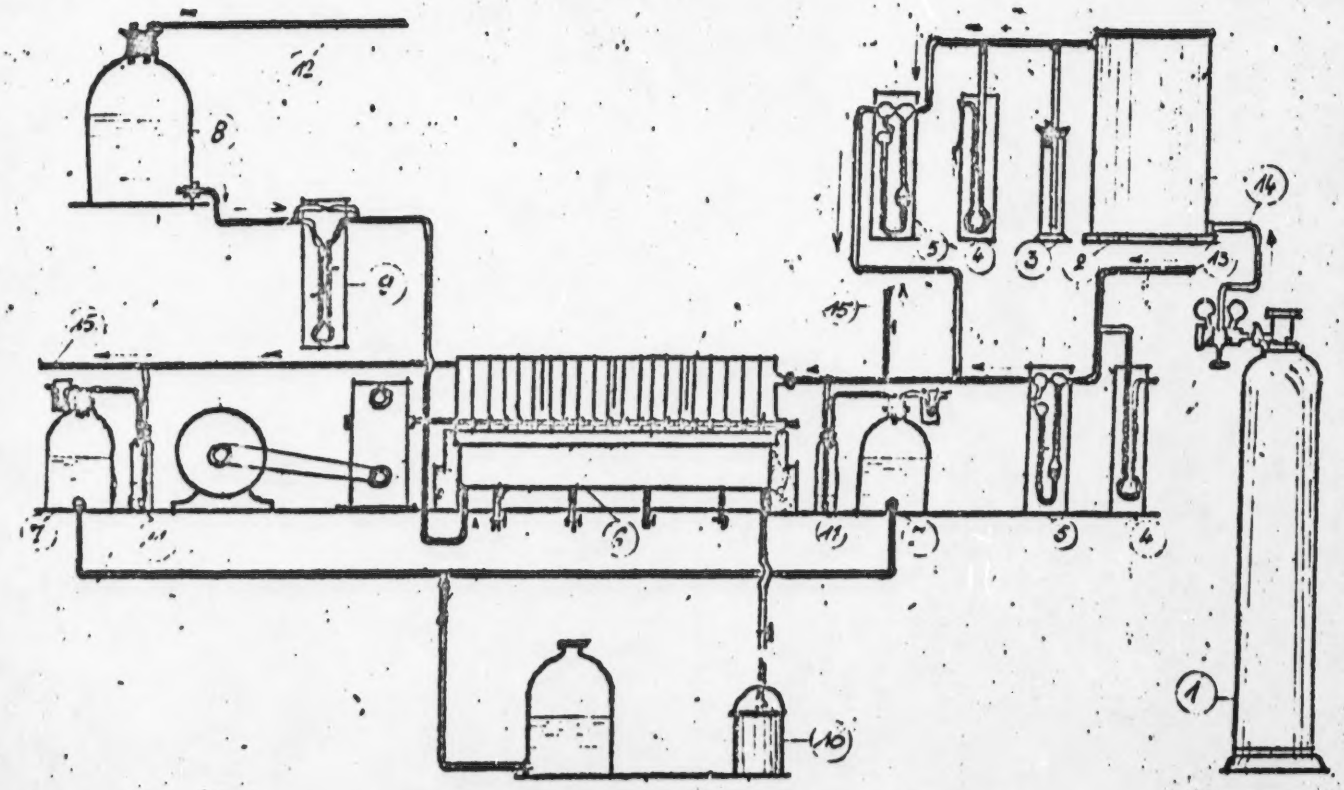

Fig. 1. Layout of the test apparatus for a Mechanical Scrubber

1-Tank containing the gas to be absorbed; 2-buffer; 3-liquid manostat; 4-U-tube manometers; 5-flow meters; 6-scrubber 7-aspirators; 8-pressure bottle; 9-flowmeter; 10-measuring tank; 11-Drexel bottle; 12-water supply line, 13-air line from blower; 14-gas line; 15-exhaust-line.

reducing valve and then through a buffer (2). The amount of air and gas was measured by flow meters (5). A liquid manostat (3) was inserted ahead of the flow-meter to keep the gas supply from the tank constant throughout the run. The static head of the gases was measured by U-tube manometers (4). Behind the flow meters, the gas supply lines were combined into the overall line through which the air-gas mixture entered the scrubber (6). The wall facing the wall through which the gas entered was fitted with an outlet for leading the gas out of the scrubber. Tubes connected to the aspirators (7) were connected to the gas inlet and outlet. The gas collected in the aspirators during the run was analyzed for its content of absorbed component.

The water that served as the absorbent was supplied from the water pipe to the pressure bottle (8), in which the level was maintained constant. From the bottle the water passed through the flow meter (9) at a fixed rate into the first section of the scrubber trough. The water passed through the section in counter flow to the gas. The water (the solution) flowed from the last – fourth – section of the scrubber into the measuring tank (10), where it was measured after the completion of the run. Samples were periodically taken in flasks of the water-solution coming from the scrubber.

The liquid in the scrubber was kept at a constant level by means of an overflow pipe. This pipe was kept at a height of 62 mm during the carbon dioxide tests, which was equivalent to 3.5 liters of liquid within the scrubber. In the ammonia tests, with absorption being effected in only one section of the scrubber, the height of the overflow pipe was lowered to 50 mm, making the volume of liquid 0.7 liter.

The tests were run under constant conditions. This was achieved by keeping the flow of liquid and gas through the apparatus constant at constant temperature and constant shaft rpm. In all our tests the gas temperature was kept at 16-17°. In the various runs the water temperature was varied from 8 to 12°. The constancy of the process conditions was confirmed by the analyses of the outgoing liquid, the composition of which varied hardly at all during any run. In fact, as we see from Table 1, the concentration of the absorbed component in the outgoing water-solution increased at the beginning of every run until it reached a certain value characteristic of the run in question, at which it remained constant. This terminal concentration was reached within 5 to 8 minutes of the start, depending upon the rate of flow of the water and the gas. The water rate of flow was 0.5 and 2.0 liters/min during these tests. The gas flowed through at a rate that varied from 5 to 24 liters/min. The resistance to the flow of gas through the scrubber varied accordingly, from 3 to 25 mm of water column. Each run lasted from 15 to 20 minutes. Up to 8 samples were taken during the course of each run. In some instances

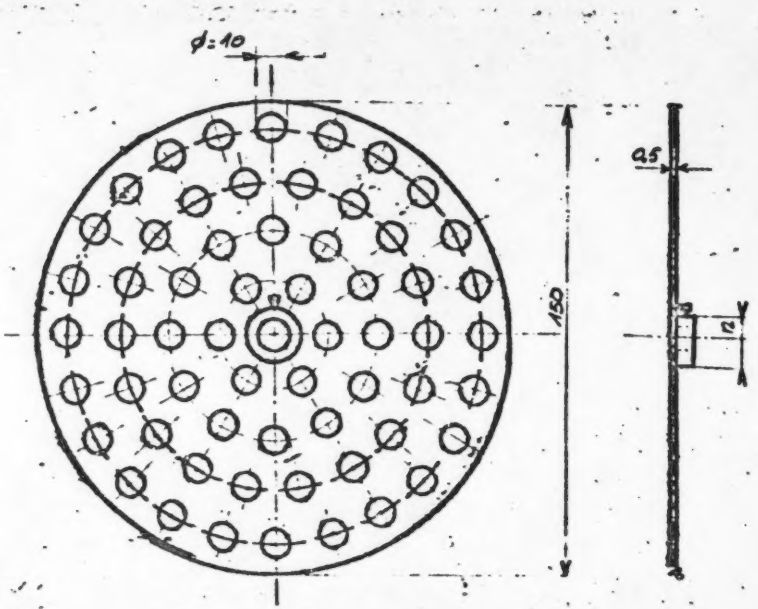

Fig. 2. Disc of the mechanical scrubber.

2 parallel samples were taken, and in others samples of the drain pipes from the first and fourth sections.

The figures in Table 1 indicate that the concentration of CO_2 in the water taken from the bottom of the last section is somewhat lower than that in the overflow. The higher concentration in the upper layer may be due to additional absorption of the gas by the surface of the water, the stirring of the liquid by the discs thus being inadequate, even at 52 rpm, to equalize the concentration throughout the liquid entirely.

The carbon dioxide in the water was determined by a method described in the literature [3].

The amount of CO_2 in the water coming from the water supply to the scrubber was determined several times during the course of the tests; it averaged no more than 0.005 g/liter. Inasmuch as this quantity was so minute, we were able to neglect it entirely in our determination of the quantity of CO_2 absorbed.

Samples of the inlet and outlet gas were taken continuously during the run by means of 2-liter aspirators. The CO_2 in these samples was determined by analysis in an Orsat apparatus.

The amount of NH_3 in the discharge water was determined by pouring the sample into a measured quantity of titrated H_2SO_4 solution and back-titrating the excess acid with caustic soda against a combined indicator: methyl red + methylene blue. To determine the NH_3 in the gas when gas samples were taken, Drexel bottles [11] containing a titrated solution of sulfuric acid were inserted in the line ahead of the aspirators to absorb the ammonia in the exhaust gas. The excess acid in the Drexel bottles after the end of the run was titrated exactly as in the case of the aqueous solution.

EVALUATION OF RESULTS

The solubility of carbon dioxide in water is extremely low. At 10°, for example, the Henry constant is $0.791 \cdot 10^6$ mm/molar fraction.* When we use this value to calculate the equilibrium concentration for a gas containing 10% CO_2, we find that it is 0.24 g/liter. As a result, the drop in the concentration of CO_2 in the gas as it passes through the apparatus is no more than 0.2-0.4% by volume for an overall CO_2 concentration of approximately 10%. The situation is different as far as the change in the concentration of CO_2 in the liquid phase is concerned. Though the water supplied to the scrubber contained 0.005 g of CO_2 per liter, the CO_2 concentration in the discharge water rose to 0.1-0.2 g per liter, i.e., twenty to forty times as much.

The gas at the inlet and outlet ends of the apparatus was analyzed each time to obtain a mean value for the run, while the liquid phase was analyzed in 6 to 8 samples for each run. Besides the use of the flow meter, the amount of water passing through the apparatus was measured directly after each run, thus eliminating any possibility of error during the tests.

In view of the foregoing, it is better and more accurate to calculate the amount of carbon dioxide absorbed from the data for the liquid phase.

Inasmuch as the principal resistance to the absorption of carbon dioxide by water is offered by the liquid stage, it is better to express the driving force as the difference in the concentrations of the dissolved gas in the liquid.

We therefore calculated the overall coefficient of absorption from the following equation:

*Cf. Technical Encyclopedia, V, p. 417.

TABLE 1

Concentration of Gases Absorbed in the Water Flowing out of the Scrubber, as Determined by Analysis of Samples Taken During the Runs, Grams/liter

Test No.	Rpm	Water rate, liters/min	Gas rate, liters/min	Concentration of gases absorbed in the water flowing out of the scrubber, in grams per liter			
				Time at which samples were taken, in minutes elapsed after start of run			
				2.5	5	7.5	10
1	52	0.5	10	–	0.200	–	0.205
2	52	0.5	10	–	–	0.204	0.204
6	52	1.0	10	0.181	0.184	0.171	0.179
10	35	0.5	10	–	0.197	0.190	0.194
18	35	1.0	10	0.136	0.141	0.138	0.140
29	17	0.5	10	0.146	0.136	0.134	0.135
26	17	1.0	10	0.094	0.103	–	0.096
4	35	0.5	10	1.25	1.25	1.23	1.22
6	35	0.5	20	2.26	–	2.19	2.21

$$K_L = \frac{W}{F \cdot \theta \cdot \Delta C} \quad \frac{kg}{hr \cdot kg/m^3} \qquad (1)$$

where W is the quantity of substance absorbed during the run, in kg; F is the absorption surface, in m^2; θ is the absorption time, in hours; ΔC is the mean logarithmetic difference in the concentrations of the absorbed component, in grams per liter, or (what amounts to the same thing) in kg/m^3. The amount of CO_2 absorbed per minute was computed from the equation:

$$W_{min.} = \frac{L}{1000} (C_o - C_i), \text{ kg/min.,} \qquad (2)$$

where L is the quantity of water flowing through, in liters/min; C_o is the concentration in the outlet water, in grams/liter; and C_i is the concentration in the inlet water, which always equals 0.005 g CO_2 per liter. When the gas and the liquid pass through in counterflow, the mean concentration difference is given by the equation:

$$\Delta C = \frac{(C_{ei} - C_i) - (C_{eo} - C_o)}{2.3 \log \frac{C_{ei} - C_i}{C_{eo} - C_o}}, \qquad (3)$$

where C_{ei} and C_{eo} are the equilibrium concentrations at the inlet and outlet ends of the apparatus. The absorption surface F is assumed to be the surface of the discs, minus the area of the holes and the portion of the disc surface that is always immersed in the liquid. The absorption surface was 0.312 m^2 for 20 discs. (The area of the surface of the water in the scrubber, which totaled 15% of the effective surface of the discs, was ignored in our calculations).

Thus, the computational equation (1) is converted into the following formula:

$$K_L = \frac{W_{min.} \cdot 60}{\Delta C \cdot 0.312 \cdot 1000} = 0.192 \frac{min.}{\Delta C} \left[\frac{kg}{m^2 \cdot hr. \cdot kg/m^3}\right]$$

TABLE 1

Concentration of Gases Absorbed in the Water Flowing out of the Scrubber, as Determined by Analysis of Samples Taken During the Runs, Grams/liter

Conc. of gases absorbed in water flowing out of scrubber, g/liter. Time samples were taken, in minutes elapsed after start of run.				Average concentration of gas in water, g/liter	Gas concentration in samples taken from bottom of section 4 of the scrubber, g/liter	Gas absorbed
12.5	15	17.5	20			
–	0.203	–	0.201	0.202	0.190 and 0.195	Carbon dioxide
0.200	0.198	0.183	0.218	0.201	–	"
–	–	0.191	0.189	0.182	–	"
–	0.191	0.188	0.180	0.190	0.181 and 0.182	"
0.142	0.131	–	0.137	0.138	0.138	"
0.145	0.143	0.137	0.127	0.138	–	"
–	0.105	–	0.095	0.099	0.080 and 0.080	"
1.19	1.27	1.26	1.29	1.25	–	Ammonia
2.20	2.20	2.20	2.21	2.21	–	"

When CO_2 is absorbed by water, the coefficient of absorption for partial pressures, i.e., K_G, is found from the expression $K_G = K_L / \alpha$, where α is the Henry constant reduced to the dimensions $\left[\frac{\text{mm Hg}}{\text{kg/m}^3}\right]$.

Ammonia is a gas that is freely soluble in water. Hence, the main resistance to its absorption is offered by the gaseous film. It is therefore better to compute the absorption coefficient in this case by expressing the impelling force in partial pressures of the absorbed gas. W do this by employing the following equation:

$$K_G = \frac{W}{F \cdot \theta \cdot \Delta P} \quad \frac{\text{kg}}{\text{m2} \cdot \text{hr.} \cdot \text{mm Hg}} \qquad (4)$$

where ΔP is the mean logarithmic difference in the partial pressures of ammonia at the inlet and the outlet ends of the apparatus. The rest of the notation is the same as that employed previously.

It should be noted that in our tests the water supplied to the absorber contained no ammonia, while the concentration of ammonia in the discharge water did not exceed 1.25-2.25 g per liter. At these concentrations and at a tempera- of 16-17°, the equilibrium partial pressure of NH_3 approaches zero, so that it may be neglected in our calculations. Hence, the motive force behind the absorption may be expressed as the mean logarithmic difference between the partial pressures of the NH_3 in the gas at the inlet and outlet ends of the apparatus, in accordance with:

$$P = \frac{P_1 - P_o}{2.3 \log \frac{P_1}{P_o}} \qquad (5)$$

where P_1 and P_o are the NH_3 partial pressures in the inlet and outlet gases, respectively.

TABLE 2

Absorption of CO_2 by Water

Test No.	Shaft rpm	Gas: Temp. °C	Gas: Total volume liters/min	Gas: CO_2 concentration % at inlet	Gas: CO_2 concentration % at outlet	Water: Amount of CO_2 absorbed, liters/min. by flowmeter	Water: Amount of CO_2 absorbed, liters/min. by direct measurement	Water: Temp. °C	Water: CO_2 concentration grams/l at outlet	Water: CO_2 concentration grams/l equilibrium at inlet	Water: CO_2 concentration grams/l equilibrium at outlet	K_L (in kg/m^2-hr.-Kg/m^3)	$K_g \cdot 10^3$ (in Kg/m^2-hr.-mm Hg)
1	52	16	10	9.2	8.8	0.5	0.5	9	0.202	0.220	0.230	0.203	0.652
2	52	16	10	9.4	9.2	0.5	0.493	9.5	0.201	0.225	0.250	0.198	0.623
3	52	16	15	10.2	10.0	0.5	0.493	10	0.210	0.240	0.245	0.185	0.573
4	52	15	20	10.4	10.2	0.5	0.487	9	0.223	0.250	0.255	0.194	0.622
5	52	16	9.9	9.6	9.0	1.0	0.97	7.5	0.177	0.235	0.250	0.234	0.792
6	52	17	10	9.6	9.1	1.0	0.98	8.0	0.182	0.235	0.245	0.257	0.854
7	52	17	20	10.0	9.8	1.0	0.99	9.8	0.180	0.246	0 250	0.241	0.785
8	52	17.5	20	10.4	9.8	1.0	0.993	10.0	0.184	0.24	0.255	0.246	0.773
9	35	16	9.65	9.3	9.8	0.5	0.494	12	0.132	0.200	0.215	0.124	0.360
10	35	17	8.82	11.1	10.7	0.5	0.453	12.5	0.190	0.235	0.245	0.23[illegible]	0.373
11	35	17	10	11.0	10.6	0.5	0.503	11.5	0.192	0.245	0.255	0.135	0.400
12	35	16	20	10.3	10	0.5	0.497	10	0.196	0.240	0.245	0.153	0.474
13	30	17	20	10	10	0.5	0.508	9.5	0.181	0.243	0.243	0.147	0.463
14	38	16.5	5	11.4	10.2	1.0	1.12	7.5	0.162	0.265	0.295	0.178	0.602
15	38	16.5	5	10.8	9.8	1.0	1.09	7.5	0.158	0.255	0.280	0.178	0.602
16	35	17	10	9.6	9.1	1.0	1.116	9.0	0.140	0.225	0.238	0.191	0.613
17	35	16	10	10.6	10.0	1.0	1.04	8.0	0.147	0.255	0.270	0.158	0.526
18	35	16.5	10	9.4	8.9	1.0	1.07	8.0	0.138	0.23	0.245	0.171	0.568
19	38	17	15	9.8	9.4	1.0	1.083	8.0	0.152	0.245	0.252	0.192	0.638
20	38	17	15	10.0	9.6	1.0	1.085	9.8	0.145	0.240	0.255	0.177	0.557
21	35	17	20	10.2	10	1.0	1.10	9.5	0.140	0.243	0.248	0.172	0.542
22	35	17	20	10.2	10	1.0	1.023	8.7	0.143	0.250	0.255	0.159	0.519
23	35	15	23.6	9.6	9.4	1.0	1.1	7.5	0.141	0.242	0.250	0.172	0.582
24	35	17	23.6	9.8	9.6	1.0	1.115	8.0	0.140	0.245	0.250	0.172	0.572
25	17	15	9.6	9.1	8.8	1.0	1.015	7.0	0.089	0.235	0.240	0.087	0.300
26	17	15.5	9.7	9.4	9.0	1.0	0.96	7.5	0.099	0.235	0.245	0.093	0.314
27	17	15	19.0	10.7	10.6	1.0	0.98	7.0	0.107	0.280	0.285	0.086	0.297
28	16	15	18.8	10.8	10.6	1.0	1.03	8.0	0.108	0.27	0.275	0.095	0.316
29	16	16.5	10	9.8	9.6	0.5	0.508	10.5	0.1158	0.227	0.232	0.088	0.267
30	16	17	10	10.4	10.2	0.5	0.5	9.0	0.141	0.250	0.255	0.076	0.244
31	16	16	20	10.6	10.4	0.5	0.508	10.0	0.132	0.250	0.255	0.070	0.217
32	16	16	20	10.6	10.4	0.5	0.508	8.5	0.144	0.260	0.265	0.076	0.247

In the ammonia tests, the absorption surface was reduced considerably. A preliminary test indicated that the NH_3 was completely absorbed in the scrubber when 20 discs, or even 10 discs, were used, none of it being found in the outlet gas. We therefore ran these tests using only 4 discs. To diminish the water surface we passed the water through only one of the sections, in which 4 discs rotated. The immersion depth was smaller, and the absorption surface totaled 0.08 m^2.

The amount of NH_3 absorbed may be expressed in terms of the gas or of the liquid. As we see in Table 3, the difference between the two is quite insignificant. But in view of the higher accuracy of the analysis data for the liquid phases, the amount of ammonia absorbed was calculated from analysis of the aqueous solution.

$$W_{min.} = LC_o \text{ grams/min}$$

where L is the quantity of water passing through the scrubber, in liters/min.; and C_o is the concentration of NH_3 in the discharge water, in grams/liter or (what amounts to the same thing) in kg/m^3.

The computational equation for K_G then reduces to:

$$K_G = \frac{C_o \cdot 60}{0.08 \cdot \Delta P \cdot 1000} = 0.75 \frac{LC_o}{\Delta P} \text{ kg/m}^2 \cdot \text{hr.} \cdot \text{mm Hg.}$$

The principal results secured in our tests on the absorption of CO_2 and NH_3 by water in a mechanical scrubber, plus the coefficients of absorption computed therefrom, are listed in Tables 2 and 3.

The absorption coefficients for carbon dioxide given in Table 2 express the value of K_L in the range of 0.07-0.25 kg/m^2 per hr. per kg/m^3, which corresponds to 0.000217 - 0.000854 kg/m^2 per hr. per mm Hg in terms of the absorption coefficient K_G as expressed for the gas phase.

For the sake of comparison we list below the values of K_L for CO_2 in the same units, as secured by various authors under different absorption conditions.

Perry's handbook [4] cites the following figures for the absorption of CO_2.

1) The gas passed over the surface of the water, which was stirred. K_L = = 0.076.

2) Absorption of pure carbon dioxide from bubbles in a current of flowing water. Temperature = 25°. K_L = 0.914.

3. Absorption by drops of water falling from a height of 50 cm through an atmosphere of pure carbon dioxide. K_L = 2.60.

4. Absorption from a mixture of carbon dioxide and air. The water was stirred with a stirrer, while the gas was not stirred. Temperature = 26°.

Per cent CO_2 by volume	100	50	25
K_L	0.098	0.088	0.079

The following figures are given for the coefficient of absorption of CO_2 by water in a paper by Prof. Shabalin [5]. When absorbed by drops bigger than 1 mm in diameter, K_L = 1.0. The value of K_L is the same for absorption from a rising bubble. K_L was found to range from 0.3 to 0.8 for different rates of trickling during absorption by a sheet of flowing water.

These figures indicate that the coefficients of absorption obtained in a mechanical scrubber are 4 to 5 times as small as in bubbling or in falling drops. They are higher, however, than the coefficients for absorption by a stirred liquid from a stationary or slowly moving gas.

The absorption coefficients measured by us are closest to those found for the absorption of the gas by a sheet of flowing liquid (at low trickling rates). This is obviously due, as we have pointed out above, to the resemblance between the hydraulic conditions prevailing during absorption in mechanical and checkerwork scrubbers.

The rate of flow of a liquid through checkerwork may be calculated from the following formula for a mean thickness of the flowing sheet:

$$V = \frac{Q}{v \cdot \gamma \cdot S},$$

where Q is the quantity of liquid, in grams/sec; v is the sheet thickness, in cm; γ is the density in $grams/cm^3$; and S is the wetted perimeter of the checkerwork, in cm.

For a 50 x 50 x 5 mm Raschig ring and a trickling rate of 30 $m^3/m^2/hr$, the thickness of the sheet is found to be 0.035 cm [6]; the wetted perimeter of these rings, which is numerically equal to the specific surface of the checkerwork, is 87.5 m.

Inserting these values in the above formula, and converting the centimeters into meters, we get the trickling rate as:

$$V = \frac{30}{3600 \cdot 2.00035 \quad 87.5} = 0.273 \text{ m/sec.}$$

The rate of flow of water through the tubes of trickle condensers is 0.15 – 0.3 m/sec [2], i.e., of the same order of magnitude as that calculated for checker work.

In our scrubber, the peripheral velocity was as follows for various disc speeds:

Rpm	7	35	52
Velocity as periphery of the disc, m/sec	0.13	0.27	0.40
Velocity halfway to the outer edge, m/sec	0.07	0.14	0.20

Hence, in our tests the rate at which the liquid was stirred by the discs is of the same order of magnitude as the trickling rate of liquid through scrubber checkerwork; it therefore introduces no essential changes into the motion of the flowing sheet. This also explains the similarity between the absorption coefficients derived for the two cases.

We likewise see from Tables 2 and 3 that it is the disc rpm that is mainly responsible for the magnitude of K_L. When the rpm is doubled, for example, K_L rises 75 to 100%. This increase is analogous to the value of K_L in a checkerwork scrubber with a higher trickling rate, i.e., with an analogous increase in the rate of flow of the liquid film.

Increasing the supply of liquid to the scrubber increased the value of K_L somewhat. When the rate of water flow was increased from 0.5 to 1.0 liter/min or 100%, for example, K_L rose from 0.14 to 0.17 at 36 rpm and from 0.195 to 0.245 at 52 rpm, or 20% and 26%, respectively.

Varying the gas velocity has no appreciable effect upon the value of K_L. We clearly see in Fig. 4 that increasing the gas flow rate from 5 to 25.6 liters per min while leaving the rpm and the water supply rate unchanged, has no effect upon the magnitude of the K_L. It should be noted that the corresponding linear velocity of the gas past a cross section of the scrubber interior was extremely low: 0.008 to 0.038 meters/sec. It is obvious that the friction caused at these gas velocities could not produce turbulence in the liquid film, which is the predominating factor in CO_2 absorption.

As we have said, a few tests were run on the absorption of ammonia by water. The following conditions were used for these tests: 35 rpm, 1.0 liter of water per minute, and a gas flow rate of from 10 to 20 liters/min. As Table 3 indicates, the corresponding absorption coefficients ranged from 0.015 to 0.23 kg/m^2 per hr per mm Hg. Increasing the gas flow rate from 10 to 20 liters/min, i.e., 100%, increased the value of K_G from 0.015 to 0.023, or 35%, on the average. Here we begin to notice the gas flow rate having an effect, which was not the case in the absorption of CO_2; But this effect is less than in trickle checkerwork, where the increase in K_G is proportional to the rise in the gas flow rate, the proportionality constant being 0.8, which in our case would have been equivalent to an increase of 74% in the value of K_G.

Perry's handbook [4] gives several values for K_G in the absorption of ammonia by water under different conditions. The numerical values, given in the

TABLE 3

Absorption of NH_3 by Water

Test No.	Gas phase				Water					Absorption coefficient, kg/m²/hr /mm Hg
	Temp. °C	Total gas volume liters/min.	Partial pressure mm Hg at inlet	Partial pressure mm Hg at outlet	Temp. °C	Volume, liters/min.	Concentration at outlet g/liter	Amount of NH_3 absorbed: gas results g/min	Amount of NH_3 absorbed: water results g/min	
1	17.5	19.9	73	13.5	13	0.483	2.25	1.09	1.3	0.023
2	16	9.9	48.5	3.5	9	0.497	0.86	0.411	0.427	0.019
3	17	10.1	81.5	6	12	0.5	1.31	0.703	0.655	0.015
4	16.5	10.3	75	7.5	11	0.5	1.25	0.637	0.625	0.016
5	17	20.1	69	17.5	11.5	0.5	2.2	0.945	1.1	0.022
6	17	20.1	72	15	10	0.49	2.21	1.05	1.08	0.022

dimensions of mole/m² per hour per atm, have been converted into the dimensions of K_G that we have used: kg/m² per hour per mm Hg. For trickling towers the value of K_G at 10° varied from 0.0383 to 0.00224 when the gas flow rate was varied from 0.48 to 0.015 m/sec, the corresponding figures at 30° being 0.0338 and 0.00224, respectively.

In a column with trickling walls, 5 cm in diameter and 81 cm high, the value of K_G varied from 0.0203 to 0.0053 kg/m² per hour per mm Hg at a temperature of 10° when the gas flow rate was varied from 0.259 to 0.049 kg/sec/m² of column cross section (0.32-0.05 m/sec).

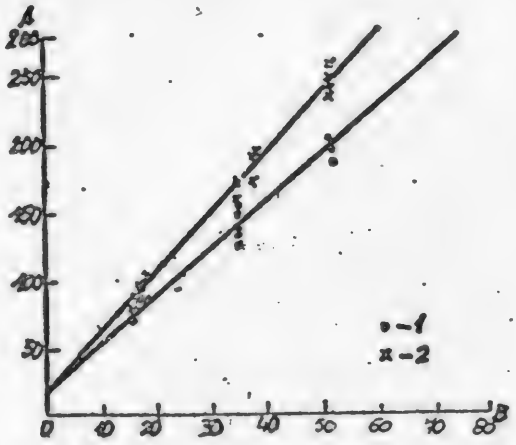

Fig. 3. Variation of the absorption coefficient for CO_2 with the disc rpm at different water flow rates.
A-Coefficient of absorption $K_L \cdot 10^3$. B-disc rpm. Water flow rate. 1-0.5 liter/min. 2-1.0 liter/min.

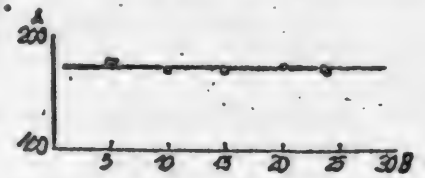

Fig. 4. Variation of the coefficient of absorption of a gas with the gas flow rate at a water flow rate of 1 liter/min and a disc rpm of 35.
A-Coefficient of absorption, CO_2 $K_L \cdot 10^3$; B-gas flow rate, liters/min.

The paper by Prof. Shabalin referred to above [5] gives the following values for the absorption coefficient of ammonia by water: K_G was 0.3 to 0.35 kg/m² per hour per mm Hg for absorption by drops whose diameter exceeded 1 mm. The values of K_G were of the same order of magnitude for rising bubbles. For trickling films, K_G lay between 0.01 and 0.04 kg/m² per hour per mm Hg, i.e., 10 to 20 times smaller than for drops or bubbles.

Comparison of the values of K_G secured in our tests and in the researches of other investigators indicates that the coefficient of absorption of a freely soluble gas in a mechanical scrubber is of the same order of magnitude as in scrubbers

employing a trickling film. But, in view of the low gas velocity employed in our tests, compared to the velocities used by the cited authors, it is likely that in mechanical scrubbers K_G will be somewhat higher, all other conditions being equal, than for a film trickling down through checkerwork.

SUMMARY

1. The values of the coefficient of absorption in mechanical scrubbers at low rpm are close to those for checkerwork scrubbers and much below the coefficients secured for bubbling or in towers employing sprayed liquid; this is true both for a slightly soluble gas (carbon dioxide) and for a freely soluble gas (ammonia).

2. Comparing the advantages of mechanical scrubbers of the foregoing type (low consumption of absorbent liquid, feasibility of securing highly concentrated solutions, lowered resistance to the passage of the gas, etc.) and their disadvantages (energy consumed for the rotating shaft, rapid wear in an aggressive medium, etc.) with those of checkerwork scrubbers, we must admit that they offer no special advantages over checkerwork.

3. The only case in which the use of mechanical scrubbers of the foregoing type may be justified is when the absorbent liquid is contaminated by a precipitate or a precipitate is formed during the absorption of the gas, i.e., when the gas is absorbed by a suspension instead of by a liquid, practically speaking. The use of other types of absorbers is hampered when this is the case by the possible clogging of the apparatus by the precipitate, of which there is no danger in mechanical scrubbers.

LITERATURE CITED

[1] M.Maizel. Handbook of Mechanical Engineering, Vol. IV, 213, 215. United Scientific and Technical Press (1935).

[2] A.G.Kasatkin. The Major Processes and Apparatus of Chemical Engineering, Vol. II, 223, 677. United Scientific and Technical Press, (1937).

[3] F.P.Treadwell and W.Hall. Treatise of Analytical Chemistry (Russ. ed.) Vol. II 84. United Scientific and Technical Press (1935).

[4] D.Perry. Chemical Engineer's Handbook (Russ. ed.), Vol. I, 584-588, 591. United Scientific and Technical Press (1937).

[5] K.N.Shabalin. Friction Between Gas and Liquid in Absorption Processes, 8-12. Metallurgy Press (1943).

[6] N.M.Zhavoronkov. The Hydraulic Principles of the Scrubber Process. 175. Soviet Science Press, Moscow (1944).

Received November 4, 1949.

THE EFFECT OF NONCONDUCTING INCLUSIONS UPON THE CONDUCTANCE OF AN ELECTROLYTE

V P. Mashovets

All-Union Aluminum and Magnesium Institute

In industrial electrolysis the electrolyte often contains nonconducting inclusions: solid impurities in suspension or, most often, gas bubbles. These inclusions reduce the conductance of the electrolyte, of course. Even conducting inclusions, such as, say particles of carbon in a molten electrolyte, increase the resistance, since polarization phenomena make it impossible for the current to pass through such inclusions.

The drop in conductivity is governed by the form and disposition of the inclusion, as well as by their quantity. When the inclusions are cylindrical in form, with their axes coinciding with the direction of the current, the reduction in the conducting cross section equals the relative packing of the volume, and the relative conductance of such a system will be:

$$K = \frac{\kappa_c}{\kappa_0} = 1 - p, \qquad (1)$$

where κ_0 is the specific conductance of the pure electrolyte; κ_c is the specific conductance of the electrolyte containing inclusions; and p is the relative packing factor, equal to the volume of the inclusions per unit total volume.

As far back as 1892, Rayleigh [1] made an analytical computation of the conductance of heterogeneous systems containing inclusions in the form of cylinders, the axes of which were perpendicular to the direction of the field, or containing spherical inclusions.

Later, Runge [2] repeated this computation and wrote the Rayleigh equation (with a few corrections) as follows for cylindrical inclusions:

$$K_c = 1 - \frac{2p}{\frac{1+\kappa_1}{1-\kappa_1} + p - 0.30584\,\frac{1-\kappa_1}{1+\kappa_1}\,p^4 - 0.013363\,\frac{1-\kappa_1}{1+\kappa_1}\,p^8 - \ldots} \qquad (2)$$

and for spherical inclusions:

$$K_c = 1 - \frac{3p}{\frac{2+\kappa_1}{1-\kappa_1} + p - 0.523\,\frac{1-\kappa_1}{\frac{4}{3}+\kappa_1}\,p^{10/3} + \ldots}, \qquad (3)$$

where κ_1 is the specific conductance of the inclusions (the specific conductance of the medium $\kappa_0 = 1$), while K_c and p denote the same quantities as in (1).

For nonconducting inclusions ($\kappa_1 = 0$), Equations (2) and (3) become:

$$K_c = 1 - \frac{2p}{1 + p - 0.306\,p^4} \qquad (2a)$$

and
$$K_c = 1 - \frac{3p}{2 + p - 0.392\, p^{10/3}} \qquad (3a)$$
while at lower relative packing factors ($p \ll 1$, ignoring higher powers of p), we get
$$K_c = \frac{1 - p}{1 + p} \sim 1 - 2p \qquad (2b)$$
and
$$Kc = \frac{1 - p}{1 + 0.5p} \sim 1 - 1.5\, p \qquad (3b)$$
Maxwell [3] gives another type of equation for heterogeneous systems with spherical inclusions, however.

We checked the equation for packings consisting of cylinders at right angles to the direction of current flow by graphically mapping the field, as well as making an experimental check.

We assume that the cylinders are arranged hexagonally, as shown in Fig. 1. We denote the distance between cylinder axes as $\underline{d} = \underline{nr}$, where $\underline{r}$ is the cylinder radius, and $\underline{n}$ is the arrangement constant. The elements of the field are the triangles I, II, and III, (Fig. 1), which differ only in their orientations. The sides of these elements are $\underline{a} = 0.5\underline{d} = 0.5\underline{nr}$ and $\underline{b} = \underline{a}\sqrt{3} = 0.866\underline{nr}$. The relative packing factor of the volume is:
$$p = \frac{0.5\pi r^2}{ab} = \frac{3.63}{n^2}. \qquad (4)$$
When the cylinders touch ($\underline{n} = 2$) the conductance of the system $K_c = 0$; then $\underline{p} = 0.909$ from (4).

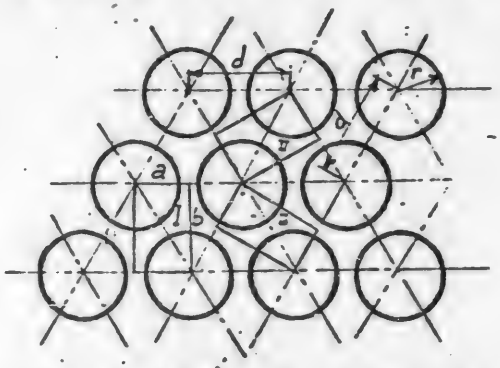

Fig. 1. Field with cylindrical inclusions.

I, II, III-Elements of the field: axes of the cylindrical inclusions at right angles to the direction of the field; a and b-element sides; r-radius of the inclusion; d-distance between cylinder axes.

It is simplest to map the field graphically by assuming the current to flow along the side $\underline{a}$ or $\underline{b}$ of the elementary cell. An example of mapping the field by the method of curvilinear squares is given in Fig. 2 for $\underline{d} = 2.2\underline{r}$ and the current flowing along the side $\underline{b}$. The number of tubes of force, $\underline{z}$, may be chosen at random, depending upon practical convenience of plotting (in Fig. 2 we have taken $\underline{z} = 4$).

Let us denote the conductance of an element of the field where there are no inclusions, and the field is homogeneous, by K_o', and the conductance of the same element when inclusions are present by K_c', and then let us compute the relative conductance
$$Kc = \frac{K_c'}{K_o'}.$$

When no inclusions are present,
$$K_o' = \varkappa \frac{a}{b} = \frac{\varkappa}{\sqrt{3}} \qquad (5)$$
(since $\underline{b} = a\sqrt{3}$ from Fig. 1), where $\varkappa$ is the specific conductance of the electrolyte.

When inclusions are present

$$K_c' = \frac{zi}{w_c u}, \qquad (6)$$

where i is the current through a single tube; u is the potential drop between two equipotential lines; and w_c is the number of equipotential lines throughout the length of the elementary cell as determined by a simple computation from Fig. 2. In Equation (6)

$$\frac{i}{u} = \kappa \frac{\Delta s}{\Delta l}, \qquad (7)$$

where Δs is the width of the tube of force; and Δl is the distance between equipotential lines. But $\Delta s = \Delta l$ from the conditions governing the mapping of the field (curvilinear squares). Hence, substituting (7) in (6), we get:

$$K_c' = \kappa \frac{z}{w_c} \qquad (8)$$

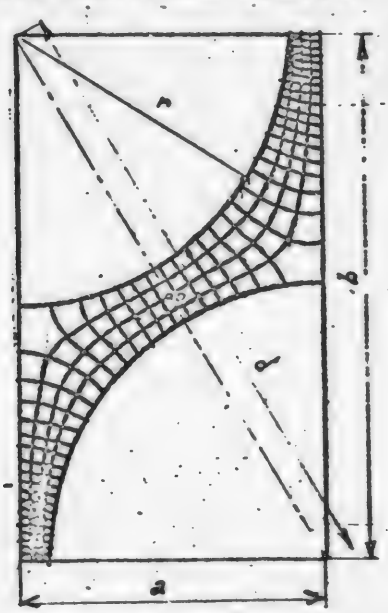

Fig. 2. Field of an elementary cell at $d = 2.2r$; direction of current flow along side b.

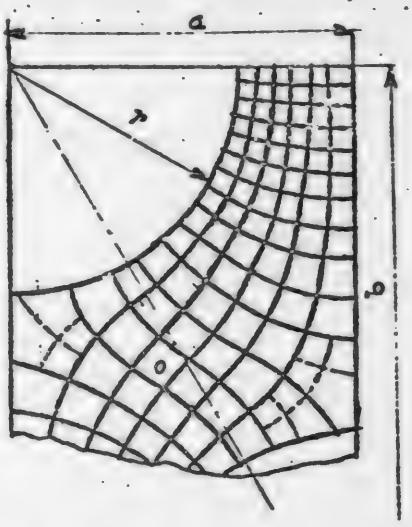

Fig. 3. Field of an elementary cell at $d = 3r$; direction of current flow along side b.

and, finally,

$$K_c = \frac{K_c'}{K_o'} = \frac{z\sqrt{3}}{w_c}. \qquad (9)$$

In addition to the field of an element with $d = 2.2r$ (Fig. 2), we also mapped the field for $d = 2.5r$, $3r$, and $5r$. For $d = 3r$, the field was mapped with the current flowing in the direction of side b (Fig. 3) as well as the direction of side a (Fig. 4). Inasmuch as the point O (Figs. 2, 3, and 4) is the center of symmetry of the field, we have reproduced only part of the elementary cell in Figs. 3 and 4.

When the current flows in the direction of side a, the conductance is:

$$K_o' = \kappa \frac{b}{a} = \sqrt{3}. \qquad (5a)$$

when no inclusions are present, and

$$K_c' = \frac{K_c'}{K_0'} = \frac{z}{v_c\sqrt{3}} \qquad (9a)$$

when inclusions are present.

We also made experimental measurements[1] of the drop in conductance when the electrolyte was filled with nonconducting cylinders. We did this by setting up plane elements 20 cm long and 11-12 cm wide. Copper electrodes were used for the end walls of the element (so that the interelectrode spacing was 20 cm), while the side walls were nonconducting. A barrier consisting of 4 rows of vertical glass cylinders 1.4 cm in diameter was set up on the hexagonal system (Fig. 1) in the middle of the element; the orientation of the barrier conformed to current flow in the direction of side b of the elementary cell I (Fig. 1).

The distance between the cylinder axes, d, was taken as 2.2r, 2.5r, 3r, and 4r. The total width of the barrier varied accordingly from 5.4 to 8.6 cm. A solution of 150 g per liter of $CuSO_4 \cdot 5H_2O$, 20 g per liter of H_2SO_4, and 50 g per liter of alcohol was poured over the bottom of the cell to a depth of 1 cm. Then the drop of potential throughout the field, within the barrier as well as outside it, was measured by the usual potentiometric method, using an electrolytic switch and a current of 50 milliamperes through the cell. The measurements indicated that the homogeneous field is appreciably distorted only in the immediate vicinity of the barrier, at a distance of about one cylinder radius from the front edge of the first row of cylinders.

Once we know the potential gradient outside the barier, $\frac{dU_0}{dl}$, and the potential drop inside the barrier per unit width of the latter, $\frac{\Delta U_c}{\Delta l_c}$, we can find the relative conductance when nonconducting inclusions are present:

$$K_c = \frac{\frac{dU_0}{dl_0}}{\left(\frac{\Delta U_c}{\Delta l_c}\right)}. \qquad (10)$$

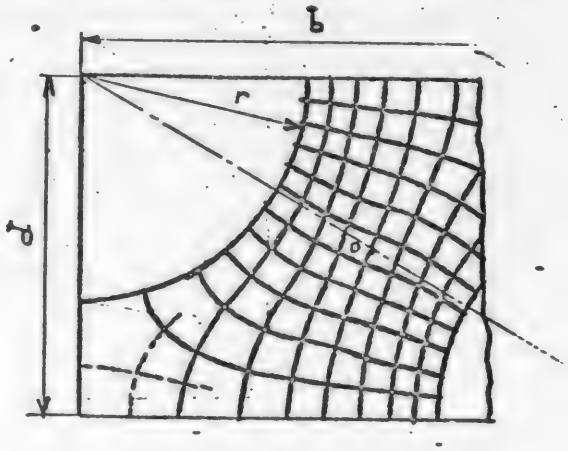

Fig. 4. Field of an elementary cell at d = 3r; direction of current flow along side a.

Table 1 gives the values of K_c, as found graphically and experimentally. The two sets of values agree perfectly. Moreover, it is worthy of note that at a given packing factor (p = 0.403), the relative conductance remains the same though the orientation of the field differs by as much as 90°.

We made only an experimental investigation of the effect of spherical inclusions, in view of the difficulties involved in graphically mapping a three-dimensional field. The principal variant employed was the cubic octahedral arrangement of the spheres (Fig. 5), in which the vertical distance between the centers of two layers of spheres $H = d\sqrt{\frac{2}{3}} = 0.816\,d$. At $H > 2r$ (or denoting $d = nr$, at $n > 2.45$), the elementary layer may be taken as the layer between a plane passing through the centers of the spheres in one layer and a plane that is 0.5H above it. Barriers of this sort were produced in a flat cell like the one described above by affixing

[1] These measurements were made by N. V. Pototskaya and L. I. Ivanova.

TABLE 1

Comparison of the Values of Relative Conductance, As Found Graphically and Experimentally When Cylindrical Inclusions are Present

Test No.	Distance between axes, $\underline{d}$	Packing factor, p	Field direction	Graphical mapping		K_c		Remarks
				Given $\underline{z}$	Resultant $\underline{w}_c$	Graphically	Experimentally	
1	$2\underline{r}$	0.908	Any	–	–	0.000	–	
2	$2.2\underline{r}$	0.750	Along side $\underline{b}$	4	49.0	0.141	0.145	
3	$2.5\underline{r}$	0.582	Along side $\underline{b}$	4	26.3	0.263	0.269	Fig. 2
4	$3\underline{r}$	0.403	Along side $\underline{b}$	6	24.3	0.426	0.433	Fig. 3
5	$3\underline{r}$	0.403	Along side $\underline{a}$	8	11.0	0.421	–	Fig. 4
6	$4\underline{r}$	0.227	Along side $\underline{b}$	–	–	–	0.640	
7	$5\underline{r}$	0.145	Along side $\underline{c}$	6	13.7	0.758	–	

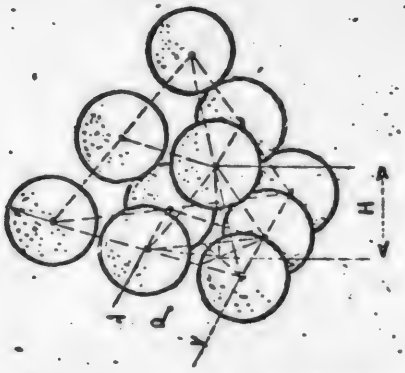

Fig. 5. Cubic octahedral arrangement of spheres.

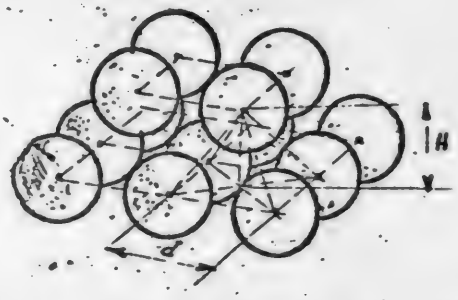

Fig. 6. Cubic octahedral arrangement of spheres with a different orientation.

four rows of hard-rubber hemispheres ($\underline{r}$ = 0.7 cm), to the bottom of the cell, for $\underline{d} = 4\underline{r}$, $3\underline{r}$ and $2.5\underline{r}$, and filling the cell with electrolyte to a depth of $0.5\underline{H}$.

Barriers with a higher packing factor were made of glass balls in contact with one another (using hard-rubber hemispheres and quarter-spheres, wherever necessary), arranging them in four different ways:

a) The cubic octahedral arrangement of Fig. 5, with $\underline{d} = 2\underline{r}$.

b) The cubic octahedral arrangement of Fig. 6, with $\underline{d} = 2\underline{r}$, the packing factor of which is the same as that of (a), though the orientation is different (rotated through 120°).

c) The hexagonal arrangement of Fig. 7.

d) The octahedral arrangement of Fig 8.

In the variants (a) and (b) the barrier was set up with three layers of balls, while in variants (c) and (d) only one layer was used, with the electrolyte poured in to a depth of $\underline{H} = \underline{d} = 2\underline{r}$. The potential gradient was measured inside and outside the barrier and the relative conductance K_c was then computed from (10). The results of these measurements are listed in Table 2. The first

TABLE 2

Relative Conductance as a Function of the Packing Factor and Orientation of Spherical Inclusions

Test No.	Arrangement of spheres	Distance from centers, d	Packing factor, p	Experimental K_c
8	Cubic octahedral (Fig. 5)	2r	0.7405	0.226
9	The same (Fig. 6)	2r	0.7405	0.226
10	Hexagonal (Fig. 7)	2r	0.6046	0.297
11	Octahedral (Fig. 8)	2r	0.5236	0.338
12	Cubic octahedral (Fig. 5)	2.5r	0.373	0.453
13	The same	3r	0.218	0.667
14	The same	4r	0.0922	0.855

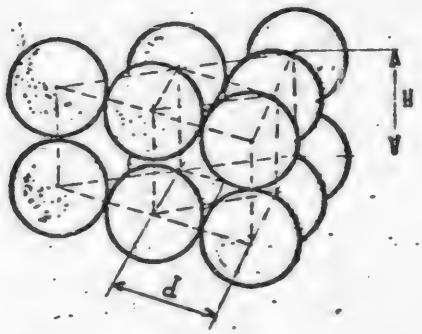

Fig. 7. Hexagonal arrangement of spheres.

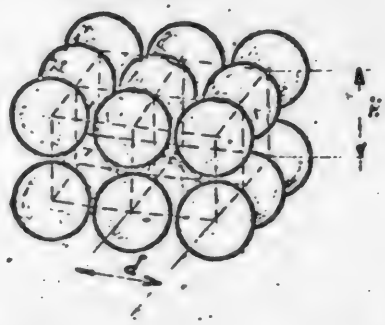

Fig. 8. Octahedral arrangement of spheres.

two lines of the table show that the conductance is independent of the orientation of the spheres, provided the packing factor is the same.

In Fig. 9, Curve I represents the Rayleigh equation for cylindrical inclusions (2a), while Curve II is for spherical inclusions (3a). Our values, both for the cylindrical inclusions (the stars represent the experimental as well as the graphical values) and for the spherical ones (circles) are fairly close to the first Rayleigh curve (2a) up to a packing factor of the order of $p = 0.4$. For any arrangement of the spheres (cubic octahedral, hexagonal, or octahedral) and for all packing factors up to the densest packing ($p = 0.7405$), the experimental values satisfy the empirical equation:

$$K_c = 1 - 1.78\,p + p^2. \qquad (11)$$

For cylindrical inclusions the experimental values satisfy both the first Rayleigh equation (2a) and our equation (11) with an accuracy that is adequate for engineering purposes up to packing factors of $p \leqslant 0.4$. At higher packing factors, cylindrical inclusions yield the singular Curve IV.

Pfleiderer [4] gives an experimental curve for the increase in the resistance of an electrolyte as a function of its filling up with gas up to $p = 0.35$. This curve, recomputed in terms of conductance, has been plotted in Fig. 9 as Curve V. At low packing factors it satisfies the second Rayleigh equation (3a) fairly well, but at higher packing factors it approaches our Equation (11). This leads us to believe that our proposed Equation (11) is a universal one, with an accuracy that is sufficient for engineering purposes, for packing factors up to

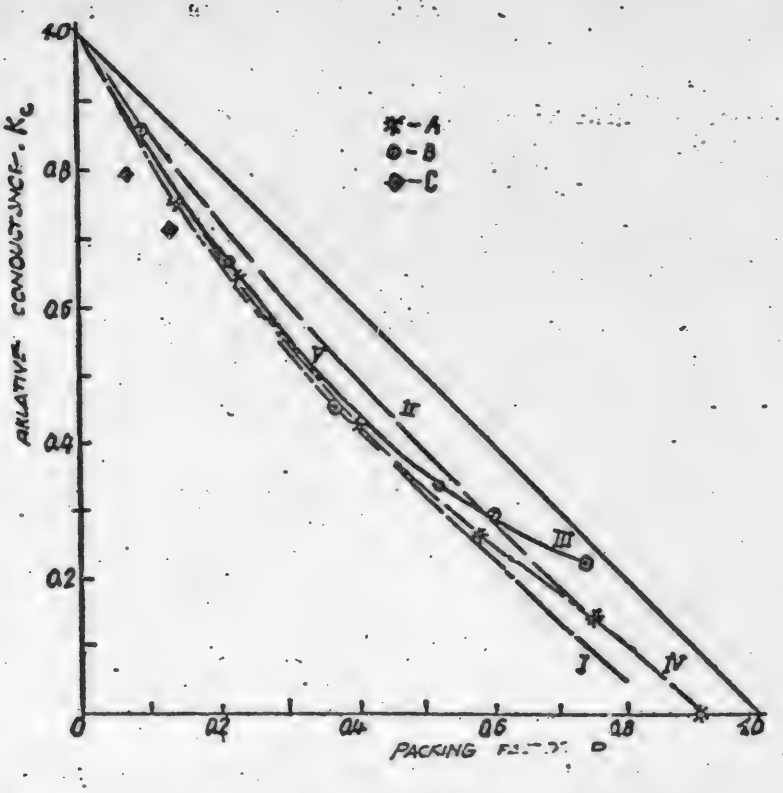

Fig. 9. Conductance as a function of the packing factor of nonconducting inclusions.

I-Rayleigh equation (2a) for cylindrical inclusions; II-Rayleigh equation (3a) for spherical inclusions; III-the author's empirical equation(11); IV-the author's experimental data for cylindrical inclusions; V-the experimental curve given by Pfleiderer. A-the author's data for cylindrical inclusions (obtained experimentally and by mapping the field graphically). B-the author's data for spherical inclusions (obtained experimentally); C-Baimakov's data.

$p = 0.4$, and that it holds good for various forms and random arrangements of the inclusions, and that for spherical inclusions of uniform diameter it holds good up to dense packing, i.e., up to $p = 0.7405$.

According to Baimakov [5], the presence of 5 and 10% (by weight) of dispersed carbon in molten cryolite – alumina increases the specific resistivity of the melt by 27% and 40%, respectively. Assuming the apparent specific gravity of the carbon as 1.5 and the specific gravity of the melt as 2.05, and converting from resistance to conductance, we get the two points denoted by the diamonds in Fig. 9. These points agree neither with our data nor with Pfleiderer's curve, and even less so with Rayleigh's equation for spherical inclusions.

SUMMARY

1. The effect of cylindrical and spherical nonconducting inclusions upon the conductance of an electrolyte has been investigated experimentally. The investigation was likewise made graphically, by mapping the field, for cylindrical inclusions.

2. An empirical formula is put forward for calculating the relative conductance, which holds good for any packing factor for spherical inclusions, and

for packing factors that do not exceed 0.4 of the total volume for cylindrical inclusions.

3. The experimental results are compared with the Rayleigh equations derived theoretically and with some of the experimental data cited in the literature.

LITERATURE CITED

[1] Rayleigh, Phil. Mag., [5], 34, 481 (1892).

[2] I.Runge, Z. tech. Phys., 6, 61 (1925).

[3] J.C.Maxwell, A Treatise on Electricity and Magnetism, I, 440 (1904).

[4] G.Pfleiderer. The Electrolysis of Water, 13. United Scientific and Technical Press.

[5] Yu.V.Baimakov. Electrolysis in Metallurgy, III, 52. Metallurgy Press, Moscow, (1946).

Received May 9, 1950.

NEW ELECTROLYTES FOR TINPLATING

V. I. Sotnikova and M. A. Loshkarev

In the overwhelming majority of cases metallic coatings are applied in electroplating in order to protect the coated part against corrosion. Accordingly, cathodic deposits of metals should be dense and homogeneous, of uniform thickness, as free from pores as possible, and should possess the best mechanical properties characteristic of the metal to be protected. Metallic coatings possessing the enumerated qualities cannot be produced by every cathodic process. In fact, a dense homogeneous deposit, possessing good protective qualities can be produced only by a cathodic process that yields a finely crystalline structure of the deposited metal. Uniformity of thickness of the electrolytic plating is achieved when good enough dispersibility and other factors are assured.

These qualities of the coatings may be easily assured in the case of metals whose cathodic deposition involves considerable chemical polarization. Iron, nickel, and cobalt are metals of this sort [1]. Copper, zinc, and cadmium, which exhibit lower chemical polarization [2], are deposited in coatings with a coarser crystalline structure, though their galvanic platings are still fairly satisfactory. Lastly, metals whose electrocrystallization occurs at extremely low overvoltages yield coarse grainy platings, which in some cases consist simply of an accumulation of individual crystals that are not bound together. This last group comprises Sn, Pb, Ag, [3], among other metals.

As we know, no electrolyte has yet been found for the refining of Ag that yields a dense, finely crystalline cathodic deposit, despite numerous endeavors in this field; with the nitric-acid electrolyte commonly employed, the silver is deposited at the cathode as individual dendritic crystals, which are removed from the cathode periodically. Nor has it been possible up to very recently to produce any satisfactory coatings of tin or lead by the cathodic deposition of these metals from solutions of simple salts. As a result, for a long time the only available method of producing electrolytic deposits of these metals that met the standards of electroplating involved the use of their complex salts as electrolyte solutions. The finely crystalline structure, the density, and the uniform thickness of the cathodic deposits secured in these electrolytes were due to the very considerable cathodic polarization that prevailed. The use of solutions of complex salts as electrolytes for electroplating involves several basic disadvantages, however: 1) the high concentration polarization in these electrolytes (low limiting C.D. and a drop in the current efficiency as the C.D. increases) allows of the use of only very low current densities, thus making it impossible to run the process at high efficiency; 2) baths of this sort are much less stable in operation than baths consisting of solutions of simple salts; 3) when complex electrolytes are used, the anodic process is much more capricious than when solutions of simple salts are employed, and is often further complicated by the tendency of the anodes to become passivated.

These disadvantages of complex electrolytes have stimulated numerous searches for electrolysis conditions that would make it possible to deposit tin, lead, and other metals in dense and finely crystalline platings from their simple salt solutions. A satisfactory solution of this problem was achieved by introducing various technical products of organic origin as additives to tin electrolytes. Without dwelling upon the papers by Lainer, Foerster, Mathers, Kern [4], Marshak [5], Kheifets [6], Kadaner [7], and other researchers, which are of considerable interest in this connection, we shall merely point out that only cresolsulfonic (3-60 g of $C_6H_3CH_3OHSO_3H$ per liter) acid sulfate electrolytes and the phenolic (ca. 10-20 g of C_6H_5OH per liter) acid sulfate electrolytes recommended by Lainer [8] have found industrial application.

In one of our own papers [9], we succeeded in proving that the addition of minute quantities of α- and β-naphthol, thymol, xylenes, diphenylamine, and some other compounds to tin-sulfate electrolytes containing up to 1 g of gelatin or sizing per liter produces very high chemical polarization, due to the formation of dense adsorbed films on the electrodes. In some instances the polarization not only exceeds the values measured by Kheifets [6] and by us [10] for the deposition of Sn from the best industrial cresolsulfonic baths, but even surpasses all the overvoltages for the cathodic deposition of metals known up to the present time. (Fig. 1).

The production of such polarization has always yielded cathodic deposits of tin that are noteworthy for their high density, the grain dimensions being of the same order of magnitude as in the cathodic deposition of the metals of the iron group (Fig. 2).* This led us to expect that simple sulfate baths containing the foregoing organic additives would yield tinplating of high industrial quality. The fact that the ameliorative action of one of these additives (β-naphthol) when added to the bath together with cresolsulfonic acid has been noted in the literature [11] lends further support to this assumption.

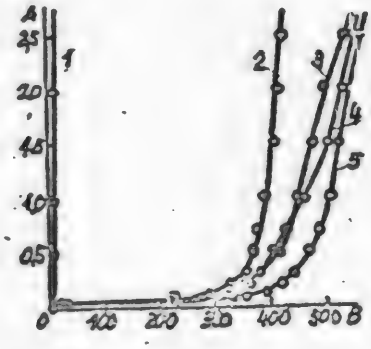

Fig. 1. Variation of polarization with current density in the cathodic deposition of tin. Electrolyte composition: $SnSO_4$ (0.25 N); H_2SO_4 (2 N); room temperature.

A-Cathode C.D. amp/sq. dm; B-η_{mv} millivolts. Bath additives: 1-Pure $SnSO_4$ solution; 2-saturated with diphenylamine; 3-saturated with thymol; 4-saturated with β-naphthol; 5-saturated with α-naphthol.

In the present paper we report the results of our investigation of the dispersibility of electrolytes, the porosity of the platings, and the consumption of organic additives in the tinplating of parts in sulfate tin baths of the following composition: 0.25 N $SnSO_4$; 2 N H_2SO_4, and 1 g gelatin per liter. The additives used were α- and β-naphthol, thymol, and diphenylamine. The researches were carried out at room temperature (20-25°C).

EXPERIMENTAL

Dispersibility. The dispersibility of baths, which is a measure of the uniformity of deposition of the metal on various portions of the part to be plated, is largely governed by three factors: the electrode polarization, the electrolyte conductance, and the variation of the current efficiency with the current density (C.D.). The higher the polarization, or, more accurately speaking, the higher it rises with an increase in the C.D., the greater will the dispersibility of the electrolyte be. As for

*See plate, page 495.

the operation of the bath as affected by the last two factors, we know that it is improved by an increase in conductance and by a drop in the current efficiency as the C.D. rises.

It is readily seen that the electrolytes under investigation must possess fairly high indexes in this respect. As Fig. 1 indicates, the cathodic deposition of tin is always accompanied by extremely high polarization of the cathode, which rises sharply as the C.D. is increased. High conductance of the electrolyte and the nature of the variation in the current efficiency as the C.D. rises must likewise exercise a favorable effect upon the dispersibility of the baths

Of all the methods of determining the dispersibility of electrolytes described in the literature, the simplest and easiest to use is the method suggested by Kudryavtsev [12]. In view of the fact that all the data in the literature on the dispersibility of tin baths are based upon the Haring and Blum method [13], however, we made our measurements by the latter method.

The following chemicals were tested as ameliorative additives: α- and β-naphthol, thymol, xylenol, and diphenylamine – all of them being added to the solution until the saturation point was reached; 10-15 g of crude phenol per liter; and 30 g of cresolsulfonic acid per liter. The variation of dispersibility with C.D. was investigated for each of these electrolytes, the C.D. being varied throughout a wide range: from 0.5 ma/cm^2 to 25 ma/cm^2. The results of our measurements, together with the corresponding polarizations, are given in Table 1 and Fig. 3.

TABLE 1

Dispersibility

C.D. ma/cm^2	β-naphthol		α-naphthol		Thymol		Diphenylamine		Cresolsulfonic electrolyte		crude phenol	
	η (mv)	dispersibility (%)	η (mv)	dispersibility (%)	η (mv)	dispersibility (%)	η (mv)	dispersibility (%)	η (mv)	dispersibility (%)	η (mv)	dispersibility (%)
0.2	3.0		4.5		14.0		4.0		17.0		9.0	
0.3	8.0		10.5				7.5		75.0	68.2	18.0	61.0
0.4												
0.5	20.5	65.2	22.0	69.4	222.0	59.6	30.0	64	245.0	74.4	290.0	65.0
1.0	334.0	76.0	357.0	73.6	303.0	74.8	283.0	65.2	331.0	74.0	387.0	59.8
1.4	347.0		395.3		337.0		316.0		360.0		422.0	
2.0	361.0	75.0	422.0	71.6	355.0	69.0	337.0	55.0	374.0	66.0	446.0	48.4
3.0	384.5	71.0	444.0	60.0	384.0	59.4	356.0	52.0	394.0	61.0	466.0	47.2
5.0	410.2	60.0	471.0	52.0	413.0	49.6	373.0	51.0	420.5	56.0	495.5	42.0
7.0	434.0	56.0	489.5	45.6	433.0	45.2	384.0	51.5	434.2	52.0	525.0	39.6
10.0	464.0	50.3	512.0	44.0	457.0	39.0	395.0	53.0	444.0	46.0	548.2	37.5
15.0	510.0	43.2	534.0	43.5	485.0	35.0	412.0	57.5	462.5	43.5	570.0	36.0
20.0	544.0	36.0	549.0	42.8	507.0	34.0	424.0	59.0	477.0	39.8	585.5	35.0
25.0	564.5	32.5	570.2	45.4	528.0	33.5	435.0	60.0	494.0	41.4	610.0	33.8

As we see from the figures in Table 1, the dispersibility varies appreciably over the entire C.D. range, its absolute value remaining rather high in all the runs, almost reaching the maximum value (80%) for some values of the C.D.

The change in dispersibility with C.D. is nearly identical for all the additives listed. The similar curves differ only quantitatively for the various additives. The dispersibility is high, some 60-70%, for all the baths at a C.D. of

some 0.5 ma/cm^2; it rises even higher for most of the baths when the C.D. is raised to 1 ma/cm^2. When the C.D. is raised to 2 ma/cm^2, the dispersibility tends to drop off somewhat in every bath, this decrease continuing in rather steep stages until 5 ma/cm^2. Finally, this decrease begins to slow down at about 5 ma/cm^2, the curves continuing nearly parallel to the axis of abscissas for most of the additives.

The dispersibility is 40-50% at the current densities used in industry; this is an entirely satisfactory value for electroplating. The dispersibility is even higher in the case of the electrolyte containing diphenylamine. It is worthy of note that Pine [14] states that the dispersibility of tin baths containing creosol ranges from 20 to 47%.

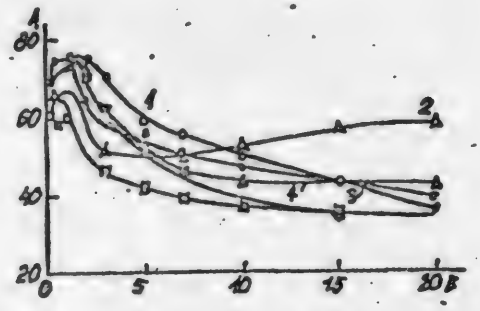

Fig. 3. Dispersibility as a function of the C.D. for electrolytes containing various additives.

A-Disersibility (by the Haring and Blum method); B-C.D., ma/cm^2. Bath additives: 1-β-naphthol, 2-diphenylamine, 3-cresolsulfonic acid (30 g/l), 4-α-naphthol; 5-thymol; 6-crude phenol (10 g/l).

As is readily seen, the maximum dispersibility occurs at current densities at which sharp potential jumps take place, which we call the limiting current density. When the C.D. rises to values corresponding to the beginning of the next section of the curve, the dispersibility drops rather steeply, the decrease slowing down and the dispersibility becoming practically constant as the C.D. is increased still further. As we see it, the specific nature of the variation in the dispersibility with changes in the C.D. may be interpreted as follows. The operation of the bath is directly dependent upon the nature of the change in polarization throughout a given C.D. range rather than upon the absolute value of the polarization; the more abrupt this change, the better the dispersibility. This is borne out by the circumstance that the dispersibility is a maximum at the limiting C.D. for all the electrolytes tested.

When we compare the curves showing the change in dispersibility with changes in C.D. for solutions to which β-naphthol and diphenylamine have been added with the potential – C.D. curves for these same solutions, we notice this characteristic feature: in the electrolyte containing β-naphthol, where the potential jump is about 400 mv when the limiting C.D. is reached, the maximum dispersibility (74%) is higher than the value (65%) in the solution containing diphenylamine, where the potential drop for the transition from the first to the third section of the curve is 100 mv smaller. That is also why the dispersibility curve for crude phenol has a less pronounced maximum than the curves for the other, more active additives. The decrease in dispersibility during the transition to the current densities obtaining along the third section of the curve is related to a decrease in the change of potential as the C.D. rises throughout this range.

Beginning at a C.D. of 10 ma/cm^2, the dispersibility is practically unaffected by the C.D. for most of the additives. Diphenylamine does exhibit a certain rise in dispersibility in this range, however. At a C.D. of 20 ma/cm^2, for instance, the dispersibility is about 35% for the solution containing thymol, while it is 60% for the diphenylamine electrolyte. This is due to the fact that in this C.D. range the current efficiency drops more steeply with a rise in the C.D. for the electrolyte to which diphenylamine has been added than for the electrolyte containing thymol or other active additives. In fact, the current

efficiency at 20 ma/cm^2 is 81.2, 70.9, 73.0, and 63.9% for thymol, α-naphthol, β-naphthol, and diphenylamine, respectively.

Thus, electrolytes containing the recommended active additives exhibit fully satisfactory dispersibility throughout the C.D. range from 0 to 2.5 amp/dm^2, which is no different from the figures given for other industrial tinplating baths.

Porosity. A study of the porosity of tin platings on a copper underlayer has shown that when the underlayer was 3.5-4 μ thick and the layer of tin was 6μ thick, the tin platings were practically nonporous in every instance, though the C.D. was varied throughout a wide range. Table 2 gives the results of measurements of porosity in solutions containing the following ameliorative additives: α- and β-naphthol, thymol, and diphenylamine; the same table gives the porosity of the copper underlayer as well.

We see from these figures that the tin platings are practically nonporous throughout the C.D. range of 1 to 20 ma/cm^2 (and even higher for some electrolytes). It is readily observed that the negligible porosity of the platings is due, apparently, to the practically complete absence of pores in the copper underlayer (less than 0.5 pore per cm^2).

Table 3 gives the variation in the porosity of platings plated directly on iron with the C.D. The thickness of the tin plating was the same as in plating over an underlayer.

TABLE 2

Porosity of Tin Plating Deposited upon A Copper Underlayer. Copperplating C.D. = = 4 ma/cm^2; Thickness of Copper Underlayer = 3.5μ; Thickness of Tin Plating 6 μ; Porosity of Copper Underlayer = ca. 0.3 pore/cm^2.

C.D. during tinplating, ma/cm^2	Porosity of the tin plating, no. of pores per cm^2			
	α-naphthol	β-naphthol	Thymol	Diphenylamine
1	0.1	0.1	0.2	0.3
3	none	none	none	none
5	none	none	none	0.1
10	0.005	none	0.1	0.2
15	0.1	0.05	0.1	0.2
20	0.1	0.1	0.3	0.2
30	0.2			
40	0.3			

TABLE 3

Variation of the Porosity of Tin Plated Directly on Iron with the Current Density. Thickness of the Tin Plating: 6μ

C.D. (ma/cm^2)	Porosity, number of pores per cm^2						
	α-Naphthol	β-Naphthol	Thymol	Diphenylamine	Phenol	Phenol + α-naphthol	Phenol + diphenyl amine
1	1.5-2	1-1.5	Many	Many	Many	4-5	4
3	0.5-0.7	0.5	3	3	1.5	1.5-2	0.5
5	0.5	0.3	0.5	1-1.5	1	0.3-0.4	0.5
10	0.5	0.2	0.7-1	0.7-1	1-1.2	0.4	0.5-0.7
15	0.5-0.7	0.5-0.7	1-1.5	1	2-2.5	0.8-1	0.8-1
20	0.7-1	0.8-1	2.2.2	1-1.2	3.5-4	1-1.3	1-1.2
30	1.5-2	2	–	2-2.5	5	2	1.5
40	5	5	Many	Many	8	2.5	1.5-2
50	–	–	–	–	–	4-5	5-6

As might have been expected, the porosity is much greater at all values of the C.D. than when a copper underlayer is employed. The nature of its variation

with the C.D. may be seen from the curves plotted from these data in Fig. 4.

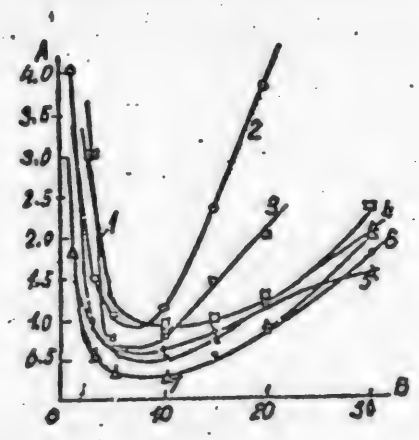

Fig. 4. Porosity of a cathodic plating as a function of the current density for electrolytes containing various additives.

A-Porosity, No. of pores per cm^2. B-C.D., ma/cm^2
Additives: 1-Diphenylamine; 2-crude phenol; 3-thymol; 4-phenol+ α-naphthol; 5-phenol + diphenylamine; 6-β-naphthol; 7-α-naphthol.

The variation of porosity with C.D. follows the same pattern for all the electrolytes tested, namely: it is fairly high (up to 5 and more pores per cm^2) at low current densities, dropping steeply as the C.D. is raised to 3-5 ma/cm^2, and reaching a minimum at 5-10 ma/cm^2. As the C.D. is raised still further, the porosity increases again, but more gradually than its fall in the low C.D. region.

The high porosity at low current densities, within the limiting C.D. range, must be attributed to low polarization. The sharp drop in porosity coincides with the transition to the region of high polarization. But when the C.D. is raised above 10 ma/cm^2 (the right-hand branch of the curve), the porosity must, of course, increase, because the potential of desorption of the capillary-active additives is reached, and because the electrolyte layer near the cathode grows poorer in Sn^{++} ions at very high currents, considerable hydrogen being evolved. When we compare these curves, we find that they differ, first of all, in the magnitude and location of their minima and, second, in the steepness of their rise in the right-hand region of the figure, i.e., the rate at which the porosity rises in the region of high C.D. The porosity minima are lowest for the electrolytes containing α- and β-naphthol. The minimum is appreciably higher for solutions to which phenol has been added. Moreover, a feature of this latter electrolyte is a much sharper rise of porosity at high C.D. than is exhibited by the baths we recommend.

It may therefore be asserted that though the nature of the variation of porosity with C.D. is of the same type, electrolytes containing our additives display better characteristics than the industrial baths employed at the present time. An interesting phenomenon was observed when crude phenol was added to the bath together with one of the pure capillary-active substances, say, α-naphthol or diphenylamine. The coating was improved and the porosity diminished through the C.D. range: the platings exhibited 4-5 pores per cm^2 at 1 ma/cm^2 instead of the numerous pores previously counted, becoming highly porous only at a C.D. in excess of 50 ma/cm^2 (5 amp/dm^2).

Hence, the growth of porosity at high current densities is much less in these baths than when a single additive is employed, and is much more reduced in comparison to an industrial electrolyte.

The results of our study of the variation of porosity with the plating thickness are given in Table 4.

As we see from the table, the porosity was 2-3 pores per cm^2 at the minimum plating thickness of 2μ, dropping sharply when the thickness was increased to 6μ, after which the decrease was more gradual. The tin platings 12μ thick, deposited at a C.D. of 10 ma/cm^2, were practically nonporous.

TABLE 4

Variation of Porosity with Thickness of Plating. C.D. = 10 ma/cm^2 (1 amp/dm^2)

Thickness of plating, μ	Porosity, number of pores per cm^2	
	α-Naphthol	Diphenylamine
2	2.5-3.0	2.7-3.0
4	1.2-1.5	1.2-1.5
6	0.5	0.9-1.2
8	0.4-0.5	0.8-1.0
10	0.3-0.4	0.3-0.5
12	0.1-0.2	0.1-0.2

TABLE 5

Variation of Porosity with Temperature. Plating Thickness: 6μ

C.D., ma/cm^2	Porosity, no. of pores per cm^2			
	α-Naphthol		Diphenylamine	
	Temperature, °C			
	28	40	18	40
1	1.5-2	Many	Many	Many
3	0.5-0.7	0.5-0.7	3	3
5	0.5	0.5-0.7	1.0-1.5	1.5-2.0
10	0.5	0.7-1	0.7-1.0	1.0-1.3
15	0.5-0.7	1.5	1	1.3-2.0
20	0.7-1	2.5	1-1.2	2.0
30	1.5-2	3	-	-
40	Many	Many	-	-

When we compare our results with those obtained by Hothersoll and Bradshaw, who found that highly porous platings were produced at a thickness of 2.5μ, we see that the figures for the same coating thickness are better for our electrolytes. Moreover, it should be stated that our results are fully satisfactory, as far as porosity is concerned, when the plating thickness is of the order of 6-8μ.

As for the effect of operating temperature upon porosity, an increase in temperature was harmful, as was to be expected, and as is the case in industrial baths (Table 5). When the temperature was raised to 40°C, the porosity was increased throughout the C.D. range, while the graininess of the coating increased.

We pointed out above the effect of temperature upon the shape of the potential – C.D. curves. it increases the limiting current. When the temperature is raised to 50-60°C, the increase in the limiting current is so great as to approach the value observed in a solution of tin sulfate without any capillary-active additive. These phenomena, together with the resultant general impairment of the deposit, are apparently due to a decrease in adsorption as the temperature is raised. Nevertheless, the platings produced have no more than 3 pores per cm^2 even at $\underline{t}$ = = 40°C, i.e., they are slightly porous platings.

Consumption of capillary-active additives. During our study of polarization and of the properties of tinplating baths we noticed that the capillary-active additives were consumed as the period of operation of the bath was prolonged. This is manifested both in an impairment of the quality of the plating (greater coarseness of crystalline structure) and in an increase in the platings's porosity. When the bath was run for a long time, we also observed an increase in the limiting current and a decrease in the polarization. Re-adding capillary-active substances to such an electrolyte until the saturation point was reached restored the initial properties of the solution, i.e., reduced the limiting C.D. to the former value and improved the appearance and the quality of the plating. This disappearance of the ameliorative additives from the solution must apparently be attributed either to the partial inclusion of the adsorbed molecules in the crystal lattice of the coating or to their reduction at the cathode.

Since baths of this sort must be corrected periodically, we were interested in determining the approximate duration of operation before periodic correction. We did this by conducting electrolysis for a long time. The freshly prepared electrolyte, saturated with a capillary-active additive (or containing the prescribed quantity of additive in the case of an industrial electrolyte) and filtered, was

Table 6

Variation of Porosity with Duration of Bath Operation. S - 20 cm^2, I - 0.2 amp., C.D. - 1 amp/cm^2, Temperature - 18°C, Volume of electrolyte - 60 cm^3, Coating thickness - 6 μ.

Additive	Time, hours													
	0		12		24		48		72		96		120	
	Nature of coating	Porosity per cm^2	Nature of coating	Porosity per cm^2	Nature of coating	Porosity per cm^2	Nature of coating	Porosity per cm^2	Nature of coating	Porosity per cm^2	Nature of coating	Porosity per cm^2	Nature of coating	Porosity per cm^2
Phenol, 10 g/l	Smooth, some luster	1.0	Smooth, dull	1.6	Smooth, dull	3.0	Dull, coarsely crystalline	Highly, porous coating	-	-	-	-	-	-
Diphenyl, saturated 0.13 g/l	smooth some luster	0.5	smooth some luster	0.3	dull, coarsely crystalline	10	coarsely crystalline gray	highly porous coating	-	-	-	-	-	-
α-naphthol, saturated 0.7 g/l	smooth lustrous	0.5	smooth lustrous	0.3	-	-	smooth some luster	1.5	smooth some luster	2	dull, more coarsely crystalline	4	dull, coarsely crystalline	highly porous
Phenol + diphenylamine saturated	smooth lustrous	0.5	smooth lustrous	0.5	smooth lustrous	0.5	smooth more coarsely crystalline	5	dull, coarsely crystalline	highly porous coating	-	-	-	-
Phenol + α-naphthol saturated	smooth lustrous	0.3	smooth, lustrous	0.3	smooth, lustrous	0.3	smooth, some luster	0.5	smooth, some luster	1	smooth, some luster more coarsely crystalline	2	More coarsely crystalline some luster	5-8

electrolyzed at the C.D. most commonly employed in industry until the quality and porosity of the platings became unsatisfactory. The porosity of the cathode coatings was measured at regular intervals, and their external appearance was recorded. The pertinent data are listed in Table 6. Electrolysis was conducted at a C.D. corresponding to the minimum porosity for most of the electrolytes, 10 ma/cm^2 (1 amp/dm^2), and at a temperature of 18°C. Inasmuch as there usually was a considerable discrepancy (as high as 20%) between the determinations of porosity with Walkers reagent in parallel tests, the tabular results represent the mean values of several determinations.

We see from Table 6 that the worst results were secured with the industrial electrolyte containing phenol; nor is the time elapsed until the plating is noticeably impaired very long for the bath containing diphenylamine, but it should be borne in mind that the concentration of diphenylamine in the bath is 70 times lower than that of the phenol. Satisfactory platings are secured for a considerably longer time with the electrolyte containing α-naphthol. The baths containing mixed additives are also worthy of note. As we see from the table, the operating life of the combined phenol + diphenylamine additive is 50% higher than that of either of these additives by itself.

The addition of α-naphthol and phenol together yields results that are somewhat better than those for an electrolyte containing α-naphthol by itself. These data may be used to calculate the approximate consumption of a capillary-active additive. Such a calculation is subjoined for the consumption of α-naphthol.

Electrolyte volume $\underline{V}$ = 60 cc; C.D. = 1 amp/dm^2; duration of electrolysis until the platings produced are unsatisfactory = 96 hours; electrode surface = = 20 cm^2; curent = 0.2 amp; solubility of α-naphthol in water = 0.7 g/liter.

Quantity of α-naphthol in our electrolyte: 0.7·0.06 = 0.042 g. Quantity of electricity: $\underline{Q} = I \cdot t = 0.2 \cdot 96 = 19.2$ amp-hr. With a current efficiency of 0.834, the quantity of Sn deposited during this time is:

$$\Delta P_{Sn} = 19.2 \cdot \frac{59.3}{26.8} \cdot 0.834 = 35.4 \text{ g.}$$

Hence, one g of α-naphthol suffices for the deposition of:

35.4/0.042 = 843 g Sn, or the deposition of 1 kg of Sn requires: 1000/843 = 1.18 g of α-naphthol. Hence, with the tin plating 6μ thick, 1 g of α-naphthol suffices for the plating of 1940 dm^2 of surface.

The results of similar calculations for the other baths are tabulated in Table 7.

As we see from Table 7, the consumption of α-naphthol and of diphenylamine is much lower than that of crude phenol. The properties of baths containing thymol, β-naphthol, and other active additives are similar.

TABLE 7

Consumption of Additives for the Deposition of 1 kg of Tin and for the Production of 100 m^2 of Plating at a Thickness of 6 μ (Without Allowing for Electrolyte Entrained with Finished Parts)

Additive	Consumption, grams	
	Per 1000 g Sn	Per 100 m^2 of plating
Phenol	63.5	273.0
Diphenylamine.	1.62	6.96
α-Naphthol ...	1.2	5.15

Therefore, bearing in mind all the data cited on polarization, structure of the coating, the dispersibility of the bath, and the porosity of the platings, we may recommend the following electrolyte compositions and operating condiations:

a) Composition: sulfate electrolyte (0.25-0.5 $\underline{N}$ $SnSO_4$, 2 $\underline{N}$ H_2SO_4), containing

1 g gelatin or sizing per liter and saturated with one or more of the following additives: α-naphthol, β-naphthol, diphenylamine, thymol, or xylenol; b) C.D. = 0.5-2 amp/dm^2; and c) room temperature.

The surface-active substances enumerated above may likewise be employed as ameliorative additives for the widely used baths employing crude phenol.

The correction of the electrolyte may be effected either periodically – by introducing additives in the solid phase or in phenol and alcoholic solutions – or continuously – by setting up racks of α-naphthol, β-naphthol, thymol, diphenylamine, or their combinations in the electrolytic bath.

In conclusion, we must add that tests of these recommended electrolytes in one of the industry's factory laboratories, independently of the authors of the present paper, have confirmed their superiority to phenol electrolytes.

SUMMARY

1. A study has been made of the dispersibility of tin sulfate electrolytes to which a colloid and one of the following surface-active substances: α-naphthol, β-naphthol, thymol, and diphenylamine, has been added. The porosity of the corresponding cathodic deposits has been determined under these conditions.

2. In accordance with the previously established presence of high chemicalpolarization during the electrolytic crystallization of tin from solutions containing the above-mentioned additives, we have established the high dispersibility of such electrolytes and the finely crystalline structure and the low porosity of the cathodic tin deposits.

3. The consumption of additives during the electrolytic crystallization of tin has been calculated. It has been found that the quality of the plating is higher than that secured in phenolic baths, while the consumption of additive is 30 to 50 times smaller than the consumption of phenol under similar conditions.

4. On the basis of these investigations new tinplating electrolytes are recommended, using additives of α-naphthol, β-naphthol, diphenylamine, and thymol.

LITERATURE CITED

[1] O.Esin and M.Loshkarev, J.Phys.Chem. USSR, 13, 186-193 (1939); V.A. Roiter, V.A.Yuza, and E.S.Poluyan, J.Phys.Chem. USSR, 13, 605-620 (1939).
[2] O.Esin and A.Levin, J.Gen.Chem. 5, 1302 (1935); 6, 1539 (1936); V.A. Roiter, E.S.Poluyan, and V.A.Yuza, J.Phys.Chem. USSR 13, 805-812 (1939).
[3] A.T.Vagramyan, J.Phys.Chem., USSR, 13, 311 (1939); 19 305 (1945).
[4] Foerster and Fischer, Z. Elektrochem., 32, 525 (1926); Mathers, Metal Ind., 17, 405 (1920); Kern and Capillon, Trans. Am. Electrochem. Soc., 45 (1924).
[5] Marshak, Metal Industry Herald (USSR) 10, 84-89 (1936).
[6] Kheifets, Symposium, The Fight Against Corrosion – A Fight for Metal. 159. United Scientific and Technical Press (1935).
[7] Kadaner. Electrolytic Tinplating (1944).
[8] Lainer and Kudryavtsev. Principles of Electroplating.
[9] M.Loshkarev, V.Sotnikov, and A.Kryukova, J.Phys.Chem. USSR, 21, 219 (1947).
[10] M.Loshkarev, O.Esin, and V.Sotnikov, J.Gen.Chem. 9, 1912 (1939).
[11] U.S.Patent 1,452,573 (Feb. 10, 1922), re-issued April 24, 1923.
[12] N.T.Kudryavtsev and A.A.Nikoforova, J.Appl.Chem. 22, 369 (1949).
[13] Haring and Blum, Trans. Am. Electrochem. Soc., 44, 141 (1923).
[14] R.Pine. Trans. Electrochem. Soc., 80, 638 (1941).

April 11, 1950.

PROTECTING METAL PARTS AGAINST CORROSION BY THE METHOD OF COLD PHOSPHATIZING*

V. S. Lapatukhin

All-Union Research Institute of Printing and the Printing Trades

Up to recently metal parts have been protected against corrosion by treating them in phosphatizing solutions at temperatures that are very close to the boiling point of these solutions (98-99°C). This temperature must be maintained with considerable care in practice, since it has been found that lowering the temperature of the phosphatizing solution by as little as a few degrees slows down the process of forming the coating and lowers its quality considerably [1,2, 3,4].

All the disadvantages involved in the hot method of treating metal parts are known: the consumption of considerable energy; certain difficulties in maintaining the exact concentration of the preparation in the solution (owing to constant evaporation); the possible inclusion of sludge in the phosphate coating when the solution simmers, resulting in a marked reduction in the latter's protective properties [1]; the difficulty (and in some instances the impossibility) of treating large-size parts; the difficulty of standardizing the process, etc.

In view of the wide application of phosphatizing in our economy, research on the development of new, more perfect methods of phosphatizing which would make it possible to treat parts at ordinary room temperature, with the shortest possible production cycle, is of considerable practical importance. This search has yielded positive results during recent years.

Some years ago it was demonstrated that cast-iron and steel parts could be phosphatized by a cold process [5]. The extremely sparse literature on this subject contains merely quite general data, rather like advertising claims, on the "cold bonderizing" process, from which it is impossible to reproduce the composition of the solution or the phosphatizing conditions required for the production of satisfactory coatings: the resistance of the resulting coatings to corrosion is sharply lowered, while the coating itself possesses slight thickness and strength and poor covering power [6]. These disadvantages have been largely eliminated in the cold phosphatizing process suggested by the present author, [7]. But even this process is far from perfect, further research in this field being indispensable. No appreciable reduction of the temperature of the phosphatizing solution can be attained by increasing the concentration of free acid, as was initially suggested [6], inasmuch as the hydrogen-ion concentration must not exceed a certain limit, at which the phosphatizing reaction is shifted to the right:

$$5Me(H_2PO_4)_2 \rightleftarrows 2MeHPO_4 + Me_3(PO_4)_2 + H_3PO_4.$$

Eberty, Gross, and Crowell [8] investigated the composition of the solution and the precipitate in the $ZnO - P_2O_5 - H_2O$ system at temperatures of 25 to 37°C and at 98°C and found that at P_2O_5 concentrations that are of interest in phosphatizing (up to 200 g per liter) the precipitate always consisted of trisubstituted

---

*D. D. Mendelevich and E. F. Gundorina participated in this research.

zinc phosphate. The constants measured by the authors for the reaction:

$$3Zn(H_2PO_4)_2 \rightleftarrows Zn_3(PO_4)_2 + 4H_3PO_4$$

$$K = \frac{[H_3PO_4]^4}{[Zn(H_2PO_4)_2]^3}$$

were found to differ widely for the extremes of temperature, being 0.71 at 98° and 0.013 at 25°. Computation indicated that at 98° one mole of zinc dihydrophosphate is in equilibrium with 0.918 mole of free phosphoric acid, but with only 3.38 mole of H_3PO_4 at 25°. Therefore, the amount of free acid required for the formation of a phosphate coating at 25° need be only 27% of the amount of free acid present at 98°. Subsequently, similar relationships were found for the other phosphates of the heavy metals. Though the researches of Eberty, Gross, and Crowell clearly indicate that the pH of a phosphatizing solution must approach that of the neutral region as the temperature is lowered, we still had to determine the allowable hydrogen-ion concentration at which phosphatizing could be effected in practice and to ascertain the necessary change in the solution pH as a function of temperature, the concentration of the preparation, the nature of the phosphate cation, the nature of the accelerator, and the concentration of the latter. As Schuster and Krauze have proved, all these factors are related [8].

It was found that a solution of zinc dihydrophosphate is best for phosphatizing at 20°C. For a phosphate concentration of 24 g P_2O_5 per liter, the solution pH should be 2.7-3, provided all the other factors are correct. The solution pH drops as the P_2O_5 concentration is raised.

When the temperature is diminished from 98° to 20°, the shift of the pH of the phosphatizing bath toward the neutral region increases as follows, depending upon the nature of the phosphate cation:

	$Ca^{\cdot\cdot}$	$Zn^{\cdot\cdot}$	$Fe^{\cdot\cdot}$	$Mn^{\cdot\cdot}$	$Cd^{\cdot\cdot}$
ΔpH	1.0	1.2	1.2	1.4	1.9

When oxidizing agents are used, this shift is somewhat less, and the pH of the phosphatizing solution is 2.8.

Optimum results were achieved in the "cold bonderizing" process when zinc dihydrophosphate solutions with a concentration of 60 points, containing 12 g of ClO_3' per liter and with up to 22 g of $Zn^{\cdot\cdot}$ ions per liter, were employed.

EXPERIMENTAL

In the light of the data cited, we prepared the following "cold bonderizing" solution: P_2O_5 concentration = 24 g per liter; $Zn^{\cdot\cdot}$ concentration = 15 g per liter; ClO_3' = 12 g per liter; total acidity ($K_{tot.}$) = 57 points; room temperature.

The pH of this solution was 2.2.

We treated plates of U-10 instrument steel 60 x 70 mm in size. The plates were first processed by polishing the surface with No. 1 emery cloth, followed by degreasing with a 5% solution of calcined soda, or by degreasing and pickling as follows:

1) The samples were washed in running water; 2) they were degreased in a solution of the following composition: 60 g caustic potash per liter; 30 g of calcined soda per liter; 20 g of trisodium phosphate per liter, and 1 liter of water; the temperature was 70-80°C and the processing lasted 10 minutes; 3) the samples were washed with hot water; 4) they were pickled in the following solution: 200 g of sulfuric acid and 50 g of sodium chloride in 1 liter of water; the temperature was 60-65°C and the treatment lasted 2-3 minutes; 5) they were washed with abundant quantities of cold water; 6) the sludge was removed by wiping the surface with

absorbent cotton; 7) they were treated with the following alkaline solution: 25 g of calcined soda to 1 liter of water; the treatment lasted 10 minutes; 8) the samples were washed with cold water; 9) phosphatization.

The processing of the samples in the phosphatizing solution was done in a 1-liter glass beaker. No more than 10 samples were phosphatized in this volume of solution to avoid "aging" of the bath.

The anticorrosion properties of the coatings were determined by the accelerated drop-test method suggested by Akimov and Ulyanov [1]. The color of the coatings was determined in the Pulfrich polarizing photometer.

The zinc dihydrophosphate used in our initial experiments on the phosphatizing of steel samples at room temperature was prepared in the laboratory. An excess of chemically pure zinc oxide was added, with constant stirring, to concentrated (85%) phosphoric acid. The solution was filtered 24 hours later; the filtrate $Zn(H_2PO_4)_2$, was then evaporated to dryness. Owing to the great hygroscopicity of the resultant product, it was stored in jars with ground-glass stoppers.

We found that the phosphatizing of the samples in this "cold bonderizing" solution yielded coatings that had unsatisfactory anticorrosion properties (10-15 seconds in the drop test) and unsatisfactory mechanical strength, besides possessing inadequate covering power, while the phosphatizing process lasted more than one hour. The evolution of hydrogen ceased after 5-8 minutes, but formation of the coating continued for another 50-60 minutes, as was readily observed by the darkening of the samples. Longer phosphatization produced no essential changes in the quality of the coatings.

At first we thought that the negative results of these initial tests were due to the fact that the specifications for the solution pH were not followed closely enough. None of our endeavors to correct the acidity of the bath by use of zinc oxide, calcium oxide, or stronger alkalies [5], making the solution pH 2.6 to 2.8, yielded the desired results, however.

It was quite obvious that the "cold bonderizing" solution did not possess the activity that is characteristic of the usual hot phosphatizing solutions. Hence, the first thing to be looked for in working out a process of phosphatizing at room temperature was a way of effectively increasing the activity of the cold phosphatizing solution.

Numerous experiments proved that fluorine derivatives were activators of the phosphatizing process, especially sodium fluoride. The amount of sodium fluoride added to the phosphatizing solution is governed chiefly by the initial acidity of the bath and the requisite optimum concentration of F' ions.

After 6 g of NaF had been added to the foregoing solution per liter, for example, the nature of the process and the phosphatizing results changed markedly. Fully satisfactory, well-bonded, finely crystalline, bright covering coatings with an anticorrosion resistance of 1.5-2 minutes in the drop test, were produced on U-10 steel at a solution pH of 2.8-3.0; the process required 40-50 minutes.

In our subsequent tests we substituted the ferromanganese preparation "Mazhef", manufactured by a Moscow factory, for the zinc dihydrophosphate, in order to make our results meet the specifications of domestic phosphatizing practice.

Effect of the concentration of sodium fluoride. Optimum pH of the phosphatizing solution. Zinc nitrate was added to the "Mazhef" solution as an accelerator, its optimum concentration being governed by the following equation, as determined in preliminary tests: $P_2O_5:NO_3 = 1:1$. The overall acidity of the solution was 78 points. The solution pH was measured by means of a potentiometer

with a glass electrode and by the pH meter turned out by the Moskip factory.

We made a study of the effect of the concentration of the sodium fluoride upon the pH of the phosphatizing solution, and the anitcorrosion properties and color of the phosphate coatings. The experimental data cited in Table 1 and Fig. 1 are the mean values of parallel measurements that were repeated many times (10-15 times) and did not differ much from one another.

TABLE 1

Total acidity, $K_{tot.}$	Additions to the basic preparation ("Mazhef")		Temperature, °C	pH	Phosphatizing time, min.	Resistance to corrosion, min.	Color of coating, % of white	Remarks
	Sodium fluoride g/liter	Zinc nitrate, g/liter						
60	–	92	19	3.0	60	Instantaneous	–	Unsatisfactory coating
78	1	92	19	3.1	55	1.5	15	Finely crystalline, light, stable coatings. Mean increase in weight of the samples after phosphatizing = 9 g/m²
78	2	92	19	3.2	50	2.0	18.5	
78	3	92	19	3.4	30	2.5	19	
78	4	92	19	3.8	50	1.0	19.5	
78	6	92	19	4.3	50	0.5	20	
78	10	92	19	–	50	0.25	22	

These tests showed that as the concentration of NaF in the phosphatizing solution was increased, the solution pH rose uniformly. The coatings formed in solutions with pH ranging from 3.1 to 3.4 had the highest anticorrosion resistance. The optimum solution pH of 3.4 corresponded to the highest resistance of the coatings to corrosion (under the given conditions). When the solution pH was raised above this optimum, the coatings' resistance to corrosion dropped off sharply. The color of the coatings likewise changed quite uniformly. For small additions of sodium fluoride, the resultant deposits were relatively dark, the color rapidly changing to light gray as the NaF concentration was increased. Moreover, the light gray color of the cold-phosphatized coatings was not a factor typical of the unsatisfactory quality of phosphate coatings, contrary to the notions of the color of coatings produced by the usual hot method (4% of white).

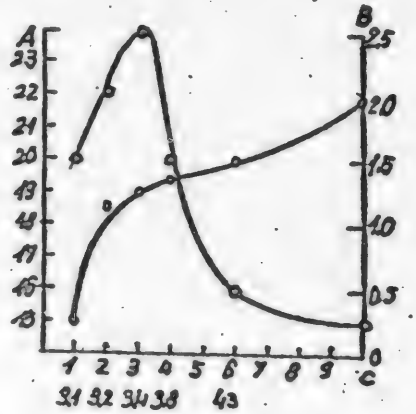

Fig. 1. Effect of the concentration of NaF upon the properties of cold-phatizing coatings.

A-Coating color, % of white; B-resistance to corrosion, min.; C-NaF concentration and pH.

1-Coating color; 2-anticorrosion resistance of coating.

Auxiliary constituents of the cold-phosphatizing solution. It has been shown above that the formation of a phosphate coating upon steel at room temperature requires that the phosphatizing solution contain a certain quantity of sodium fluoride, without which the phosphatizing process is extremely slow, and the resulting

phosphate coatings have little resistance to corrosion and are too weak mechanically, no matter whether the specifications concerning the solution pH, the concentration of the basic preparation, and the other conditions have been complied with or not. It was observed, however, that the coatings formed from a solution that contained only the indispensable constituents (the "Mazhef" preparation and sodium fluoride) had a relatively coarselycrystalline structure and was not very effective in protecting the metal against corrosion notwithstanding the great thickness of the coating and its covering power. Moreover, the phosphatizing process was extremely slow.

To eliminate these deficiencies, we found it useful to add auxiliary constituents to the phosphatizing solution – accelerators, which are essentially a combination of one oxidizing agent or another with a substance that diminishes the free acidity of the solution. Substances of this sort are, for example, zinc oxide, calcium oxide, etc.; it is not advisable to add strong alkalies to the solution.

We have found that optimum results are obtained when the acid value of the phosphatizing process, given by the ratio of the total to the free acidity ($\eta = K_{tot}/K_{free}$), is no lower than 12-15, whereas the optimum value of the acid number is 7-8 for the ordinary hot process [3, 8].

As we see in Figs. 2 and 3, (see Plate, page 495), the phosphate coatings produced at room temperature have an extremely fine and uniform crystalline structure, compared to the coatings produced by hot phosphatizing; they possess high covering power and are firmly bonded to the metal. They have somewhat lower resistance to corrosion than ordinary coatings.

Duration of the cold-phosphatizing process. In the experiments described above, the phosphatizing time was long enough to eliminate this factor in studying the properties of the coating. It was assumed that 40-50 minutes of treatment in the phosphatizing solution would suffice to form the coating completely, especially as the cold phosphatizing process does not require more than 30 minutes according to the data in the literature [6, 13].

It should be noted that the usual method of checking the end of the phosphatizing process, (the end of the evolution of hydrogen – the "boil") is useless in this case. The visible generation of gas bubbles comes to an end within the first 3-5 minutes during cold phosphatizing, though the process of forming the coating is far from complete by that time.

TABLE 2

Phosphatizing time, minutes	Mean increase in wt. of samples g/m^2	Resistance to corrosion of the coatings, min.	Remarks
10	7.3	0.25	Phosphatizing was done at 19°C, with a solution pH of 3.4
20	8.7	0.75-1.0	
30	8.9	2-2.5	
50	9.2	2.5	

The actual phosphatizing time was determined by making a study of the changes in weight of the samples and of the resistance of the phosphate coatings to corrosion. The experimental results are listed in Table 2.

These figures indicate that the minimum time for phosphatizing in a cold solution must be 30 minutes for the formation of a high-quality coating.

Effect of temperature. We noticed that the temperature of the phosphatizing solution affects the length of time required for phosphatizing in cold baths, as well as the quality of the coatings themselves. When the temperature is lowered by as little as 3-4°, the time required for the process is lengthened considerably,

while the quality of the coatings grows noticeably worse. Raising the solution temperature by 20-30° likewise has a pronouncedly unfavorable effect. We therefore concluded that there must be some optimum temperature at which the process would yield the best results. This conclusion was subsequently borne out during a study of the effect of temperature upon the protective properties of the coatings (Fig. 4).

It was found that the temperature optimum lay in the 20-30°C range. Raising or lowering the temperature beyond the otpimum impaired the protective properties of the coatings pronouncedly. The coatings produced at a temperature of 25-26°C had the highest resistance to corrosion (6 minutes for the drop test).

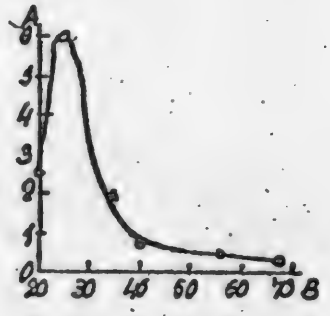

Fig. 4. Effect of the temperature of the phosphatizing solution upon the resistance of the phosphate coatings produced.

A-Corrosion resistance of coating (min.); B-Temperature-°C.

Electrophosphatization. The suggestion has been advanced that the phosphatization process rate be speeded up by treating steel parts in a phosphatizing solution through which an alternating current is passed [10].

In contrast to the ordinary process, electrophosphatization is effected with zinc dihydrophosphate at 65-75°. The electric current depolarizes the hydrogen evolved when the metal reacts with the solution, thus speeding up the formation of a dense, finely crystalline coating, the thickness of which is as much as 0.012 mm according to Rivkind [11]. It has also been shown that raising the process temperature above the specified level impairs the quality of the coating, due, apparently, to further hydrolytic decomposition of the zinc phosphate and an increase in the free acidity of the solution above the optimum value [12]. Electrophosphatization in hot solution is effected with a voltage of 15-20 volts across the terminals and a C.D. of 3-5 amp/dm^2. According to Kudryavtsev, increasing the current density to 10-12 amp/dm^2 improves the coating [12].

Our experiments on electrophosphatization in hot baths have shown that applying a current promotes the phosphatization process enormously, the process time being shortened to 4-8 minutes. Zinc phosphate as well as the "Mazhef" preparation may be employed for hot phosphatizion. Though the operating conditions for the two substances are somewhat different, the resulting phosphate coatings are quite similar. These coatings possess a uniform, extremely fine crystalline structure, their thickness being 0.07-0.1 mm.

Outstanding features of hot electrophosphatized coatings are their extremely high mechanical strength and their light gray color (20% of white). Their resistance to corrosion is somewhat less than that of coatings produced in the usual hot baths, however (2-4 minutes by the drop test).

There is a suggestion in the literature that electrophosphatization in cold solutions ought to yield coatings, the protective properties of which would not be inferior to those produced in the usual hot baths, though the process time would be shortened considerably [8]. No data are cited in support of this proposal, nor is any information given concerning the process conditions.

We made our tests of cold electrophosphatization to ascertain the process conditions as well as to establish the properties of electrophosphatized coatings. The steel samples were treated in the solution used for the cold chemical method

of phosphatizing under the following conditions: solution pH = 3.2-3.4; temperature = 20°C; distance between electrodes = 8.5 cm; electrode material = No. 3 steel; alternating current at 12 volts; usual preparatory treatment of the samples before phosphatization.

We began by learning the effect of the c.d. upon the resistance to corrosion of the coatings. The processing time was fixed at 15 minutes for all the samples. The experimental data are listed in Table 3.

TABLE 3

Current density, amp/dm^2	Resistance to corrosion, sec.	Remarks
0.1	40	The coatings were bright, with good covering power, finely crystalline
0.3	90	
0.5	60	
1.0	30	The coatings were dark, thin, with typical passivation of the surface at the samples' edges.

We see from Table 3 that the optimum c.d., yielding the highest anti-corrosion properties (under the given conditions), was 0.3 amp/dm^2.

We then made a study of the kinetics of electrophosphatization at this optimum c.d.; we tested the gain in weight of the samples and the resistance to corrosion of the coatings. Our results are shown graphically in Figs. 5 and 6. The following conclusions may be drawn from these results.

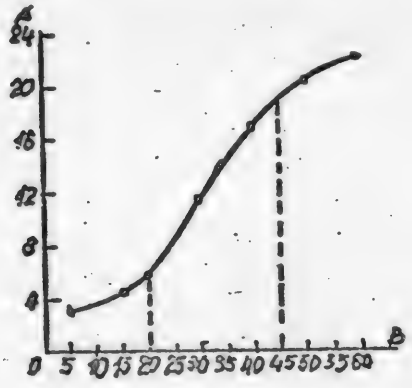

Fig. 5. Gain in weight of samples as a function of the electrophosphatizing time in cold baths. c.d. = 0.3 amp/dm^2; voltage: 12 volts.
A-Gain in weight, g/m^2; B-phosphatizing time, min.

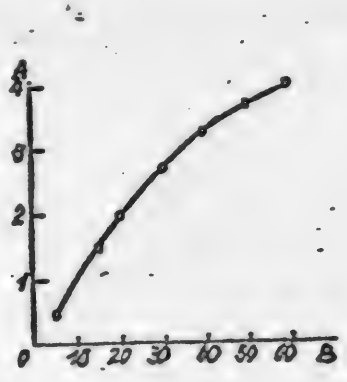

Fig. 6. Change in the anticorrosion properties of coatings as a function of the electrophosphatizing time in cold baths. c.d. = 0.3 amp/dm^2; voltage: 12 volts.
A-Resistance to corrosion, min.; B-Phosphatizing time, min.

1. As the phosphatizing time is prolonged, the weight of the samples increases continuously, slowly at first (during the first 20 minutes) and then directly proportional to the time – up to about 45 minutes. The gain in weight then

slows down perceptibly. The coatings produced are bright and quite thick (up to 22 g/m^2), and possess good covering power, uniform finely crystalline structure, and high mechanical strength.

The anticorrosion properties of the coating rise sharply with the phosphatizing time, reaching a value of 3 minutes by the drop test after 30 minutes of processing. The resistance to corrosion is increased to 8 minutes when electrophosphatizing is carried out at 25°.

Thus, the application of an alternating current during cold-bath phosphatizing increases the anticorrosion properties, the mechanical strength, and the thickness of the coatings over the respective values for coatings produced by chemical treatment alone in the same baths. The following operating conditions are recommended: c.d.: 0.3 amp/dm^2; voltage: 10-12 volts; temperature: 20-25°; processing time: 30 minutes.

General notes on cold phosphatizing processes. Phosphatizing at room temperature, with the production of high-quality phosphate coatings, became feasible only after an effective agent was found for increasing the activity of solutions of the usual phosphatizing salts. We were the first to point out that some of the derivatives of fluorine, sodium fluoride in particular, might serve as these activating agents. When certain specifications concerning the concentration of the basic preparation, the solution pH, the ratio of total to free acidity, the nature and the concentration of the accelerators, etc., are complied with, the presence of sodium fluoride yields bright, strong, very finely crystalline coatings of good covering power at room temperature, which are distinguished by their high adsorption and adhesion properties with respect to protective lacquers and paints and possess satisfactory anticorrosion properties themselves.

As our investigations have shown, the concentration of the solution of the iron-manganese preparation ("Mazhef"), together with the obligatory and auxiliary additives, must be 60-70 points, while the solution pH must be kept within the 3.0-3.4 range. Raising the acid number (the ratio of the total to the free acidity) from 7-8 (the value for the ordinary hot process) to 12-15 promotes the formation of high-quality coatings and shortens the processing time at room temperature. In this case, the most efficient way of preparing the parts for phosphatizing is sandblasting.

The cold-phosphatizing processing time depends largely upon the specifications the resultant coatings are to meet. The formation of the coating does not cease when the visible evolution of hydrogen comes to an end (3-5 minutes); the coating thickness and its anticorrosion properties increase parallel with the sample's gain in weight. High resistance of the cold-phosphatizing coatings to corrosion can be achieved, however, only when the requisite bath temperature is maintained, inasmuch as it has been found that raising or lowering the temperature of the phosphatizing solution above or below the optimum (19-30°C) greatly impairs the protective properties of the coatings.

Electrophosphatizing in cold solutions under the specified conditions further increases the resistance of the coatings to corrosion, greatly increases their resistance to abrasion, and shortens the process time somewhat.

Numerous experiments and industrial tests of the method we have developed * have demonstrated that the cold-phosphatizing solutions are highly stable, thus effecting a saving in the consumption of the "Mazhef" preparation and the accelerators over the usual consumption figures, while greatly shortening the loss of time involved in correcting the bath during the continuous process.

---

*This method of cold chemical phosphatizing and electrophosphatizing has been widely tested in establishments of the printing industry in the preparation of litho-offset printing forms from carbon steel.

The great stability of the solution and the constancy of the results obtained in large-scale phosphatizing make it possible to introduce rigid standardization of the process.

It is no longer necessary to employ hot washing of the parts before they are immersed in the phosphatizing solution and after completion of the process. Cold washing can be substituted for hot washing without adverse effects.

Another advantage of the new process is the fact that processing parts in cold-phosphatizing solutions does not involve perceptible changes in the mechanical properties of the metal, in contrast to what happens in the usual hot process [14].

The use of the cold-phosphatizing process for the mass treatment of parts in assembly-line installations or for the processing of large parts by spraying is of especial practical importance.

SUMMARY

1. An experimental check of the previously suggested process of "cold bonderizing" has confirmed the feasibility of phosphatizing ferrous metals at room temperature and has revealed basic disadvantages of this process, involving its low efficiency in so far as the protective and mechanical properties of the resultant coatings are concerned.

2. It has been shown that lowering the temperature of the phosphatizing process to room temperature, though achieving positive results with regard to the properties of the phosphate coatings, requires a sharp increase in the activity of the solution of the usual phosphatizing salts by the addition of some activator to the solution, and the strict compliance with the specified optimum solution pH, acid number (n) , concentration of the preparation and of the accelerators, etc.

3. A new method is put forward for the cold phosphatizing of metals, yielding high resistance to corrosion together with the requisite mechanical strength. The method involves the formation of protective phosphate coatings in the temperature range of 19-30°C, using solutions that contain fluorine compounds as obligatory additives to the standard iron-manganese preparation, together with accelerators that lower the free acidity of the solution and promote the depolarization of the hydrogen evolved during phosphatization. The optimum processing conditions have been worked out for chemical phosphatizing at room temperature and for cold electrophosphatizing using alternating current.

4. Numerous experiments and industrial tests have confirmed the practical value of the new method, both in so far as the effectiveness of its protection against corrosion and the marked simplification of the technology of phosphatizing are concerned and from the standpoint of the savings involved.

5. Owing to the high adsorption and adhesion properties of cold-phosphatizing coatings, this new method is particularly effective in the multiple protection of parts against corrosion, involving the subsequent treatment of the phosphate layer with organic fillers or the application of paint or lacquer protective films.

LITERATURE CITED

[1] G.V.Akimov and A.A.Ulyanov: Accelerated Methods of Protecting Parts Against Corrosion. Symposium published by the USSR Acad. Sci., ed. G.V.Akimov, Corresp. Member USSR Acad.Sci., p. 83, Moscow (1946).

[2] I.I.Khain. Corrosion and Its Prevention. 1-2, 80 (1939).

[3] A.Burkhardt and G.Sachs. Korrosion, 11, 47 (1933).

[4] O.Macchia. Das Phosphatrestschutz. Berlin. Verlag Chemie. 109 (1940).

[5] German Patent 741,937 (1941).

[6] L.Schuster and R.Krauze, Korrosion u. Metallschutz, 18, 87 (1942); 20, (5), 153 (1944).

[7] Certificate of Authorship No. 72,714 (1948).

[8] Eberty, Gross, and Crowell, J.Am.Chem.Soc., 42, 1433 (1920).

[9] O.Macchia, Korrosion u. Metallschutz, 12, 197 (1936).

[10] French Patent 783,250 (1935); E.S.Gurevich. Protecting Metals Against Corrosion. Patent symposium, 364 (1938).

[11] A.Z.Rivkind, Corrosion and Its Prevention, No. 1-2, 38 (1938).

[12] N.T.Kudryavtsev, Corrosion and Its Prevention, No. 1-2, 114 (1939).

[13] Roesner and Schuster, Chem.Fabrik, 1, Jan. (1941).

[14] K.M.Domnich, Corrosion and Its Prevention, No. 1-2 (1939).

Received June 16, 1949.

A SUSPENDED LAYER OF SPHERICAL PARTICLES*

N. I. Smirnov and Li De En

Chair of Synthetic Rubber Technology, Lensoviet Institute of Technology, Leningrad

In our preceding report [1] we showed that a layer of solid spherical particles suspended in a liquid or gaseous stream may be described hydrodynamically by means of the equation:

$$Eu = 8.58\, Re^{-2.2}\, Ar G_1^{0.5} G_2^{0.33} G_3^{0.33} \qquad (1)$$

This equation was derived from a large quantity of experimental data. The present report describes the conditions under which these experiments were performed and the results of processing the data obtained, thus enabling us to assess the accuracy of Equation (1).

EXPERIMENTAL

Experimental method. The device in which the suspended layer of solid spherical particles was investigated was a vertical glass column. Most often we used a glass tube with an internal diameter of 24.6 mm, though we sometimes employed a tube whose inner diameter was 16.5 mm. Both tubes were 550 mm high. A copper screen was attached 60 mm from the bottom end of the tube. When liquid flow was employed, we used the setup shown in Fig. 1. A layer of dry spheres was first placed on the copper screen until it reached a certain height. The layer heights usually employed were 6, 8, and 10 cm. Then the liquid was allowed to rise through the tube slowly by turning the speed regulator (stopcock B), constantly replenishing the liquid in the level regulator A, until all the bubbles had been driven out of the layer of solid particles. We then set the desired liquid flow rate and measured the height of the suspended layer. The initial and terminal heights of the layer were read off on a scale graduated in millimeters, attached alongside the tube.

When the tube was kept strictly vertical, the height of the layer remained practically unchanged throughout a run. It fluctuated considerably when the tube was not quite vertical.

The liquid flow rate was measured several times during the run by using a 1/10 second stopwatch to read off the time required for the liquid flowing out of the upper end of the tube to fill a measuring cylinder D of known capacity. The liquid flow was uniform as a rule, the time required for filling the cylinder remaining invariant for the individual samples. The temperature of the discharge liquid was measured by a thermometer graduated in tenths of a degree.

The pressure drop in the liquid was measured with a differential manometer F, one end of which was attached to the tube at a point 25 mm below the screen, while the other end was connected to a point 450 mm above the screen. The pressure

---

*Report V of a series on the motion of a body within a medium.

drop was measured to the nearest 0.1 mm of water column.

Two liquids were employed in these tests: water and kerosene. We always used ordinary tap water without any prior treatment, the kerosene being distilled prior to use. The necessary characteristics of the water (specific gravity, viscosity) were taken from a handbook [2], while we measured these constants for the kerosene. The viscosity of the kerosene was measured with an Ostwald viscosimeter at 15, 20, and 25°, its specific gravity being measured in a pyknometer at the same temperatures. A logarithmic graph of viscosity versus temperature was plotted, the specific gravities for various temperatures being found by simple interpolation.

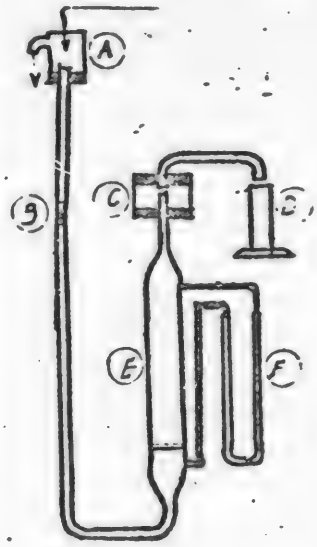

Fig. 1. Apparatus for studying a layer suspended in streams of liquid.

A-Level regulator; B-regulator of liquid flow; C-trap; D-measuring cylinder; E-column; F-differential manometer.

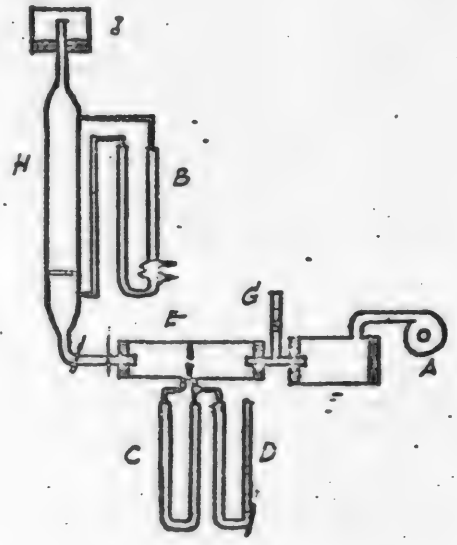

Fig. 2. Apparatus for studying a layer suspended in streams of gas.

A-Blower; B and C-differential manometers; D-manometer; E-tube containing diaphragm; F-oil separator; G-gas flow regulator; H-column; I-trap.

The setup used for the experiments on particles suspended in a current of gas was somewhat different (Fig. 2). A tube containing a diaphragm, E, a gas flow regulator G, an oil separator F, and a gas blower A was connected to the bottom of the column. The diaphragm tube served as a device for measuring the velocity of gas flow through the column. The tube diameter was less than 50 mm, so that the diaphragm was specially calibrated during operation, and its constant determined. The gas velocity through the column was calculated from the following equation [3]:

$$W = \frac{4K}{\pi D_2} \sqrt{hp} \sqrt{\frac{273}{\delta t}}, \qquad (2)$$

where W is the velocity of the gas through the column, in meters/sec; K is the diaphragm constant; D is the diameter of the column, in meters; h is the pressure drop across the diaphragm, in mm of water column, p is the absolute gas pressure

in the diaphragm tube, in kg/m^2; δ is the specific gravity of the gas in terms of air; and t is the temperature in degrees Kelvin.

After a layer of spherical particles had been placed in the column up to a certain height (usually 4,6,8, or 10 cm), the gas flow regulator was manipulated to produce a suspended layer of a given height. While this was going on, the differential manometer C was measuring the pressure drop across the diaphragm, and the manometer D was measuring the residual pressure in the diaphragm tube, these two quantities being required for computing the gas velocity through the column from Equation (2). The pressure drop in the column was measured to the nearest 0.1 mm of alcohol column by the differential manometer B and then converted to kg/m^2. The temperature of the gas was measured at the outlet end by a thermometer graduated in tenths of a degree.

Two gases were employed in these tests: air and carbon dioxide. The air was taken directly from the room by means of a gas blower, while the carbon dioxide, supplied in tanks, was first evaporated into a gasometer. The viscosity and specific gravity of air and of carbon dioxide, needed for our calculations, were taken from a handbook, [2].

Description of the solid spherical particles. Glass and lead balls were utilized in these tests. The glass balls were specially manufactured, while the lead balls were the usual lead shot used for shotgun shells. Glass rods of the same grade were used in making the glass balls. The rods were heated in a Bunsen burner flame and drawn out into a fine, long thread, which was wound on a large wooden drum. To keep the glass thread from breaking as it cooled on the drum, the latter was set up at a distance of 5 to 6 meters from the Bunsen burner. Since it traversed so long a path, the thread solidified by the time it was wound on the drum. This enabled us to secure an unbroken glass thread several thousand meters long. The resultant thread was automatically unwound from the drum at constant speed by means of a mechanical device and fed into the hot flame of a soldering torch. The minute balls of molten glass that were formed at the end of the thread grew to a certain size and broke away, dropping on a sloping sheet of cardboard, down which they rolled into the collecting bin. The well-adjusted apparatus, once set up, operated continuously for days at a time, needing practically no attention.

TABLE 1

Description of the Spherical Particles Used In the Tests

Particle material	Arithmetical mean diameter, 10^{-3} m.	Deviation from the arithmetical mean diameter, %		Density of the ball material, kg/m^3
Glass	0.805	Not more than ± 5	59*	2434.0
		From ± 5 to ±10	33	
		From ±10 to ±12	8	
	1.157	Not more than ± 5	45	2434.0
		From ± 5 to ±10	24	
		From ±10 to ±15	29	
		From −15 to −20	2	
	1.691	Not more than ± 5	68	2434.0
		From ± 5 to ±10	29	
		From ±10 to ±12	3	
Lead	1.972	Not more than ± 5	85	10000.0
		From ± 5 to ±10	15	

The glass balls thus prepared were screened to secure fractions of uniform diameter. 100 balls were chosen from each fraction, and their diameters were measured by a micrometer graduated in thousandths of a millimeter. The arithmetical sum of these diameters was taken as the diameter of all the balls in the fraction.

*The figures in this column indicate the percentage of the particles that deviated from the mean diameter.

TABLE 2

Suspended Layers of Spherical Particles

Test No.	Temp °C	Column diameter 10^{-3} meter	Particle diameter 10^{-3} meter	Density of particles, kg/m^3	Density of the medium kg/m^3	Viscosity of the medium kg/sec/m^2	Loss of head kg/m^2	Velocity of the medium meters/sec.	Initial layer hgt, 10^{-2} meter	Hgt. of suspended layer 10^{-2} meter	Value of Euler's criterion		
											Observed	Computed	Discrepancy, %
1	2	3	4	5	6	7	8	9	10	11	12	13	14
					Glass balls in water								
1	7.0	24.5	1.691	2434.0	999.9	1.457	68.50	0.05564	6	12	217.15	248.65	+14.5
2	7.0	24.5	1.691	2434.0	999.9	1.457	80.20	0.07318	6	16	146.92	149.78	+ 1.9
3	7.0	24.5	1.691	2434.0	999.9	1.457	87.50	0.09349	6	24	99.21	100.20	+ 2.2
4	7.0	24.5	1.691	2434.0	999.9	1.457	95.20	0.10861	6	32	79.17	79.16	0
5	6.8	24.5	1.691	2434.0	999.9	1.466	87.80	0.04791	8	14	375.25	400.94	+ 6.8
6	7.2	24.5	1.691	2434.0	999.9	1.466	91.90	0.07579	8	22	156.90	169.47	+ 8.0
7	7.2	24.5	1.691	2434.0	999.9	1.466	99.20	0.09275	8	30	113.10	120.55	+ 6.7
8	6.8	24.5	1.691	2434.0	999.9	1.466	99.60	0.09568	8	34	106.74	117.64	+10 1
9	7.0	24.5	1.691	2434.0	999.9	1.457	105.50	0.04211	10	16	611.15	598.70	- 2.4
10	7.0	24.5	1.691	2434.0	999.9	1.457	113.00	0.06802	10	24	239.78	238.60	- 0.5
11	7.0	24.5	1.691	2434.0	999.9	1.457	114.50	0.08842	10	36	104.60	111.70	+ 6.7
12	12.0	24.5	0.805	2434.0	999.5	1.261	63.80	0.03316	6	12	569.50	604.97	+ 6.2
13	12.0	24.5	0.805	2434.0	999.5	1.261	64.70	0.04358	6	16	334.35	366.0	+ 9.5
14	12.0	24.5	0.805	2434.0	999.5	1.261	66.20	0.05660	6	24	202.82	235.09	+15.8
15	12.0	24.5	0.805	2434.0	999.5	1.261	67.40	0.06197	6	32	172.26	212.00	+22.4
16	12.5	24.5	0.805	2434.0	999.5	1.244	73.70	0.02678	8	14	1008.40	1093.10	+ 8.5
17	12.5	24.5	0.805	2434.0	999.5	1.244	76.00	0.04390	8	22	388.00	428.35	+10.4
18	12.5	24.5	0.805	2434.0	999.5	1.244	78.00	0.05394	8	30	263.10	300.51	+14.2
19	12.5	24.5	0.805	2434.0	999.5	1.244	78.80	0.05752	8	34	233.70	273.32	+16.9
20	12.0	24.5	0.805	2434.0	999.5	1.261	92.20	0.02264	10	16	1765.30	1826.90	+ 3.5
21	12.0	24.5	0.805	2434.0	999.5	1.261	94.90	0.03835	10	24	633.25	655.93	+ 3.5
22	12.0	24.5	0.805	2434.0	999.5	1.261	97.70	0.04754	10	32	424.20	450.09	+ 5.1
					Lead balls in water								
23	13.0	16.5	1.972	10000.0	999.3	1.221	381.50	0.21463	6	12	81.29	88.52	+ 8.8
24	13.0	16.5	1.972	10000	999.3	1.221	405.30	0.30987	6	20	41.63	45.93	+10.3
25	13.0	16.5	1.972	10000	999.3	1.221	418.50	0.36441	6	28	30.94	35.81	+15.7
26	13.0	16.5	1.972	10000	999.3	1.221	521.00	0.18378	8	13.8	151.43	140.35	- 7.3
27	13.5	16.5	1.972	10000	999.3	1.221	545.50	0.31029	8	26	55.62	54.76	- 1.6
28	13.5	16.5	1.972	10000	999.3	1.221	553.50	0.35883	8	34	42.20	43.90	+ 4.0
29	13.5	16.5	1.972	10000	999.3	1.221	609.20	0.96040	10	11.8	648.30	598.57	- 7.7
30	13.5	16.5	1.972	10000	999.3	1.221	650.50	0.27589	10	28.4	83.90	78.85	- 5.4
31	13.5	16.5	1.972	10000	999.3	1.221	662.00	0.31616	10	36.0	66.68	62.98	- 5.5
					Glass balls in kerosene								
32	17.0	24.5	1.691	2434.0	938.6	1.769	79.41	0.05899	6	12	238.49	255.73	+ 7.2
33	17.0	24.5	1.691	2434.0	938.6	1.769	83.54	0.07802	6	16	143.34	152.90	+ 6 6
34	17.0	24.5	1.691	2434.0	938.6	1.769	86.07	0.09167	6	20	106.99	114.96	+ 7.4
35	17.0	24.5	1.691	2434.0	938.6	1.769	83.54	0.10969	6	28	75.73	86.44	+14.1
36	17.0	24.5	1.691	2434.0	938.6	1.769	102:48	0.04996	8	14	428.81	426.85	- 0.4
37	17.0	24.5	1.691	2434.0	938.6	1.769	109.56	0.08046	8	22	177.13	173.65	- 1.9
38	17.0	24.5	1.691	2434.0	938.6	1.769	111.45	0.09674	8	30	124.64	128.87	+ 3.4
39	17.0	24.5	1.691	2434.0	938.6	1.769	112.39	0.10598	8	34	104.59	109.80	+ 5.0
40	17.5	24.5	1.691	2434.0	938.5	1.753	119.65	0.04283	10	16	681.85	673.73	- 1.2

TABLE 2 (Continued)

See page 422 for column headings

1	2	3	4	5	6	7	8	9	10	11	12	13	14
Glass balls in kerosene													
41	17.5	24.5	1.691	2434.0	938.5	1.753	125.54	0.07157	10	24	256.60	249.13	- 2.9
42	17.5	24.5	1.691	2434.0	938.5	1.753	128.10	0.09011	10	32	165.19	164.51	- 0.4
43	17.5	24.5	1.691	2434.0	938.5	1.753	136.32	0.09669	10	36	152.44	146.33	- 4.1
44	18.8	24.5	1.157	2434.0	938.3	1.712	71.79	0.05012	6	12	295.34	318.17	+ 8.1
45	16.5	24.5	1.157	2434.0	938.7	1.785	74.52	0.07486	6	20	139.03	160.42	+15.3
46	16.5	24.5	1.157	2434.0	938.7	1.785	76.12	0.08871	6	28	102.29	123.55	+20.7
47	19.1	24.5	1.691	2434.0	938.2	1.702	90.35	0.04323	8	14	505.10	520.24	+ 3.0
48	19.1	24.5	1.691	2434.0	938.2	1.702	93.06	0.06753	8	22	213.33	225.49	+ 5.7
49	19.1	24.5	1.691	2434.0	938.2	1.702	96.54	0.08249	8	30	148.36	161.87	+ 9.1
50	18.9	24.5	1.691	2434.0	938.2	1.708	113.34	0.03382	10	16	1036.05	1031.30	- 0.4
51	18.9	24.5	1.691	2434.0	938.2	1.708	115.46	0.04685	10	20	549.80	525.93	- 4.3
52	18.7	24.5	1.691	2434.0	938.2	1.718	117.66	0.06460	10	28	294.30	292.05	- 0.7
53	18.7	24.5	1.691	2434.0	938.2	1.718	118.68	0.07605	10	36	212.78	219.97	+ 3.3
54	20.4	24.5	0.805	2434.0	938.1	1.662	76.10	0.04907	6	16	334.52	334.68	+ 0.1
55	20.4	24.5	0.805	2434.0	938.1	1.662	77.77	0.06436	6	24	194.00	206.14	+ 6.2
56	20.4	24.5	0.805	2434.0	938.1	1.662	78.05	0.07369	6	32	148.92	172.37	+15.7
57	20.4	24.5	0.805	2434.0	938.1	1.662	100.09	0.02796	8	14	1330.50	1232.20	- 7.3
58	20.4	24.5	0.805	2434.0	938.1	1.662	102.35	0.04824	8	22	460.20	426.47	- 7.3
59	20.4	24.5	0.805	2434.0	938.1	1.662	103.76	0.05924	8	30	309.18	300.15	- 2.9
60	20.4	24.5	0.805	2434.0	938.1	1.662	104.03	0.06359	8	34	276.46	271.31	- 1 8
61	20.4	24.5	0.805	2434.0	938.1	1.662	117.75	0.02485	10	16	2009.30	1778.50	-11.4
62	20.4	24.5	0.805	2434.0	938.1	1.662	120.60	0.04251	10	24	700.83	624.40	-10.9
63	20.4	24.5	0.805	2434.0	938.1	1.662	124.07	0.05600	10	36	420.34	395.17	- 5.1
Lead balls in kerosene													
64	19.0	16.5	1.972	10000.	938.3	1.705	443.30	0.19415	6	11.5	122.96	123.44	+ 0.3
65	19.0	16.5	1.972	10000	938.3	1.705	453.20	0.29995	6	20	52.67	57.01	+ 8.2
66	19.0	16.5	1.972	10000	938.3	1.705	467.70	0.38994	6	32	32.16	37.45	+16.4
67	19.5	16.5	1.972	10000	938.2	1.686	587.80	0.17592	8	14	198.61	180.32	- 9 3
68	19.5	16.5	1.972	10000	938.2	1.686	593.40	0.27364	8	21.5	82.87	78.73	- 4.9
69	19.5	16.5	1.972	10000	938.2	1.686	606.50	0.36414	8	34	47.83	48.92	+ 2.3
70	18.4	16.5	1.972	10000	938.3	1.725	700.90	0.16565	10	16	266.96	232.67	-12.8
71	18.4	16.5	1.972	10000	938.3	1.725	707.90	0.24058	10	24	127.89	116.96	- 8.5
72	18.4	16.5	1.972	10000	938.3	1.725	725.30	0.30189	10	32	83.21	78.13	- 6.0
73	18.4	16.5	1.972	10000	938.3	1.725	730.30	0.30189	10	36	76.26	73.03	- 4.2
Glass balls in air													
74	20.2	24.5	1.691	2434.0	1.220	001845	73.40	0.53643	4	4	1901.30	2089.70	+ 9.9
75	20.2	24.5	1.691	2434.0	1.220	0.01845	72.90	0.78440	4	5.0	952.75	1067.90	+10.8
76	20.5	24.5	1.691	2434.0	1.218	0.01847	105.90	0.61866	4	5.5	2228.50	2253.80	+ 1.1
77	20.5	24.5	1.691	2434.0	1.218	0.01847	106.80	0.72890	4	7.0	1619.00	1614.00	- 0.2
78	20.0	24.5	1.691	2434.0	1.221	0.01847	141.30	0.54790	8	8.2	3687.20	3489.60	- 5.4
79	20.0	24.5	1.691	2434.0	1.221	0.01847	147.30	0.65180	8	8.7	2785.70	2429.00	-12.8

TABLE 2 (Continued

See page 422 for column headings

1	2	3	4	5	6	7	8	9	10	11	12	13	14
Glass balls in air													
80	20.0	24.5	1.691	2434.0	1.221	0.01847	150.20	0.77200	8	9.5	2024.80	1724.00	-14.9
81	19.8	24.5	1.691	2434.0	1.222	0.01843	148.70	0.59948	10	10.5	3322.70	3345.70	+ 0.6
82	19.8	24.5	1.691	2434.0	1.222	0.01843	154.80	0.67936	10	11.0	2693.60	2580.40	- 4.2
83	19.8	24.5	1.691	2434.0	1.222	0.01843	156.30	0.75256	10	11.5	2216.60	2091.00	- 5.6
84	19.8	24.5	1.157	2434.0	1.222	0.01843	72.00	0.49618	4	4.5	2347.70	2460.40	+ 4.8
85	19.8	24.5	1.157	2434.0	1.222	0.01843	73.40	0.62890	4	5.0	1490.10	1548.40	+ 3.9
86	17.7	24.5	1.157	2434.0	1.230	0.01833	106.80	0.46990	6	6.5	3833.40	3676.00	- 4.1
87	17.7	24.5	1.157	2434.0	1.230	0.01833	109.70	0.57130	6	7.0	2691.50	2459.60	- 8.6
88	17.7	24.5	1.157	2434.0	1.230	0.01833	119.60	0.47122	8	8.5	4294.10	4331.70	+ 0.8
89	17.7	24.5	1.157	2434.0	1.230	0.01833	124.80	0.55597	8	9.0	3218.50	3075.50	- 4.4
90	17.7	24.5	1.157	2434.0	1.230	0.01833	149.20	0.51600	10	10.5	4466.00	4121.60	- 7.7
91	17.7	24.5	1.157	2434.0	1.230	0.01833	151.10	0.56873	10	11.0	3722.50	3363.00	- 9.6
92	17.7	24.5	1.157	2434.0	1.230	0.01833	155.20	0.60525	10	11.5	3375.00	2975.90	-11.8
93	17.7	24.5	0.805	2434.0	1.230	0.01833	69.70	0.40586	4	4.5	3373.00	3382.40	+ 0.3
94	17.7	24.5	0.805	2434.0	1.230	0.01833	70.80	0.50152	4	5.0	2243.20	2250.00	+ 0.3
95	17.7	24.5	0.805	2434.0	1.230	0.01833	96.90	0.38974	6	6.5	5087.70	4897.00	- 3.7
96	17.7	24.5	0.805	2434.0	1.230	0.01833	100.30	0.45880	6	7.0	3795.70	3504.90	- 7.7
97	17.7	24.5	0.805	2434.0	1.230	0.01833	113.40	0.40933	8	8.5	5395.50	5289.70	- 1.9
98	17.7	24.5	0.805	2434.0	1.230	0.01833	118.20	0.45270	8	9.0	4594.30	4320.10	- 5.9
99	17.7	24.5	0.805	2434.0	1.230	0.01833	122.70	0.49596	8	9.5	3974.00	3598.20	- 9.5
Glass balls in carbon dioxide													
100	17.5	24.5	1.691	2434.0	1.836	0.01498	93.20	0.45905	6	6.5	2351.70	2161.90	+ 0.8
101	17.5	24.5	1.691	2434.0	1.836	0.01498	93.70	0.56616	6	7.0	1553.90	1767.30	+13.6
102	15.5	24.5	1.691	2434.0	1.854	0.01488	122.50	0.53050	8	8.5	2310.40	2201.20	- 4.7
103	15.5	24.5	1.691	2434.0	1.854	0.01488	123.40	0.59940	8	9.0	1821.00	1755.00	- 3.6
104	15.5	24.5	1.691	2434.0	1.858	0.01486	141.70	0.57040	10	10.5	2299.40	2543.70	+10.6
105	15.0	24.5	1.691	2434.0	1.858	0.01486	143.10	0.64421	10	11.0	1820.70	1644.40	- 9.6
106	16.5	24.5	1.157	2434.0	1.845	0.01493	89.00	0.42623	6	6.5	2602.60	2667.20	+ 2.4
107	16.5	24.5	1.157	2434.0	1.845	0.01493	90.80	0.53358	6	7.0	1695.50	1667.90	- 1.6
108	16.4	24.5	1.157	2434.0	1.846	0.01492	114.40	0.47037	8	8.5	2747.60	2575.90	- 6.2
109	16.4	24.5	1.157	2434.0	1.846	0.01492	118.20	0.54901	8	9.0	2083.30	2195.30	+ 5.3
110	16.4	24.5	1.157	2434.0	1.846	0.01492	137.90	0.47081	10	10.5	3306.50	2971.00	-10.1
111	16.4	24.5	1.157	2434.0	1.846	0.01492	142.20	0.52894	10	11.0	2700.40	2335.60	-13.5
112	16.4	24.5	1.157	2434.0	1.846	0.01492	143.60	0.56508	10	11.5	2389.50	2049.70	-14.2
113	18.7	24.5	0.805	2434.0	1.826	0.01503	61.70	0.36765	4	4.5	2451.00	2598.10	+ 6.0
114	18.7	24.5	0.805	2434.0	1.826	0.01503	63.50	0.45126	4	5.0	1669.20	1710.50	+ 2.4
115	19.0	24.5	0.805	2434.0	1.823	0.01505	90.30	0.35684	6	6.5	3858.30	3958.60	+ 2.9
116	19.0	24.5	0.805	2434.0	1.823	0.01505	92.70	0.42010	6	7.0	2826.70	3553.40	- 9.7
117	19.0	24.5	0.805	2434.0	1.823	0.01505	93.20	0.46302	6	7.5	2338.80	2110.90	- 9.5
118	18.0	24.5	0.805	2434.0	1.823	0.01505	118.20	0.36707	8	8.5	4723.60	4051.70	-14.2
119	18.0	24.5	0.805	2434.0	1.852	0.01505	119.10	0.39837	8	9.0	4042.60	3449.30	-14.7

Three of the fractions of glass balls were used in our tests.

The same method was used to determine the size of the lead balls. The density of the substance from which the balls were made was determined by means of a pycnometer at 20°. A complete description of the balls is given in Table 1.

A total of 281 experiments was run with spherical particles under various conditions, counting both the main and parallel tests. In the overwhelming majority of cases the parallel tests yielded results that were very close to those secured in the main tests; we therefore have enumerated only the results of the main tests in Table 2 to avoid unnecessary bulkiness of the tabular data.

In our preceding report [1], we have shown that, on the assumption that the phenomenon of a suspended layer consists of three elementary processes, we can represent this phenomenon theoretically by means of the following criterial equation:

$$Eu = C\,Re^{-2\cdot2}\,Ar^{p}\,G_2^{0.33}G_3^{0.33} \qquad (3)$$

The expressions for calculating the similarity criteria are given in that same report. There are two unknowns in Equation (3): the coefficient C and the exponent p. These unknowns may be readily computed from the experimental data listed in Table 2, thus yielding the final equation for the hydrodynamics of a suspended layer of spherical particles, as given by Equation (1). The three last columns of Table 2 give the observed values of Euler's criterion, the corresponding values as calculated from Equation (1), and the discrepancy between. In the vast majority of instances these are quite small, as is strikingly shown by the data plotted in Fig. 3.

Equation 3 was derived on the assumption of turbulent flow (Reynolds number higher than 7). In our experiments, the value of the Reynolds number varied from 4.3 to 630, however, though there were very few tests in which the number fell below 7. Still, these tests yielded satisfactory agreement of the observed and the computed values of Euler's criterion, but the deviations were all on one side of the curve, as we see at the bottom of Fig. 3. Thus, at Re < 7 there is a tendency for the computed values of Euler's criterion to depart from the observed values. This points to the necessity of describing the hydrodynamics of a suspended layer in the region of laminar flow by means of a special equation. Such an equation can probably be derived and tested by the method described in our preceding [1] and present reports. This will be the subject of our next report.

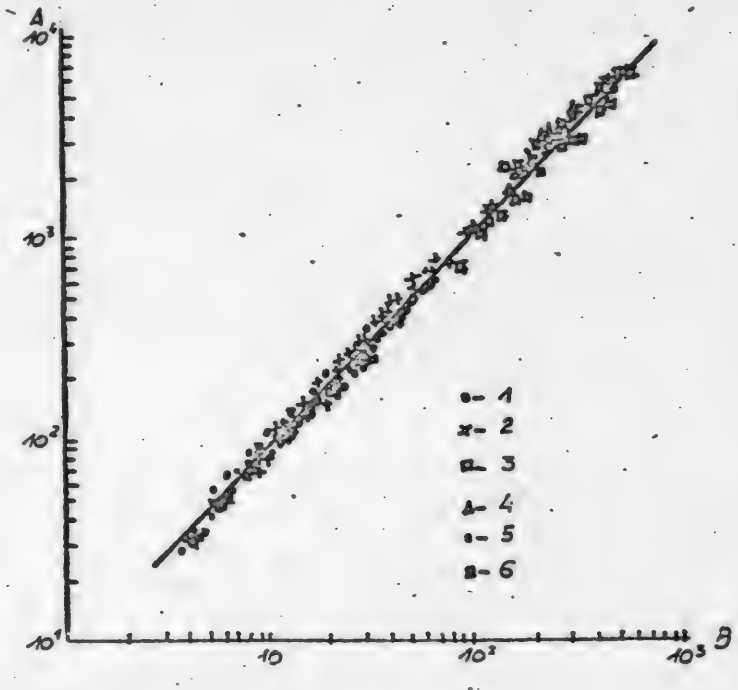

Fig. 3. Results of tests on spherical particles.

1-Glass balls in water 2-glass balls in kerosene; 3-glass balls in air; 4-glass balls in carbon dioxide; 5-lead balls in water 6-lead balls in kerosene. A-Euler's criterion, Eu; B-$Re^{-2.2}\,Ar\,G_1^{0.5}\,G_2^{0.33}\,G_3^{0.33}$.

We wish to express our profound gratitude to V.L.Rubana, who suggested the

method of producing the glass balls, and who adjusted the apparatus set up to produce them by the method described herein.

SUMMARY

1. Experimental data have been utilized to determine the unknown coefficient and exponent in the theoretically derived equation for the hydrodynamics of a suspended layer of solid spherical particles.

2. The applicability of the criterial equation to Reynolds numbers ranging from 7 to 630 has been tested in the formation of suspended layers of glass and lead balls with diameters ranging from 0.8 to 1.97 mm in water, kerosene, air, and carbon dioxide.

3. A method has been mapped for studying the hydrodynamics of a suspended layer in the region of laminar flow.

LITERATURE CITED

[1] N.I.Smirnov and Li De En, J.Appl.Chem. 24, 1 (1951).*

[2] Handbook of Physical, Chemical, and Engineering Data, Soviet Encyclopedia Press (1931).

[3] S.I.Tsepkin. Control, Measuring, and Regulating Instruments in the Chemical Industry. State Chemical Press (1945).

Received October 18, 1950.

---

*See CB translation p. 65 ff.

THE AQUEOUS HYDROLYSIS OF OAKWOOD

A. F. Zaitseva and N. I. Nikitin

Forest Institute of the USSR Academy of Sciences

The mild preliminary treatment of wood with hot water is beginning to be employed in various branches of the industry, such as the production of crystalline xylose. Deciduous wood, rich in pentoses, is usually employed for this purpose [1]. The hydrolysis of wood at a temperature higher than 100° has likewise been introduced into the cellulose industry recently [2]. The humification of wood polysaccharoses that occurs when mineral acids are employed is much less during aqueous hydrolysis.

In their investigation of aqueous hydrolysis, most authors concluded that an important factor was the splitting out of acetic and formic acids, which break down the bond between the lignin and the carbohydrates [3]; Sharkov and Efimov [4] believe that the hydrolysis of hemicellulose is accelerated in aqueous solution by organic acids to different degrees, depending upon the presence of these readily split-out acids in the plant fiber. These authors heated ground pinewood to 100° for 6 hours in pure water, dissolving 5.6% hemicellulose (by weight of the original wood). They dissolved 12.1-12.9% of the hemicellulose by heating the wood to 174° in an autoclave for 60 minutes. Increasing the length of the water treatment to 120 minutes under the same conditions raised the percentage of hemicellulose that entered solution to 15.3-15.8%. Zherebov and his associates [5] extracted Siberian deciduous woods with water, securing 9 to 20% of gum. They made a study of the serviceability of this gum as material for hydrolysis and subsequent saccharification, the study yielding a positive result. Kurbatov [6] recovered hemicellulose from sphagnum mosses by boiling with water for 200-250 hours. He extracted some 40% of carbohydrates by this method. Analyzing the hydrolyzates, the author found (in percentages by weight of reducing sugars): 26% xylose; 6.4% mannose; 23-30% galactose, and 40% glucose. Aranovsky and Gortner [7] have shown that the aqueous hydrolysis of poplar (at 186° for 12 hours) hydrolyzes not only the hemicelluloses, but some 37% of all the cellulose in the wood as well.

Schütz and Sarten [8] treated birchwood with hot water at 100, 135, and 165°, dissolving 5 to 35% of the ripe wood. The authors cite proof that the solution contains substances in the shape of the entire ligneous complex, preserving the elementary composition of the original wood. Their rather general ultimate analysis led these authors to deny the existence of lignin as a special aromatic substance in wood, inasmuch as the lignin ought to have a high percentage of carbon , differing appreciably from the percentage of carbon in the wood as a whole. Our objections to these notions will be cited below.

In the present research, using oakwood, we had as our objective: recovering the principal soluble products by means of the mildest possible aqueous hydrolysis; identifying them chemically as completely as possible; and making a microscopic

study of the changes in the cell walls caused by the elimination from these walls of some of their principal constituents in prolonged mild aqueous hydrolysis.

EXPERIMENTAL

In our research we utilized samples of oakwood of the species Quercetum fontinale according to Tellerman's classification, from trees about 60-75 years old, yielding logs 28-30 cm in diameter, cut off at a height of 1.25-1.35 meters above the ground.

After the bark and the bast fiber had been removed, a sawdust mixture was prepared from an average sample of the wood. Sawdust passing through a 1-mm screen and held on a 0.2-mm screen was taken for analysis. The prepared sawdust mixture was freed from resin (by extraction with ethyl ether) and from tanning agents (by boiling it for 3 hours with water over a water bath with a reflux condenser, and then washing it with hot water until the wash water was colorless). The individual batches of sawdust were air dried and then subjected to prolonged renewable aqueous extraction for 50, 100, 500, and 1000 hours. Extraction with water was effected at 100°, using electrical [illegible] with a reflux condenser and a mechanical stirrer, the sawdust and water proportions being 1:50. Every 4 hours the water was separated from the sawdust by decantation, fresh water was poured over the sawdust, and extraction was begun again. The extracts of the 50-hour and 100-hour aqueous treatments were collected separately and evaporated in vacuum (5-10 mm Hg) at 35-40°, the evaporated hydrolyzate being analyzed chemically.*

The original sawdust (with the resin and tanning agents removed) and the residues left after 50, 100, 500, and 1000-hour aqueous extraction were analyzed chemically. The quantity of water-soluble substances was determined from the dry extract residue and the sawdust's loss in weight. The analysis was made for the percentages of the following constituents: cellulose, lignin, pentosans, methylpentosans, galactan,-mannan, uronic acids, methoxy groups (total and readily split out), substances soluble in 4% NaOH, acetyl groups, nitrogen, and ash. An ultimate analysis was also made. We used, in the main, the method described in our preceding report [9] for determining the constituents of the wood, except for determination of the acetyl groups and the nitrogen. The acetyl groups were determined by the Freudenberg method [10], as subsequently elaborated (for wood) by Freeman and others [11].

A sample of the wood is treated by heating it over a water bath with absolute alcohol and p-toluenesulfonic acid. The acetyl groups that split out enter into reaction with the absolute alcohol, forming ethyl acetate. The latter is driven off into a titrated alcoholic solution of alkali, where it saponifies after reheating. The number of acetyl groups is calculated from the consumption of alkali.

The nitrogen in the wood was determined by the Kjeldahl method [12].

We also investigated the overall reducing properties of the water-soluble hydrolyzates. In the hydrolyzates secured from the wood residues left after prolonged water processing, we determined the percentages of readily and difficultly hydrolyzable substances, and fermenting and nonfermenting sugars, the latter being identified quantitatively.

The readily hydrolyzable reducing substances in the initial sawdust and in the sawdust after extraction with water for 50, 100, and 500 hours were determined

*Until they were evaporated, the aqueous extracts were stored under toluene in glass bottles with ground-glass stoppers; after evaporation, the concentrated hydrolyzates were transferred to Erlenmayer flasks and boiled for 5 minutes on a hot plate, after which the flasks were quickly plugged with sterile absorbent cotton. This operation was repeated every time a sample was taken for analysis.

by boiling the sawdust with 2.5% sulfuric acid over a water bath for 5 hours, using a 1:50 sawdust-acid ratio [13]. The resultant hydrolyzates were subjected to a Bertrand analysis to determine their percentages of reducing substances; they were then neutralized with barium carbonate (pH 4.5-5) and, after the resulting precipitate had been filtered out, the reducing substances they contained were again determined by the Bertrand method and expressed in terms of glucose. The loss of reducing substances caused by neutralization totaled 6-9%. The neutralized hydrolyzates were evaporated in vacuum (5-10 mm Hg) until their concentration of sugar totaled 3-4%. The evaporated hydrolyzate was divided into two parts – in one part the hexose was eliminated by fermentation with baker's yeast at 28-32°. 1.5 g of yeast was used per 100 cc of hydrolyzate. Fermentation was done in small flasks fitted with a Meisl seal. The completeness of fermentation was checked by the flask's loss of weight. As a rule fermentation was complete after two or three days. After fermentation was over, the mash was separated from the yeast by filtration after a brief period of boiling. The total reducing substances in the resultant filtrate were then determined by the Bertrand method. The difference in the reducing substances before and after fermentation was the total fermented sugar. The nonfermenting sugars (after the mineral salts had been eliminated from the solution with alcohol) were then analyzed to determine their xylose content – as the bromocadmium salt of xylonic acid [14], their arabinose content being found as the diphenylhydrazone hydrochloride [15], and their uronic acids by the Tollens-Le Fevre method [9].

The mineral salts were eliminated from the second half of the neutralized and evaporated hydrolyzate by adding alcohol to the solution, after which its galactose was determined via mucic acid by the Van der Haar method [16] and its mannose was determined as a phenylhydrazone insoluble in acetone or alcohol [17].

The reducing substances that were hard to hydrolyze were determined in the sawdust residue (after the readily hydrolyzable reducing substances had been removed) with 80% sulfuric acid by the Kiesel and Simiganovsky method [18,19]. The resultant hydrolyzate was analyzed by the same method used for the analysis of the readily hydrolyzable portion.

In our investigation of the reducing properties of the substances that had dissolved in the water, we noticed that additional hydrolysis with 2.5% sulfuric acid for 5 hours resulted in a diminished yield of reducing substances (56-60% instead of 68-70%). We therefore ran a series of auxiliary experiments and then made several changes in the conditions governing the hydrolysis of the water-soluble substances. Hydrolysis was effected as follows: the water-soluble substances (from the 50-hour and 100-hour aqueous extracts) were boiled for 3 hours with 5% sulfuric acid (1 part of acid to 50 parts of extract) with a reflux condenser. This procedure produced the highest yield of reducing substances.

In our quantitative identification of the sugars (xylose, arabinose, etc.), we checked the methods we were using by applying them to the pure sugars. Our research has resulted in the introduction of several changes in the procedures specified in the literature at the present time.

Our first series of tests yielded a characteristic picture of the changes in the chemical composition of sawdust as a function of the water-extraction time. These results (the mean values of two or more determinations) are listed in Table 1.

We see from Table 1 that the percentage of water-soluble substances rises continuously as extraction is continued. The loss of weight of the sawdust totaled 11.2% after 50 hours of extraction with water, 32.0% after 100 hours, 51.5% after 500 hours, and 65.6% after 1000 hours. The average ultimate analysis of the

Table I

Changes in the Chemical Composition of Oakwood after Aqueous Extraction

Analysis for:	Initial oak sawdust (without resin or tanning agents)	Sawdust after extraction with water for 50 hours (%)		Sawdust after extraction with water for 100 hours (%)		Sawdust after extraction with water for 500 hours (%)		Sawdust after extraction with water for 1000 hours (%)		Oak sawdust after extraction with a reflux condenser for 296 hours over a water bath (%)	
		Dry residue	original wood	Dry residue	original wood	Dry residue	Original wood	Dry residue	Original wood	Dry residue	Original wood
Loss of weight of the sawdust after aqueous extraction	-	-	11.2	-	32.0	-	51.5	-	65.6	-	38.9
Dry residue	100	-	88.8	-	68.0	-	48.5	-	34.4	-	61.1
Ultimate analysis (%) C	48.85	48.99	-	50.23	-	49.91	-	49.71	-	48.64	-
Ultimate analysis (%) H	6.21	6.15	-	5.96	-	6.14	-	6.21	-	5.23	-
Kurschner cellulose free of pentosans	40.7	44.9	39.9	58.1	39.5	67.3	32.6	75.4	25.9	59.1	36.1
Lignin, by the Storch and Muller method	24.9	25.6	22.7	24.5	16.7	24.4	11.8	17.6	6.0	21.6	13.2
Pentosans, corrected for uronic acids and methylpentosans	22.4	20.5	18.2	10.42	7.1	6.97	3.37	5.43	1.8	12.6	7.7
Methylpentosans	0.65	0.14	0.12	0.29	0.19	0.34	0.16	0.29	0.09	-	-
Galactan	0.24	0.10	0.09			-	-	-	-	-	-
Mannan	none	-	-	-	-	-	-	-	-	-	-
Uronic acids (in terms of the glucuronic	5.7	4.1	3.7	1.7	1.3	0.7	0.4	0.7	0.2	-	-
Total Methoxy groups*	6.7	6.8	6.0	5.8	3.9	4.9	2.4	4.1	1.4	5.3	3.3
Readily detachable methoxy groups	1.7	1.6	1.4	1.4	0.9	0.4	0.2	0.4	0.1	1.2	0.7
Substances soluble in 4% NaOH**	18.4	21.1	18.8	-	-	10.7	5.2	-	-	-	-
Acetyl groups	3.0	1.9	1.7	2.4	1.6	0.6	0.3	0.4	0.1	-	-
Nitrogen	0.25	0.19	0.16	0.13	0.08	0.12	0.05	0.07	0.02	-	-
Ash	0.06	0.07	0.06	0.09	0.06	0.11	0.05	0.13	0.04	-	-
Sum total	99.6	99.1	88.0	99.0	66.8	100.9	48.9	100.4	34.3	-	-

*The total methoxy groups were not entered into the sum total, as part of them is contained in the lignin.

**The substances soluble in 4% NaOH were not entered into the sum total, as most of them are included with the pentosans.

insoluble sawdust residue remained close to that of the initial sawdust. The changes in the composition of the wood were by no means uniform, however. The pentosans and uronic acids dissolved in water best, lignin somewhat less so, and cellulose much less so. The pentosans left in the sawdust totaled 18.2% after 50 hours of extraction with water (as against 22.4% in the original sawdust), 7.1% after 100 hours, and only 1.8% after 1000 hours. This means that 90% of the pentosans in the original wood were dissolved. The same picture is observed when we examine the changes in the percentage of the uronic acids, which totaled only 0.2% in the sawdust residue after 1000 hours of aqueous extraction. Hence, 96% of the uronic acids originally present in the wood dissolved in the water. The lignin left in the wood residue totaled 22.7% after 50 hours of extraction (as against 24.9% in the original sawdust), while 75% of the total wood lignin was dissolved after 1000 hours. It was found that the cellulose resisted repeated aqueous extraction most tenaciously, being practically unaffected by the first 100 hours of extraction, and only 36% of its initial content entered solution after 1000 hours of extraction (the residue containing 25.9% by weight of the initial wood, as against 40.7%).

The foregoing dissolved constituents or their hydrolysis products were found in the aqueous extracts evaporated in vacuum. The results of these analyses are listed in Table 2.

TABLE 2

Chemical Composition of Aqueous Extracts

Analysis for:	Extract after 50 hours of extracting the sawdust with water,		Extract after 100 hrs. of extracting the sawdust with water,	
	Per cent of dry residue	Per cent of original wood	Per cent of dry residue	Per cent of original wood*
Anhydrous residue	–	11.2	–	30.8
Ultimate analysis, per cent C	48.11	–	48.22	–
Ultimate analysis, per cent H	5.76	–	5.77	–
Lignin**	17.6	1.9	24.3	7.5
Pentosans, corrected for uronic acids and methylpentosans	43.8	4.9	49.3	15.3
Methylpentosans	1.0	0.11	1.70	0.52
Galactan	1.25	0.14	0.44	0.13
Mannan	none	none	none	none
Uronic acids	12.3	1.4	12.9	3.9
Total methoxy groups	2.8	0.3	8.0	2.4
Readily detachable methoxy groups	0.12	0.01	3.5	1.1
Nitrogen	0.50	0.05	0.70	0.21
Ash	0.10	0.01	0.09	0.03

When we examine Table 2, we see that the aqueous extracts contain a high percentage of pentosans (or of products of their hydrolysis). The percentage of these substances in the extracts is of the same order of magnitude as their loss in the sawdust. The drop in the percentage of pentosans in the sawdust was 4.2% after 50 hours of extraction, for example, while the 5 hour aqueous extract indicated it contained 4.9% of pentosans (in terms of furfural). The percentage

* We took as the original wood the wood freed from its resin and tanning agents (the resin removed after extraction of the sawdust with ether totalled 0.6%, while the tanning agents removed by 3 hours of extraction with water totalled 9.4%).

** The lignin was found to contain 58.6% carbon, 5.9% hydrogen and 18% methoxy groups.

of pentosans in the sawdust dropped 15.3% after 100 hours of aqueous extraction, the same percentage being found in the 100-hour aqueous extract in terms of furfural. The same picture is seen in the changes in the percentage of uronic acids. The changes in the percentage of lignin likewise agree with the percentages found in the evaporated extracts.

In determining the percentage of lignin in the aqueous extracts we made a change in the usual method employed for determining lignin in wood. Enough 80% sulfuric acid was added to a given volume of the aqueous hydrolyzate, evaporated in vacuum and containing at least 0.5 g of dry residue, to make the acid concentration in the total volume amount to 64%. One part of dry residue was taken to 25 parts of acid. The reaction mixture was then allowed to stand for 16 hours at 20°, after which it was diluted with 200 cc of water and boiled for 3 minutes on a hot plate. The resulting insoluble (condensed) lignin was filtered cut, washed with water, and dried to constant weight at 105°.

As we see from Tables 1 and 2, the sawdust lost 2.2% of lignin after boiling for 50 hours, while the extract was found to contain about 2%. After 100 hours of extraction with water the sawdust had lost 8% lignin, while the extract was found to contain 7.5%.

The mean ultimate analysis of the substances dissolved in water (Table 2) and the composition of the water-insoluble sawdust residue were both close to the mean ultimate analysis of the initial sawdust.

For the sake of comparison we also ran a 396-hour extraction with water over a boiling water bath, using a reflux condenser and changing the water every 4 hours, the sawdust-water proportions being the same: 1 to 50. The results of this test were compared with the results obtained in electrical air heating (Table 3).

TABLE 3

Results of Extraction by Boiling Over a Water Bath and by Electrical Air Heating

Extraction No.	Boiling with air heat and a reflux condenser		Extraction No	Boiling over a water bath with a reflux condenser	
	Extraction time, hrs.	Sawdust's loss of weight, %		Extraction time, hrs.	Sawdust's loss of weight, %
31	124	35.4	42	168	29.7
42	168	38.3	99	396	38.9
55	220	40.9			
100	400	49.4			

As we see in Table 3, the sawdust is gradually dissolved even when heating is done over a water bath, being partially hydrolyzed during prolonged aqueous extraction, but the rate of hydrolysis is somewhat slower. No essential difference is observed, as is borne out by the chemical analyses (cf the last column in Table 1).

The figures listed in Table 4 indicate that the reducing substances are largely dissolved in polymer form when sawdust is extracted with water, the monosaccharides being formed only after additional hydrolysis of these substances with 5% sulfuric acid.

When we compare the data on the change in the percentage of readily and

difficultly hydrolyzable reducing substances listed in Table 5, we see that the readily hydrolyzable sugars are diminished in the hydrolyzates made from the sawdust residues left after prolonged extraction with water. As Table 5 shows, this change occurs at the the expense of the nonfermenting portion of the hydrolyzate. The hydrolyzates of the original sawdust contained 17.1% of readily hydrolyzable nonfermenting sugars, whereas the hydrolyzates of the sawdust residue left after 50 hours of extraction with water contained only 8.1%, the 100-hour residue hydrolyzates containing 5.5%, and the 500-hour residue hydrolyzates only 0.2% (in terms of the original wood). All this is in conformity with the data of our general chemical analyses, as listed in Tables 1 and 2, which indicate a change in the percentage of the pentosans and uronic acids during aqueous hydrolysis. The difficultly hydrolyzable reducing substances in the original sawdust contain somewhat less nonfermenting sugar than the readily hydrolyzable portion, and the sugar is likewise

TABLE 4

Change in the Reducing Substances in Aqueous Extracts (Per Cent by Weight of the Extract's Anhydrous Residue

Material	Reducing substance found	
	Before hydrolysis	After hydrolysis with 5% H_2SO_4
Extract after 50 hrs. of extraction with water.....	14.9	68.5
Extract after 100 hrs. of extraction with water	15.1	72.2

TABLE 5

Identification of the Reducing Portion of Oak Sawdust

Reducing Substance (R.S.)		Original sawdust (without resin or tanning agents	Oak sawdust after 50 hours extraction with water		Oak sawdust after 100 hours extraction with water		Oak sawdust after 500 hours extraction with water	
			% of anhydrous residue	% of original wood	% of anhydrous residue	% of original wood	% of anhydrous residue	% of original wood
Readily hydrolyzable R.S.		22.8	15.1	13.4	16.2	11.0	0.9	0.4
Including	Fermenting	5.7	6.0	5.3	8.1	5.5	0.4	0.2
	Galactose	0.1	tr.	tr.	tr.	tr.	–	–
	Mannose	none	none	none	none	none	–	–
	Glucose (diff.)..	5.6	6.0	5.3	8.1	5.5	–	–
	Nonfermenting ...	17.1	9.1	8.1	8.1	5.5	0.5	0.2
	Xylose	12.2	7.6	6.8	6.3	4.3	–	–
	Arabinose	0.2	0.1	0.08	0.1	0.07	–	–
	Uronic acids	4.3	1.9	1.7	0.9	0.6	–	–
Difficultly hydrolyzable RS:		55.1	58.7	52.2	59.3	40.3	73.2	35.1
Including	Fermenting	44.9	49.9	44.4	53.1	36.1	71.7	34.4
	Galactose	0.2	0.1	0.08	tr.	tr.	–	–
	Mannose	none	none	none	none	none	–	–
	Glucose (diff.)..	44.7	49.8	44.3	53.1	36.1	–	–
	Nonfermenting ...	10.2	8.8	7.8	6.2	4.2	1.5	0.7
	Xylose	5.1	4.5	4.0	4.1	2.8	–	–
	Arabinose	0.2	tr.	tr.	tr.	tr.	–	–
	Uronic acids	2.2	–	–	–	–	–	–

diminished in the hydrolyzates of the wood residues left after extraction with water. In the hydrolyzates of the original sawdust the sugars totaled 10.2%, for example, while they amounted to no more than 0.7% in the hydrolyzate of the wood residue left after 500 hours of extraction with water.

We also see in Table 5 that the tested oakwood had no mannose at all, and merely traces of galactose and arabinose, whereas the xylose totaled as much as 12.2% in the readily hydrolyzable reducing substances and 5.1% in the reducing substances that are hard to hydrolyze (both in per cent of the initial wood). The uronic acids were 4.3% in the readily hydrolyzable and 2.2% in the difficultly hydrolyzable reducing substances, though the percentage of glucose (after hydrolysis of the cellulose) is 44.7% in the reducing substances that are hard to hydrolyze; in addition, up to 5.6% of glucose was found in the readily hydrolyzable reducing substances. The glucose found in the readily hydrolyzable substances owes its origin to glucane, as well as to the most readily hydrolyzable amorphous part of the cellular tissue [20].

The second stage of the research was a study of the localization of the various substances in the cell walls by the methods of anatomic research and microchemical reactions [21,22].

We therefore took two samples of sawdust: the original sawdust (freed from resin and tanning agents) and the sawdust after 1000 hours of extraction with hot water (65% of the substances in the anhydrous wood having been dissolved). In these samples we measured the width of the cellular cavities and the width of the bordering pores. Completely measuring the mechanical (libriform) fibers involved previous maceration breaking down the intercellular substance by boiling with strong nitric acid and potassium chlorate, followed by washing the macerated sawdust with water.

Measuring the width of the hollows in the mechanical fibers and their overall diameter in the middle of their wide section was done at a magnification of 500 times, with an accuracy of 0.01 mm. The mean values were taken of 50 parallel measurements (the deviations between individual measurements were insignificant). Microphotographs were made of various sawdust preparations.

The extracted and macerated sawdust had fibers that were much thinner than those in the original sawdust. At high magnifications the thickness of the walls of the mechanical (libriform) fibers is readily visible in these same macerated sawdusts. In the original sawdust, the libriform walls are thick, while the interior cavities are comparatively narrow (Fig. 1 [see plate, page 495], and Table 6.

TABLE 6

Comparative Data on the Decrease in Cell Wall Thickness After Extraction With Water

Dimensions of cell walls, μ	Original sawdust, (macerated)	Sawdust after extraction for 1000 hours with water (macerated)
Mean cell width, including cavity	1.80	1.16
Mean cavity width	0.46	0.79
Mean thickness of 2 walls (difference)	1.34	0.37
Decrease in thickness of walls from original value	-	72.5%

In the extracted sawdust (Fig. 2 [see plate, page 495] and Table 6), the walls of the mechanical fiber have become considerably thinner. The diameter of the slitlike and bordering pores has increased considerably. The degree to which

the constituent substances have been washed out of the cell walls after prolonged extraction with hot water is indicated more accurately by our measurements and chemical analyses.

Our measurements of the overall thickness of the mechanical fiber cells together with their cavities and of the thicknesses of the walls separately demonstrated that the mean thickness of the two cell walls combined was 1.34 μ in the original sawdust, while it was no more than 0.37 μ in the sawdust after 1000 hours of extraction with water. Hence, the walls of the extracted sawdust had grown 72.5% thinner. The circumstance that the diameter of the cell cavity had likewise increased considerably in the extracted sawdust (0.79 μ as against 0.46 μ in the original sawdust) is also worthy of note. We see, therefore, that the extraction of the constituents takes place in the internal layers of the cell tissue as well as in its outer layers.

Since it was impossible to make a cross section of the sawdust in order to trace the localization of the individual substances in the cell walls more closely by employing microchemical reactions, we extracted oak chips for a long time with hot water.

The chips were prepared from the same sample of oak, 3 x 6 x 20 mm chips being taken separately from the heartwood and the sapwood. After the sample chips had been freed of their resins and tanning agents, some of the chips were extracted for 600 hours at 100° with water, using a reflux condenser, the water being changed every 8 hours. The other chips served as the raw material for comparative investigations.

Chemical analysis of the heartwood and sapwood chips (the original chips and chips after 600 hours of extraction with water) was performed by the same methods as those described above for the analysis of the sawdust. The results of the analyses of the chips are listed in Table 7. As we see from this table, 49.4% of the substances in the heartwood chips and 52.1% of those in the sapwood chips dissolved after 600 hours of extraction with hot water.

The mean ultimate analysis of the insoluble chip residue was close to the ultimate analysis of the original chips. The individual constituents of the wood entered solution at various rates, thus confirming the results obtained with the sawdust.

We see from Table 7 that 95% of the uronic acids contained in the original chips dissolved from both the heartwood and the sapwood after 600 hours of extraction with water, the corresponding figures being 75-76% for the pentosans, 52-55% for the lignin, and only 15-13% for the cellulose.

The localization of the individual constituents in the cell walls was studied in cross sections of the chips. The microphotographs in Figs. 3 and 4 (see plate, page 495) are cross sections of the sapwood in the original state and after extraction.

These microphotographs clearly show the changes in the structure of the sapwood after prolonged extraction with hot water. In the original sapwood (Fig. 3) the mechanical (libriform) fibers constitute an interlinked network, with relatively blurred intercellular boundaries, whereas the cells of the mechanical fibers seem to fall apart in the sapwood that has been extracted with water (for 600 hours), each cell possessing its isolated external wall.

When the original samples of heartwood and sapwood were stained with zinc chloroiodide, the whole preparation turned yellow (lignin reaction); after 600 hours of extraction, however, the heartwood and the sapwood were stained violet by zinc chloroiodide (cellulose reaction). This again proves that part of the lignin in the original oakwood lies in the intercellular substance, as well as in

TABLE 7

Change in the Chemical Composition of Oak Heartwood and Sapwood After Pro-Prolonged Extraction with Water

Analysis for:	Original oakwood chips (with resin and tanning agents removed)		Oakwood chips after 600 hours of extraction with water				Loss of the individual constituents, in % of their content in the original wood	
			Heartwood substances		Sapwood substances			
	Heartwood substances	Sapwood substances	% of anhydrous residue	% of original wood	% of anhydrous residue	% original wood	Heartwood substances	Sapwood substances
Loss in weight of chips after extraction with water	–	–	–	49.4	–	52.2	–	–
Anhydrous residue ..	100	100	–	50.6	–	47.8	–	–
Ultimate analysis, % C..	49.11	48.98	49.01	–	49.00	–	Almost no change	
Ultimate analysis, % H..	6.02	6.10	6.00	–	5.98	–		
Kürschner cellulose, free of pentosans..	40.4	36.9	65.4	33.1	66.7	31.9	15.5	13.5
Lignin (with 64% H_2SO_4)	24.6	25.2	23.1	11.7	23.5	11.2	52.8	55.5
Pentosans, corrected for uronic acids ..	21.4	20.5	10.3	5.2	10.4	4.9	75.7	76.0
Methylpentosans	0.40	0.42	0.15	0.07	0.18	0.8	82.5	80.9
Galactan	0.49	0.65	trace	trace	trace		Almost 100%	
Uronic acids (in terms of the glucuronic)	6.2	7.3	0.5	0.25	0.6	0.3	97.2	95.8
Methoxy groups (total)*	6.9	6.9	5.2	2.63	5.7	2.7	63.3	60.8
Detachable methoxy groups	1.7	1.7	0.4	0.2	0.8	0.3	88.2	82.3
Nitrogen	0.24	0.27	0.10	0.05	0.08	0.03	79.1	88.8
Ash	0.05	0.12	0.09	0.04	0.10	0.04	20.0	66.6
Acetyl groups	3.15	5.12	1.02	0.52	0.80	0.38	83.4	92.5
Sum total	98.6	98.2	101.1	51.48	103.2	49.1	–	–

the primary and more superficial (secondary) layers of the mechanical cells. After part of the lignin has been removed (50% of the original total), the cellulose predominates, the deeper-lying lignin being protected by the whole mass of secondary cellulose layers.

Figures 5 and 6 (see plate, page 495) are microphotographs of tangential sections of the sapwood, originally and after extraction.

In the tangential section of the sapwood that has undergone 600 hours of extraction (Fig. 6) we see the ruptured cells of the medullary rays (dark areas), the thinned and ruptured (in spots) cell walls of the libriform, and the nearly total absence of the wood parenchyma. The tangential section of the original

---

*The total methoxy groups were not entered into the sum total, as part of them is contained in the lignin.

heartwood (Fig. 5), however, shows the wood parenchyma, the whole cells of the medullary rays, and the rather well-shaped rows of libriform.

The investigation of the localization of the various constituents in the cell walls of the wood was done in the chair of plant physiology and anatomy of the Academy of Forestry, with the active participation of Asst. Prof. N.L.Kossovich and Senior Laboratory Assistant N.A.Baidalina of that chair, to whom we are deeply indebted.

SUMMARY

1. The prolonged retreatment of oakwood with boiling water at 100° results in the formation of a large quantity of water-soluble substances. The following percentages of the sawdust entered solution as the result of aqueous hydrolysis: 32.0% after 100 hours; 51.5% after 500 hours; and 65.6% after 1000 hours. After 600 hours, 49.4% of heartwood chips dissolved, and 52.1% of sapwood chips.

2. Investigation of the ultimate analysis of the wood residue that was insoluble in water and of the mean composition of the substances dissolved in the water as the result of hydrolysis has shown that these ultimate analyses are hardly different. This may lead one to the incorrect conclusion that the wood enters solution as a sort of uniform complex.

3. It was found, however that the various substances in wood dissolve at very different rates during mild aqueous hydrolysis. The pentosans and uronic acids dissolve fastest, lignin dissolving somewhat more slowly, and cellulose very much more slowly. After 1000 hours of extraction with water, we were able to dissolve up to 90% of all the pentosans present in the original wood, 95% of the uronic acids, 75% of the lignin, and only 36% of the cellulose.

4. These figures prove that lignin exists in wood as a substance possessing its own properties and containing a much higher percentage of carbon (64-66% than the carbohydrates. If the wood did not contain aromatic lignin, it would be impossible to obtain a hydrolyzate with nearly the same average ultimate analysis (49.9% C and 6.14% H) after mild aqueous hydrolysis as in the original wood (48.8% C and 6.15% H).

5. The wood carbohydrates largely enter aqueous solution in polymer form. After additional hydrolysis with 5% sulfuric acid the reducing power of the aqueous hydrolyzates was increased by a factor of 4-5.

6. Xylose is the predominating sugar in the aqueous hydrolyzates of oakwood; we also found that they contained traces of galactose and arabinose. No mannose was found at all in oakwood.

7. The percentage of readily hydrolyzable reducing substances in wood hydrolyzates drops gradually as the water extraction is repeated, only traces of these substances being left after 500 hours of extraction.

8. Anatomical investigation and microchemical reactinns of cross sections have shown that the prolonged extraction with water involves intensive leaching out of the constituents of the wood, not only in the surface layers of the cells, but also to a considerable degree in the internal portions of the cells as well. Measurements of the libriform have shown that its walls had grown 72% thinner after 1000 hours of extraction with water (the cell cavities, on the other hand, growing wider) than the walls of the libriform cells that had not been extracted with water.

LITERATURE CITED

[1] A.D.Mishin. The Hydrolysis of Birchwood to Produce Crystalline Xylose.

Sverdlovsk (1942).

[2] V.I.Sharkov. Hydrolytic Production, II, 119 (1948)

[3] Overbeck and Müller, Ber., 75, 547 (1942).

[4] V.I.Sharkov. Op.cit., I, 180 (1945).

[5] L.P.Zherebov, Zubkova-Gitler and Zalmason. Trans. Inst. of Wood Chem., 2, 82 (1933).

[6] M.Kurbatov. Coll. Rep. Belorussian Inst. of Minsk, 17, 107 (1945).

[7] Aranovsky and Gortner, quoted in Sharkov, op.cit., II, 117 (1948).

[8] F.Schutz and P.Sarten, Cellulosechemie, 4 (1944).

[9] Nikitin, Rudneva, Zaitseva, and Chochieva, J.Appl.Chem. 22, 67 (1949).

[10] Freudenberg, Anal., 433 230 (1923); Z.Angew.Chem. 38, 280 (1925).

[11] Freeman and Peterson, Ind. Eng. Chem., 13, 803 (1941).

[12] N.Ya.Demyanov and N.D.Pryanishnikov. General Methods of Analysis of Vegetable Substances, 262 (1934).

[13] V.I.Sharkov. Op.cit., I, 40 (1945).

[14] Tollens-Elsner. Short Handbook of the Chemistry of the Carbohydrates, 153 (1938).

[15] L.Wise, F.Peterson, Ind.Eng.Chem. 22, 362 (1930).

[16] N.Ya.Demyanov and N.D.Pryanishnikov. Op.cit., 122 (1934).

[17] Schorger, Ind.Eng.Chem. 9, 748 (1917).

[18] Kiesel and Simiganovsky, Ber., 60, 332 (1927).

[19] N.Ya.Solechnik. The Hydrolysis of Wood, 146 (1933).

[20] Hägglund. Holzchemie. 113 (1939).

[21] L.I.Ivanov. The Anatomy of Plants, 111 (1939).

[22] S.I.Vanin. Trans. Academy of Forestry, 67, 185 (1949).

Received August 7, 1950

THE POLYTHERM OF THE TERNARY SYSTEM $MgO-P_2O_5-H_2O$*

S. Ya. Shpunt, A. P. Belopolsky and M. N. Shulgina

Laboratory of Physicochemical Analysis of the

Scientific Research Institute for Fertilizers and Insectofungicides

Our preceding report set forth the results of our investigation of the $MgO - P_2O_5 - H_2O$ system at 25 and 80° [1].

To establish the temperature limits within which the various crystal hydrates of monomagnesium phosphate can exist when in contact with phosphoric acid solutions we plotted the following isotherms: 0, 10, 50, and 58°. As we shall see below, invariant points with three saturated solid phases at the bottom occur at temperatures of 10 and 58°.

EXPERIMENTAL

50° isotherm We investigated this isotherm at P_2O_5 concentrations ranging from 1.3 to 63.7%. Our results are listed in Table 1 and shown in Fig. 1. As the

TABLE 1

$MgO - P_2O_5 - H_2O$ System. 50° Isotherm

Points	Percentage in the solution by weight		Per cent neutralization	Percentage in the "residues" by weight		Percentage in the washed precipitate by weight		Solid phases
	MgO	P_2O_5		MgO	P_2O_5	MgO	P_2O_5	
1	0.4	1.3	–	–	–	–	–	
2	1.6	6.0	95.3	–	–	–	–	
3	2.6	9.3	98.8	22.6	41.0	–	–	$MgHPO_4 \cdot 3H_2O$
4	4.6	16.8	96.4	–	–	23.0	42.0	
5	7.0	27.2	90.8	22.4	41.1	–	–	
A	8.9	37.3	83.9	19.7	42.1	–	–	$MgHPO_4 \cdot 3H_2O + Mg(H_2PO_2)_2 \cdot 4H_2O$
6	8.3	39.6	73.7	13.2	48.8	14.3	49.3	$Mg(H_2PO_4)_2 \cdot 4H_2O$
A_1	7.2	41.8	60.8	14.0	51.8	14.7	53.3	$Mg(H_2PO_4)_2 \cdot 4H_2O + Mg(H_2PO_4)_2 \cdot 2H_2O$
7	5.0	53.4	32.9	15.3	55.3	–	–	$Mg(H_2PO_4)_2 \cdot 2H_2O$
A_2	3.9	57.5	23.8	–	–	–	–	$Mg(H_2PO_4)_2 \cdot 2H_2O + Mg(H_2PO_4)_2$
8	2.2	62.7	12.3	9.0	64.4	–	–	
9	1.5	63.7	8.3	8.4	64.6	–	–	$Mg(H_2PO_4)_2$

*Report II of a series on physical and chemical investigations of magnesium phosphates.

figure shows, the isotherm consists of the following saturation branches: 1) $MgHPO_4 \cdot 3H_2O$; 2) $Mg(H_2PO_4)_2 \cdot 4H_2O$; 3) $Mg(H_2PO_4)_2 \cdot 2H_2O$; 4) $Mg(H_2PO_4)_2$. Dimagnesium phosphate trihydrate saturates the solutions containing up to 37.3% P_2O_5, its branch coinciding with the corresponding branches for the 25 and 80° isotherms. This is followed by a short branch representing saturation with monomagnesium phosphate tetrahydrate, extending from 37.3% to 41.8% P_2O_5. The branch representing monomagnesium phosphate dihydrate extends from 41.8% to 57.5% P_2O_5. In the region of higher concentrations, anhydrous dimagnesium phosphate is in equilibrium with the solutions.

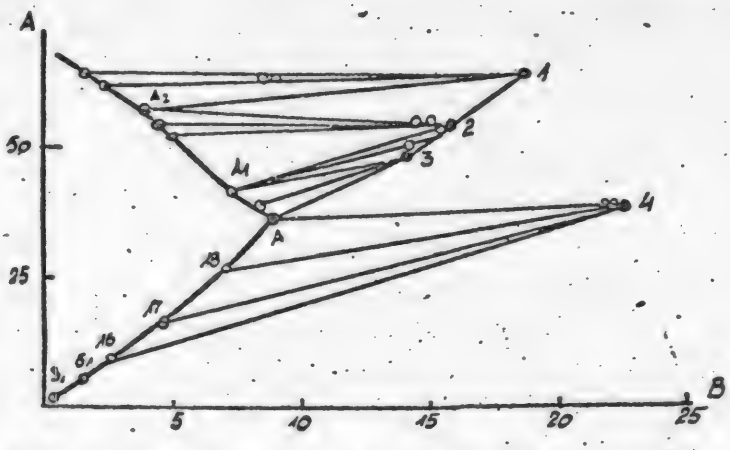

Fig. 1. The MgO – P_2O_5 – H_2O System. 50° Isotherm.

A-% P_2O_5; B-Percent MgO. 1-$Mg(H_2PO_4)_2$; 2-$Mg(H_2PO_4)_2 \cdot 2H_2O$; 3-$Mg(H_2PO_4)_2 \cdot 4H_2O$, 4-$MgHPO_4 \cdot 3H_2O$.

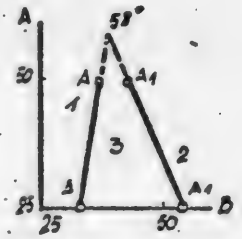

Fig. 2. Extrapolation of the invariant point.

A-Temperature °C; B-% P_2O_5;
1-$MgHPO_4 \cdot 3H_2O$;
2-$Mg(H_2PO_4)_2 \cdot 2H_2O$,
3-$Mg(H_2PO_4)_2 \cdot 4H_2O$.

When we compare this figure with the isotherms for 25 and 80° [1], we find that the region in which the monomagnesium phosphate tetrahydrate exists has been shortened considerably; on the other hand, the branch for the crystallization of monomagnesium phosphate dihydrate has increased perceptibly, in contrast with the 25 and 80° isotherms. The respective figures are compared in the following table.

Isotherm	Range in which $Mg(H_2PO_4)_2 \cdot 4H_2O$ exists – % P_2O_5
25°	33.1-53.3
50	37.3-41.8

The shortening of the tetrahydrate branch was natural, since the rise in temperature evidently ought to entail an increase in the dehydrating action of the phosphoric acid upon the crystal hydrates of the monomagnesium phosphate.

The approximate temperature and composition of the invariant point with three saturated solid phases: $MgHPO_4 \cdot 3H_2O$ + $Mg(H_2PO_4)_2 \cdot 4H_2O$ + $Mg(H_2PO_4)_2 \cdot 2H_2O$ can be found by extrapolating the data cited. As we see in Fig. 2, linear extrapolation gives the temperature as 58° and the P_2O_5 concentration as 40%. Above 58°, the isotherms of the MgO – P_2O_5 – H_2O system must consist of the saturation branches $MgHPO_4 \cdot 3H_2O$, $Mg(H_2PO_4)_2 \cdot 2H_2O$, and $Mg(H_2PO_4)_2$, which agrees with the direct investigation of the 80° isotherm,[1].

58° Isotherm. To fix the temperature and the composition of the liquid phase at the invariant point $A_{58°}$, above which monomagnesium phosphate tetrahydrate is no longer in stable equilibrium with phosphoric acid solutions, we made

the appropriate experimental determinations. Large excesses of dimagnesium phosphate trihydrate and of monomagnesium phosphate tetra- and dihydrates were added to a solution containing about 40% P_2O_5 and 9.5% MgO. The suspension was agitated for a long time (7 days) in a thermostat at 58°.

Once equilibrium was attained, as was carefully checked by means of repeated samples taken from the liquid phase and by microscopic examination of the precipitate, we found that all three of the solid phases introduced into the vessel were present at the bottom. Therefore, the figures obtained by rough extrapolation coincided with the results of direct experiment: 58° actually is the temperature of the invariant point $A_{58°}$, with the solid phases: $MgHPO_4 \cdot 3H_2O$ + $Mg(H_2PO_4)_2 \cdot 4H_2O$ + + $Mg(H_2PO_4)_2 \cdot 2H_2O$.

The equilibrium composition of the solution at this point is given by the following data: 9.5% MgO and 38.5% P_2O_5.

Interpolating between the 50° and 80° isotherms, we found that the the junction point A_2, where the 58° isotherm meets the solid phases: $Mg(H_2PO_4)_2 \cdot 2H_2O$ + + $Mg(H_2PO_4)_2$, the solution contains 4.5% MgO and 58% P_2O_5. We also determined several other intermediate points along the lines of saturation of the anhydrous monomagnesium phosphate and its dihydrate by interpolation. As for the branch representing saturation with dimagnesium phosphate, it is almost certain that it practically coincides with the corresponding branch in the 25, 50, and 80° isotherms, where this coincidence has been proved experimentally.

The experimental and interpolation values are listed in Table 2, while the 58° isotherm is plotted in Fig. 3.

TABLE 2

$MgO - P_2O_5 - H_2O$ System. +58° Isotherm.

Points	Percentage by weight in solution		Per cent neutralization	Solid phases
	MgO	P_2O_5		
1	0.4	1.3	–	
2	1.6	6.0	95.3	
3	2.6	9.3	98.3	$MgHPO_4 \cdot 3H_2O$
4	4.6	16.8	96.4	
5	7.0	27.2	90.8	
$A_{58°}$	9.5	38.5	82.7	$MgHPO_4 \cdot 3H_2O + Mg(H_2PO_4)_2 \cdot 4H_2O +$ $+ Mg(H_2PO_4)_2 \cdot 2H_2O$.
6	6.3	50.0	44.4	$Mg(H_2PO_4)_2 \cdot 2H_2O$
7	5.1	55.0	32.5	
A_2	4.5	58.0	27.2	$Mg(H_2PO_4)_2 \cdot 2H_2O + Mg(H_2PO_4)_2$
8	3.3	60.0	19.3	$Mg(H_2PO_4)_2$
9	2.1	63.0	11.7	

10° Isotherm. Comparison of the 80, 58, 50, and 25° isotherms discloses an interesting peculiarity of the system in question. As will be shown below, the P_2O_5 concentration range within which monomagnesium phosphate dihydrate is in equilibrium with the solutions is diminished when the temperature is lowered below 58° as well as when it is raised above that point, which might have been expected.

The foregoing becomes particularly obvious when we examine Fig. 4, where these concentration ranges are plotted as a function of temperature. The graph

Isotherm	Range in which $Mg(H_2PO_4)_2 \cdot H_2O$ exists – % P_2O_5
80°	44.8-56.5
58	38.5-58.0
50	41.8-57.5
25	53.3-59.6

shows that the dihydrate branch is longest at the invariant temperature of 58°. The perceptible shortening of the dihydrate branch on either side of 48° forces us to assume that there are two limits between which this salt is in stable equilibrium with phosphoric acid solutions.

1) An upper limit, where there is an invariant point with the solid phases: $MgHPO_4 \cdot 3H_2O + Mg(H_2PO_4)_2 \cdot 2H_2O + Mg(H_2PO_4)_2$ – above this temperature the regions of saturation of the dimagnesium phosphate and the anhydrous monomagnesium phosphate adjoin each other; and 2) a lower limit, where there is an invariant point with the solid phases $Mg(H_2PO_4)_2 \cdot 4H_2O + Mg(H_2PO_4)_2 \cdot 2H_2O + Mg(H_2PO_4)_2$ – below this point the regions of saturation of the tetrahydrate and the anhydrous monomagnesium phosphate must be in direct contact with each other.

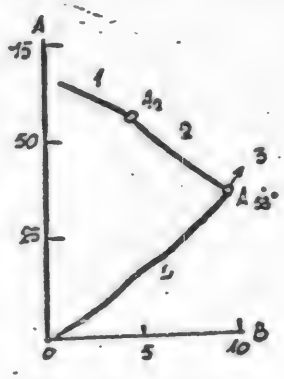

Fig. 3. $MgO - P_2O_5 - H_2O$ System. +58° isotherm.

A-% P_2O_5; B-% MgO. 1-$Mg(H_2PO_4)_2$; 2-$Mg(H_2PO_4)_2 \cdot 2H_2O$; 3-$MgHPO_4 \cdot 3H_2O$ + $Mg(H_2PO_4)_2 \cdot 4H_2O$ + $Mg(H_2PO_4)_2 \cdot 2H_2O$; 4-$MgHPO_4 \cdot 3H_2O$.

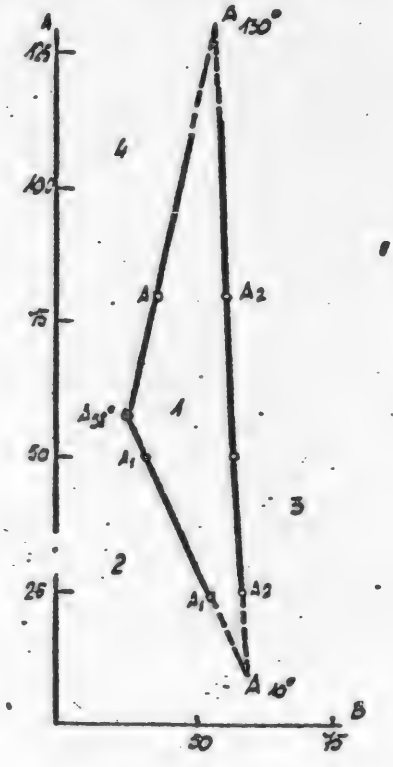

Fig. 4. Extrapolation of the invariant point.

A-Temp. °C; B-% P_2O_5.
1-$Mg(H_2PO_4)_2 \cdot 2H_2O$; 2-$Mg(H_2PO_4)_2 \cdot 4H_2O$; 3-$Mg(H_2PO_4)_2$; 4-$MgHPO_4 \cdot 3H_2O$.

The existence of the upper limit is quite natural. As the temperature is raised, a point must be reached at which the vapor pressure of the saturated water vapor above the phosphoric acid solution, which is in equilibrium with the anhydrous monomagnesium phosphate and its dihydrate, attains a value that equals the dissociation pressure of the system:

$$Mg(H_2PO_4)_2 \cdot 2H_2O \rightleftarrows Mg(H_2PO_4)_2 + 2H_2O.$$

Above this temperature the monomagnesium dihydrate is no longer stable when in contact with the phosphoric acid solution, and the branch representing the

anhydrous monomagnesium phosphate intersects the dimagnesium phosphate branch directly.

What is unusual is the presence of the lower limit, which corresponds to equilibrium of the two crystal hydrates and the anhydrous form of the same salt. At any rate, we have not come across an instance of this sort in the literature. As a rule, a change in temperature results in the successive hydration or dehydration of the crystal hydrates, any given crystal hydrate not appearing (or disappearing) as a stable phase before its neighbor on the scale of crystallization water appears (or disappears). Moreover, in this case, the order in which the crystal hydrates of monomagnesium phosphate appear as the temperature is gradually lowered is as follows:

$$Mg(H_2PO_4)_2$$

$$Mg(H_2PO_4)_2 + Mg(H_2PO_4)_2 \cdot 2H_2O$$

$$Mg(H_2PO_4)_2 + Mg(H_2PO_4)_2 \cdot 2H_2O + Mg(H_2PO_4)_2 \cdot 4H_2O$$

$$Mg(H_2PO_4)_2 + Mg(H_2PO_4)_2 \cdot 4H_2O$$

Extrapolation of the curve in Fig. 4 demonstrates that the lower limit at which monomagnesium phosphate dihydrate exists is located at 10° and a P_2O_5 concentration of 59%.

TABLE 3

$MgO - P_2O_5 - H_2O$ System. +10° Isotherm.

Points	Per cent by weight in solution		Per cent neutralization	Per cent by weight in "residues"		Solid phases
	MgO	P_2O_5		MgO	P_2O_5	
1	1.8	6.2	98.3	–	–	$MgHPO_4 \cdot 3H_2O$
2	4.7	16.8	98.6	–	–	
A	8.2	31.0	93.2	–	–	$MgHPO_4 \cdot 3H_2O + Mg(H_2PO_4)_2 \cdot 4H_2O$
3	4.4	50.5	30.6	10.5	49.0	
4	3.9	54.5	25.1	–	–	$Mg(H_2PO_4)_2 \cdot 4H_2O$
5	3.4	57.5	20.9	12.0	56.2	
$A_{10°}$	3.2	58.9	19.2	–	–	$Mg(H_2PO_4)_2 \cdot 4H_2O + Mg(H_2PO_4)_2 \cdot 2H_2O + Mg(H_2PO_4)_2$.
6**	0.4	62.0	2.3	5.9	64.1	
7	0.3	63.8	1.7	4.8	65.4	$Mg(H_2PO_4)_2$

We checked these figures by making an experimental investigation of the 10° isotherm. Our results are given in Table 3 and Fig. 5. The point $\underline{A}_{10°}$, at which the solution ought to be in equilibrium with all three forms of the monomagnesium phosphate: $Mg(H_2PO_4)_2 + Mg(H_2PO_4)_2 \cdot 2H_2O + Mg(H_2PO_4)_2 \cdot 4H_2O$ according to our extrapolation, was plotted with especial care. The experimental results were in good agreement with the extrapolated value. The composition of the solution at the invariant point $\underline{A}_{10°}$ is as follows: 3.2% MgO; 58.9% P_2O_5.

After prolonged agitation in the thermostat, all the three phases:

$$Mg(H_2PO_4)_2 \cdot 4H_2O + Mg(H_2PO_4)_2 \cdot 2H_2O + Mg(H_2PO_4)_2,$$

were found in the bottom phase.

Evidently, the saturated water vapor pressure above this solution is the same as the dissociation pressure for the systems:

* The $Mg(H_2PO_4)_2 \cdot 2H_2O$ introduced as an additive was converted into $Mg(H_2PO_4)_2 \cdot 4H_2O$.

** The $Mg(H_2PO_4)_2 \cdot 2H_2O$ introduced as an additive was converted into $Mg(H_2PO_4)_2$.

1) $Mg(H_2PO_4)_2 \cdot 4H_2O \rightleftarrows Mg(H_2PO_4)_2 + 4H_2O$
2) $Mg(H_2PO_4)_2 \cdot 2H_2O \rightleftarrows Mg(H_2PO_4)_2 + 2H_2O$
3) $Mg(H_2PO_4)_2 \cdot 4H_2O \rightleftarrows Mg(H_2PO_4)_2 \cdot 2H_2O + 2H_2O$.

The singularity of this result forced us to make a particularly careful investigation of the composition of the solid phases in the vicinity of the invariant point $A_{10°}$. An excess of monomagnesium phosphate dihydrate was added to a solution containing about 57% P_2O_5 and 3.5% MgO. After three days had elapsed, all the dihydrate had been converted into the tetrahydrate, as was proved by the Schreinemakers residue method and by microscopic examination of the precipitate. The dihydrate added to a solution containing about 62% P_2O_5 and 0.5% MgO, on the other hand was converted into the anhydrous monomagnesium phosphate within three days (Table 3). This is convincing proof that the lower limit at which the dihydrate can exist actually exists and that below 10° the saturation regions of the tetrahydrate and the anhydrous salt directly adjoin each other.

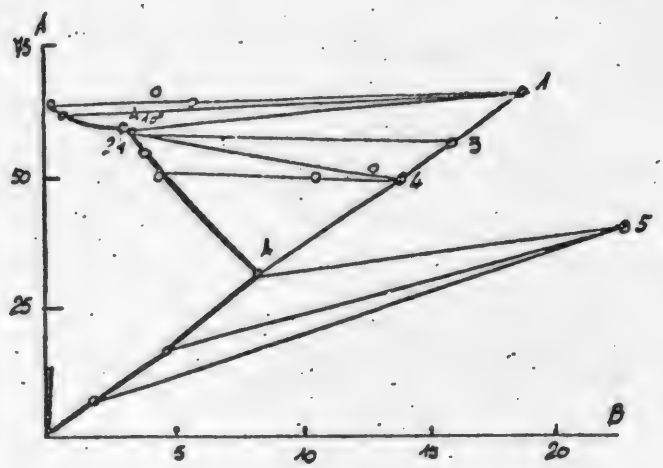

Fig. 5. MgO – P_2O_5 – H_2O System. 10° isotherm.

A-% P_2O_5; B-% MgO. 1-$Mg(H_2PO_4)_2$; 2-$Mg(H_2PO_4)_2 \cdot 4H_2O$ + + $Mg(H_2PO_4)_2 \cdot 2H_2O$ + $Mg(H_2PO_4)_2$; 3-$Mg(H_2PO_4)_2 \cdot 2H_2O$; 4-$Mg(H_2PO_4)_2 \cdot 4H_2O$; 5-$MgHPO_4 \cdot 3H_2O$.

To obtain further confirmation we made an investigation of the 0° isotherm.

0° Isotherm. The results of our investigation of the MgO – P_2O_5 – H_2O system at 0° are given in Table 4 and Fig. 6. In accordance with what has been set forth above, the 0° isotherm consists of three saturation branches: 1) $MgHPO_4 \cdot 3H_2O$; 2) $Mg(H_2PO_4)_2 \cdot 4H_2O$; and 3) $Mg(H_2PO_4)_2$. The absence of the dihydrate in the bottom phase was proved by microscopic examination and by the residue method.

The branch representing dimagnesium phosphate trihydrate was plotted in the range of 6.5 to 29.5% P_2O_5. At the latter concentration we reach the junction point A, where the solution is saturated with two salts: $MgHPO_4 \cdot 3H_2O$ + $Mg(H_2PO_4)_2 \cdot 4H_2O$. In the interval from 29.5% to 58.4% P_2O_5, the solutions were saturated with monomagnesium phosphate tetrahydrate, while at higher phosphoric acid concentrations the anhydrous monomagnesium phosphate is in equilibrium with the solutions. It has thus been demonstrated by direct experiment that the junction points A_3 actually exist below 10°, at which the solution is in equilibrium with the anhydrous monomagnesium phosphate and its tetrahydrate (Fig. 6).

130° Isotherm. Extrapolation of the curve in Fig. 4 yields the approximate location of the invariant point $A_{130°}$, where the monomagnesium phosphate dihydrate is no longer in equilibrium with phosphoric acid solutions. This extrapolation shows that this point, with the solid phases $MgHPO_4 \cdot 3H_2O$ + $Mg(H_2PO_4)_2 \cdot 2H_2O$ + $Mg(H_2PO_4)_2$ is located at 130°.

Our extrapolation is justifiable only if the hydration of the dimagnesium phosphate at 130° is the same as at lower temperatures. As Graham and Schiffer have pointed out [2], when dimagnesium phosphate trihydrate is heated in the

TABLE 4

$MgO - P_2O_5 - H_2O$ System. 0° Isotherm.

Points	Per cent by weight in solution		Per cent neutralization	Solid phases
	MgO	P_2O_5		
1	1.9	6.3	–	$MgHPO_4 \cdot 3H_2O$
2	4.6	16.5	98.2	
A	8.0	29.5	95.5	$MgHPO_4 \cdot 3H_2O + Mg(H_2PO_4)_2 \cdot 4H_2O$
3	4.4	49.6	31.3	$Mg(H_2PO_4)_2 \cdot 4H_2O$
4	3.9	52.5	26.1	
5	4.1	53.2	27.0	
A_3	3.1	58.4	19.4	$Mg(H_2PO_4)_2 \cdot 4H_2O + Mg(H_2PO_4)_2$
6	2.2	59.7	12.9	$Mg(H_2PO_4)_2$
7	0.4	62.6	2.2	
8	0.4	64.8	2.1	

TABLE 5

$MgO - P_2O_5 - H_2O$ System. 130° Isotherm

Points	Per cent by weight in solution		Per cent neutralization	Solid phases
	MgO	P_2O_5		
1	0.8	3.0	93.3	$MgHPO_4 \cdot 3H_2O$
2	3.1	10.6	–	
3	4.9	18.5	93.5	
4	6.8	26.1	91.5	
5	8.0	31.3	90.0	
6	9.6	39.4	85.8	
$A_{130°}$	12.7	54.0	82.7	$MgHPO_4 \cdot 3H_2O + Mg(H_2PO_4)_2 \cdot 2H_2O + Mg(H_2PO_4)_2$
7	6.2	60.0	36.3	$Mg(H_2PO_4)_2$
8	4.1	63.0	22.8	

TABLE 6

Invariant Points of the $MgO - P_2O_5 - H_2O$ System

Points	Temperature, °C	Per cent by weight in solution		Solid phases
		MgO	P_2O_5	
$A_{58°}$	58	9.5	38.5	$MgHPO_4 \cdot 3H_2O + Mg(H_2PO_4)_2 \cdot 4H_2O + Mg(H_2PO_4)_2 \cdot H_2O$
$A_{10°}$	10	3.2	58.9	$Mg(H_2PO_4)_2 \cdot 4H_2O + Mg(H_2PO_4)_2 \cdot 2H_2O + Mg(H_2PO_4)_2$
$A_{130°}$	130	12.7	54.0	$MgHPO_4 \cdot 3H_2O + Mg(H_2PO_4)_2 \cdot 2H_2O + Mg(H_2PO_4)_2$

absence of a solution, it loses its crystallization water only at 170°. It may be confidently asserted, therefore, that it is $MgHPO_4 \cdot 3H_2O$ that is in contact with the phosphoric acid solution at 130°. It follows that the polythermal curve demarcating the saturation regions of dimagnesium phosphate and monomagnesium phosphate dihydrate is continuous up to 130°. Extrapolation indicates that the

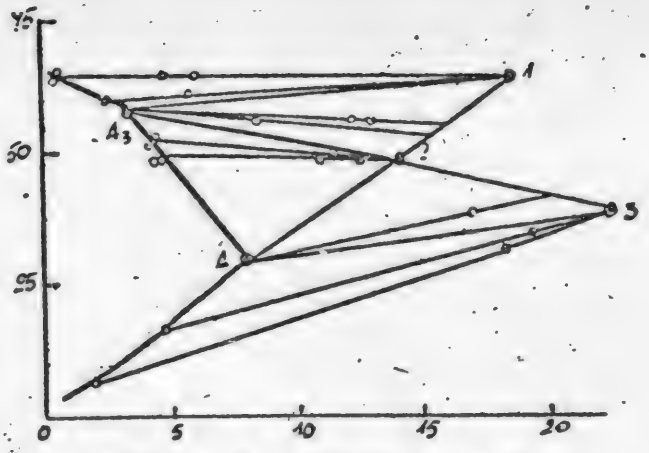

Fig. 6. $MgO - P_2O_5 - H_2O$ System. 0° Isotherm.

A-% P_2O_5; B-% MgO. 1-$Mg(H_2PO_4)_2$; 2-$Mg(H_2PO_4)_2 \cdot 4H_2O$; 3-$MgHPO_4 \cdot 3H_2O$.

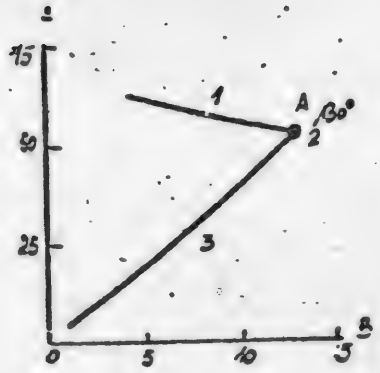

Fig. 7. $MgO - P_2O_5 - H_2O$ System. 130° Isotherm.

A-% P_2O_5; B-% MgO. 1-$Mg(H_2PO_4)_2$; 2-$MgHPO_4 \cdot 3H_2O$ + $Mg(H_2PO_4)_2 \cdot 2H_2O$ + $Mg(H_2PO_4)_2$; 3-$MgHPO_4 \cdot 3H_2O$.

composition of the solution at the invariant point $A_{130°}$ is 12.7% MgO and 54.0% P_2O_5. We likewise found the compositions of the solutions along the $MgHPO_4 \cdot 3H_2O$ and $Mg(H_2PO_4)_2$ branches by extrapolation (Table 5). The 130° isotherm is shown in Fig. 7.

Polytherm of the ternary system $MgO - P_2O_5 - H_2O$. Once we possess the solution compositions at the junction points of the following isotherms: 0, 10, 25, 50, 58, 80, and 130°, we can plot the complete polytherm of the $MgO - P_2O_5 - H_2O$ system over that temperature range. The vertical projections of the polytherm on the % P_2O_5 – 0 – t° and MgO – 0 – t° coordinate planes are shown in Fig. 8. The projection on the % P_2O_5 – 0 – t° plane, where the saturation regions are not superposed on each other, is the clearer of the two. In the vertical projection on the % Mg – 0 – t° plane, the regions of the various crystal hydrates of monomagnesium phosphate are shown against the "background" of the dimagnesium phosphate trihydrate's region. This region is nearly flat and is perpendicular to the horizontal plane of projection. As a result, the isothermal branches representing saturation with dimagnesium phosphate practically coincide within the temperature range investigated.

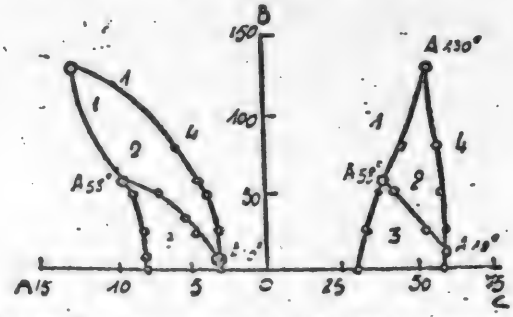

Fig. 8. Polytherm of the $MgO - P_2O_5 - H_2O$ System.

A-% MgO; B-Temp. °C; C-% P_2O_5. 1-$MgHPO_4 \cdot 3H_2O$; 2-$Mg(H_2PO_4)_2 \cdot 2H_2O$. 3-$Mg(H_2PO_4)_2 \cdot 4H_2O$. 4-$Mg(H_2PO_4)_2$.

SUMMARY

1. The 0, 10, 50, 58, and 130° isotherms of the ternary system $MgO - P_2O_5 - H_2O$ have been plotted experimentally, as well as by interpolation and extrapolation, it being found that dimagnesium phosphate crystallizes out of phosphoric acid solutions in the 0-130° temperature range as the crystal trihydrate.

2. The monomagnesium phosphate exists in the form of two crystal hydrates: $Mg(H_2PO_4)_2 \cdot 4H_2O$ and $Mg(H_2PO_4)_2 \cdot 2H_2O$, and the anhydrous salt $Mg(H_2PO_4)_2$ in this same temperature range.

The upper limit at which the tetrahydrate is stable is 58°. The dihydrate is in stable equilibrium with the solution from 10 to 130°. The anhydrous salt is stable throughout the investigated temperature range.

3. Three invariant points, with three solid phases at the bottom, have been found between 0 and 130°; the compositions of the liquid and solid phases at these points is given in Table 6.

4. The data obtained have been used to plot the polytherm of the $MgO - P_2O_5 - H_2O$ system from 0° to 130°.

LITERATURE CITED

[1] A.P.Belopolsky, S.Ya.Shpunt and M.N.Shulgina, J.Appl.Chem. 23, 8, (1950).*

[2] Graham and Schiffer, Gmellin. Handbuch.d.anorg.Chem., 27 (B), (403) (1937).

Received November 15, 1949.

---

*See CB translation p. 879 ff.

BLANK
PAGE

THE KINETICS OF THE ABSORPTION OF CARBON DIOXIDE BY SOLUTIONS OF SODIUM HYDROXIDE IN A HIGH-SPEED PROPELLER AGITATOR

M. Kh. Kishinevsky and M. A. Kerdivarenko

Laboratory of Physical Chemistry, Kishinev State University

In many research papers devoted to a study of the absorption processes that involve chemical reactions, apparatus is employed in which the absorption process takes place under conditions that are far from those employed industrially. The apparatus is often fitted with an agitator that provides very weak stirring, at which the surface of separation remains mirror-smooth. Such process conditions are quite artificial, however, since in industrial absorption installations the process is carried out with stirring of the separation surface as well as of the entire volume. For this reason, there is little justification for the application of the laws found to govern these artificial setups to actual industrial processes.

The present paper is a report of research on the process of absorbing carbon dioxide by solutions of sodium hydroxide, using a high-speed propeller agitator. The surface separating the phases was kept constant in the various tests by using the method worked out by Kishinevsky and Pamphilov [1], based on keeping the solution viscosity constant by combined selection of the temperature and solution concentration. This method eliminates the need for knowing the magnitude of the surface of separation and makes it possible to study a system under any desired hydrodynamic conditions.

EXPERIMENTAL

The layout of the apparatus is shown in Fig. 1.

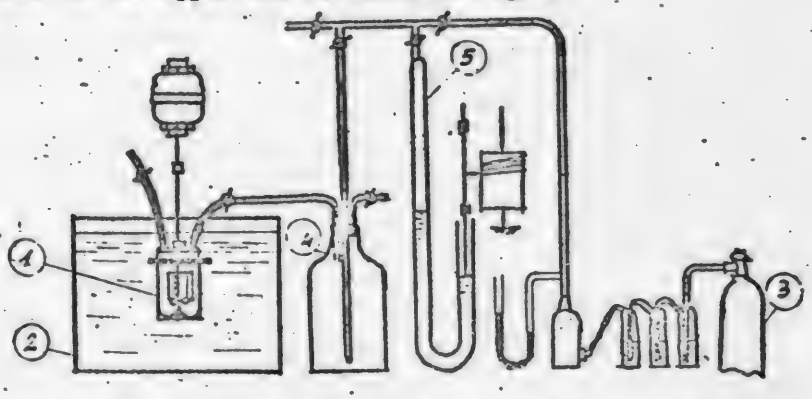

Fig. 1. Layout of experimental apparatus.

1-Propeller agitator; 2-thermostat; 3-gas tank; 4-buffer vessel; 5-gas buret.

The carbon dioxide was absorbed by alkali solutions in the 1-liter cylindrical propeller agitator 1, made of steel and immersed in the water thermostat 2. The temperature was kept constant within ±0.05°C up to 40°C and within ±0.1°C from 40 to 70°C. The agitator was equipped with a diffuser and fitted with four longitudinal ribs to prevent the formation of eddies at high propeller speed. The propeller, located in the lower section of the diffuser, forced the liquid upward in four symmetrical streams into the spaces between the ribs.

The source of the gas was the tank 3, from which the gas passed through three wash bottles containing strong sulfuric acid and an 11-liter buffer bottle before reaching the agitator. Prior to every run, the whole system ahead of the agitator was subjected to a careful checkup. The agitator itself was separately blown out before the motor was turned on. The blow-off conditions remained the same for all the tests.

The float in the open elbow of the gas buret 5 was attached to a needle which recorded the rate at which a vacuum was formed on a soot-covered recording cylinder that was rotated by a synchronous motor at a speed of 60 rpm.

The accuracy of the adopted method of recording the rate was tested by a cinematographic method; the rate at which the meniscus of the sealing liquid in the open elbow dropped was photographed on film at a speed of 4 frames per second.

TABLE 1

Rate of Absorption of CO_2 by NaOH Solutions at 1800 Propeller Rpm

Concentration of the NaOH solutions at the test temp., gram-equiv/liter	Solution temperature, °C	CO_2 partial pressure, atm	Solubility of CO_2 in NaCl solutions at a partial pressure of 1 atm	Absorption rate, moles/min	Absorption rate corrected for a CO_2 partial pressure of 1 atm
0.10	14.2	0.955	0.0470	0.065	0.068
0.40	16.5	0.940	0.0399	0.095	0.096
0.90	20.5	0.935	0.0316	0.133	0.142
1.60	26.9	0.926	0.0242	0.173	0.187
1.96	30.5	0.917	0.0198	0.188	0.206
2.60	35.0	0.905	0.0157	0.211	0.234
2.96	40.0	0.894	0.0131	0.221	0.247
4.00	50.0	0.856	0.0084	0.232	0.271
5.00	59.4	0.805	0.00475	0.228	0.283

600 ml of solution was poured into the agitator. So large a quantity of absorbent ensued that the rate at which a vacuum was produced remained constant for a period of time that exceeded the period during which the rate was recorded on the rotating cylinder, even at a solution concentration of 0.1 N. This made it unnecessary to extrapolate the rate back to the start.

The temperature and the solution concentration were so chosen as to keep the viscosity constant through the tests at 1.20 centipoises.

Conversion of the readings on the recording device into moles/min of CO_2 absorbed was done on the basis of the system volume, the gas temperature in the system, and the outside pressure.

Two series of tests were made. The first set was run at 1800 rpm of the propeller, the second being run at 1200 rpm.

The results of the first and second series of tests are given in Tables 1 and

TABLE 2

Rate of Absorption of CO_2 by NaOH Solutions at 1200 Propeller Rpm

Concentration of the NaOH solutions at the test temp., gram-equiv/liter	Solution temperature, °C	CO_2 partial pressure, atm	Solubility of CO_2 in NaCl solutions at partial pressure of 1 atm	Absorption rate, moles/min	Absorption rate corrected for a CO_2 partial pressure of 1 atm
0.10	14.2	0.955	0.0470	0.0104	0.0109
0.40	16.5	0.940	0.0399	0.0202	0.0215
0.90	20.5	0.935	0.0316	0.0325	0.0348
1.60	26.9	0.926	0.0242	0.0454	0.0490
1.96	30.5	0.917	0.0196	0.0502	0.0548
2.60	35.0	0.903	0.0157	0.0578	0.0639
2.96	40.0	0.894	0.0131	0.0618	0.0681
3.60	46.1	0.875	0.0101	0.0677	0.0774
4.00	50.0	0.856	0.0085	0.0707	0.0826
5.00	59.4	0.805	0.0047	0.0746	0.0926
6.04	69.5	0.741	–	0.0726	0.0980

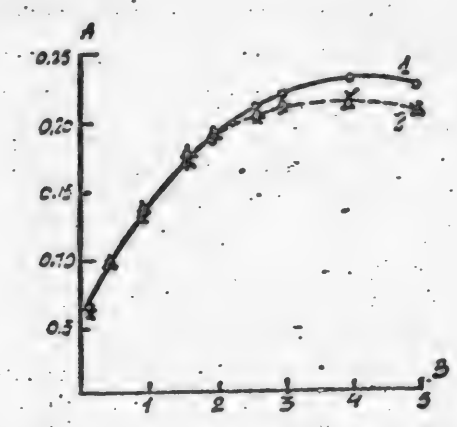

Fig. 2. Rate of absorption of CO_2 by NaOH solutions of varying concentration in a propeller agitator at 1800 rpm.

A-CO_2 absorption rate, moles/min.; B-concentration of NaOH solutions, moles/liter.

1-Experimental curve; 2-curve plotted computationally.

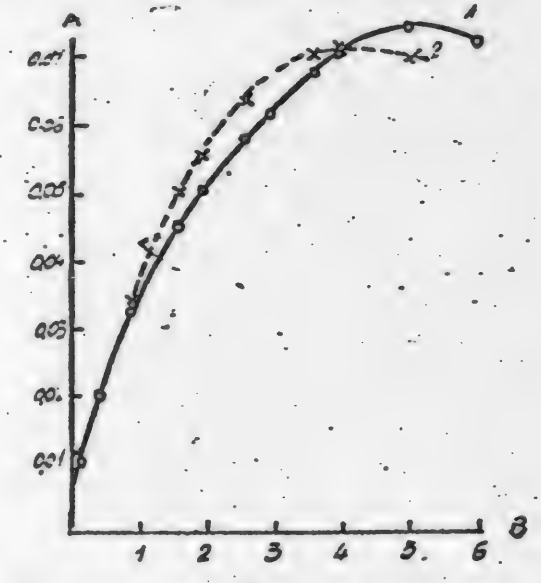

Fig. 3. Rate of absorption of CO_2 by NaOH solutions of varying concentration in a propeller agitator at 1200 rpm.

A-CO_2 absorption rate, moles/min; B-concentration of NaOH solutions, moles/liter.

1-Experimental curve; 2-curve plotted computationally.

2. The listed data represent the mean values of several runs. The error did not exceed 2%.

The experimental data are represented by the solid lines in Figs. 2 and 3.

EVALUATION OF RESULTS

These experimental results were worked up on the basis of the equation put forward by Kishinevsky for the kinetics of absorption in absorption processes that

involve first-order reactions:

$$\frac{d\omega}{\sigma d\tau} = \frac{mc\left[1 - e^{-\left(P - \frac{d\omega}{\sigma d\tau}\beta\right) HK_c\Delta\tau}\right] + HP}{\frac{1}{V_n} + \frac{H}{\beta}} . \qquad (1)$$

In the process under study the chemical reaction involved is of the second order. The concentration of free molecules of the gas in the surface layer may be taken as constant, however, owing to the minuteness of $\Delta\tau$ at high propeller speed.

Inasmuch as we do not know the size of the phase separation surface during the tests, the experimental data are referred to the overall surface of separation, so that Equation (1) is rewritten as

$$\frac{d\omega}{d\tau} = \frac{mc\left[1 - e^{-\left(P - \frac{d\omega}{\sigma d\tau}\beta\right) HK_c\Delta\tau}\right] + HP}{\frac{1}{V_\sigma} + \frac{H}{\beta_\sigma}} , \qquad (2)$$

where $\frac{d\omega}{d\tau}$ is the rate of absorption per unit time; m is the stoichiometric coefficient of the reaction; c is the concentration of the chemsorbent; P is the partial pressure of the absorbed gas; H is the solubility of the gas; $\Delta\tau$ is the period during which the surface of separation is renewed; K_c is the specific reaction rate; β_σ is the hydrodynamic constant of the gas phase: $\beta_\sigma = \beta \cdot \sigma$; V_σ is the hydrodynamic constant of the liquid phase: $V_\sigma = V_n \cdot \sigma$; V_n is the hydrodynamic constant of the liquid phase, equaling the linear velocity of mass flow normal to the surface of separation.

The applicability of Equation (2) to the experimental data secured at 1800 propeller rpm was confirmed by computing the activation energy of the reaction between carbon dioxide and hydroxyl ions.

Inasmuch as the physical solubility of carbon dioxide in solutions of sodium hydroxide, which is a factor in Equation (2), is unknown, we employed the values of H for sodium chloride solutions of corresponding concentrations. It is obvious that this assumption must result in increasing discrepancies as the concentration of sodium hydroxide is increased. The upper concentration limit at which this assumption is still permissible was established by comparing the experimental curve of the absorption rate recorded by Kishinevsky and Pamfilov [1], using an intensive agitation apparatus at 400 rpm, with the curve showing the rate of this same process, as calculated from Equation (2) on the basis of the hydrodynamic constants found in their experiments.

The discrepancy becomes perceptible at a concentration of 2 N. The pertinent data are listed in Table 3 and shown graphically in Fig. 4.

The rate of sorption was calculated as follows. We first determined the product $K_c \cdot \Delta\tau$ at a sodium hydroxide concentration of 0.4 N and the corresponding temperature (we shall henceforth denote this product by K) from the experimental value of the absorption rate at the given concentration and the experimental values of the hydrodynamic constants β_σ and V_σ. The values of K for other temperatures were determined from the equation

$$\log \frac{K}{K_{16.5°}} = \frac{E}{2.3R}\left(\frac{T - 289.7}{T \cdot 289.7}\right) , \qquad (3)$$

TABLE 3

Rate of Absorption of CO_2 by NaOH Solutions in an Intensive-Agitation Apparatus at 400 rpm

Concentration of NaOH solutions, gram-equiv/liter	Solution temperature, °C	CO_2 partial pressure, atm	Solubility of CO_2 in NaCl solutions at a partial pressure of 1 atm	Absorption rate, moles/min	
				Experimental	Computed
1.96	30.5	0.959	0.0198	0.122	0.122
2.97	39.6	0.935	0.0131	0.128	0.127
3.99	57.0	0.857	0.0058	0.125	0.122

in which the value of the activation energy was taken to equal that found by the same authors in the intensive-agitation apparatus at 400 rpm.

The absorption rates at other temperatures and concentrations were computed from Equation (2), in which all the parameters were now known.

As we see from Fig. 4, the discrepancy between the experimental absorption rates and those computed by the method

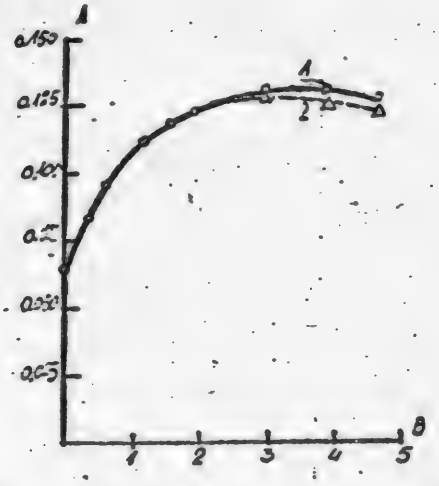

Fig. 4. Rate of absorption of CO_2 by NaOH solution of varying concentration in an intensive-agitation apparatus at 400 rpm.

A-CO_2 absorption rate, moles/min.; B-NaOH solution concentration, moles/liter. 1-Experimental curve; 2-curve plotted computationally.

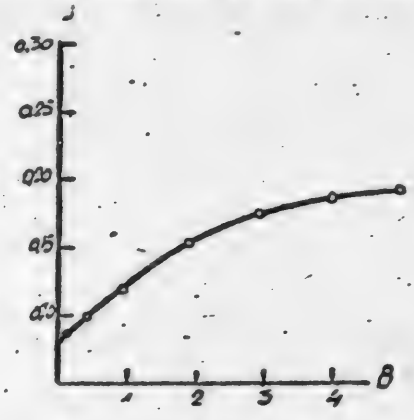

Fig. 5. $\frac{d\omega}{d\tau}$ as a function of concentration.

A-CO_2 absorption rate, in terms of a CO_2 partial pressure of 1 atm; B-NaOH solution concentration, moles/liter.

described above begins to be perceptible at the concentration of 2N. Thus, up to this concentration, the solubility of carbon dioxide in sodium hydroxide solutions is practically the same as its solubility in solutions of sodium chloride. This justifies the computation of the activation energy from Equation (2) up to a concentration of 2N, using the values of the solubility of carbon dioxide in solutions of sodium chloride.

To compute the activation energy from the data of our experiments run at 1800 propeller rpm, we began by calculating the hydrodynamic constants V_0 and β_0.

We determined β_0 on the assumption that $\frac{d\omega}{d\tau}/P$ approaches a limit as the

concentration and temperature increase. Inspection of the equation of mass transfer in the gas phase:

$$\frac{d\omega}{d\tau} = \beta_\sigma (P - P_1), \qquad (4)$$

indicates that the existence of this limit depends upon the tendency of P_1 to approach zero. Hence, β_σ is the limit of $\frac{d\omega}{d\tau}/P$.

The variation of $\frac{d\omega}{d\tau}/P$ with concentration is shown graphically in Fig. 5.

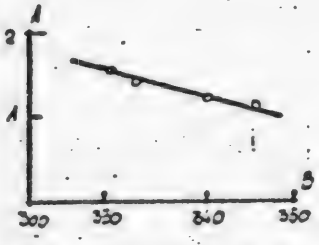

Fig. 6. Log K as a function of $1/\tau$.

A-Logarithm of the velocity coefficient; B-reciprocal of the temperature, expressed in degrees on the absolute scale.

TABLE 4

Rate of Absorption of CO_2 by NaOH Solutions Above 2N, and Calculated Values of the Constant K

Solution concentration at experimental temperature, gram-equiv/l.	Solution temp., °C	Velocity coefficient K, computed from Equation (3)	Computed rate of absorption	
			From Equation (2)	From Equation (5)
0.10	14.2	9.0	0.062	0.063
0.40	16.5	–	0.095	0.096
0.90	20.5	14.7	0.132	0.137
1.60	26.9	23.7	0.173	0.179
1.96	30.5	30.7	0.188	0.190

Graphical extrapolation yielded the value of β_σ as 0.283 mol/min/atm.

The hydrodynamic constant V_σ of the liquid phase was determined from Equation (2) for zero concentration of the active portion of the absorbent. The equation then takes on this form:

$$\frac{d\omega}{d\tau} = \frac{HP}{\frac{1}{V_\sigma} + \frac{H}{\beta}}, \qquad (5)$$

in which all the variables are known with the exception of V_σ. Computation gave 1.26 liters/min as the value of V_σ.

The constant K was computed from Equation (2). Its values are listed in Table 4. Figure 6 shows the variation of log K with $1/\tau$.

The activation energy, calculated by the method of least squares, proved to be 13,200 cal, which is in complete agreement with the data given in the paper by Kishinevsky and Pamfilov [1] and with the results of direct measurement.

There can therefore be hardly any doubt about the applicability of Equation (2) to absorption processes taking place under conditions that resemble those existing in the propeller agitator at 1800 rpm.

We were also interested in ascertaining the departure from the experimental curve involved in using values of the solubility of CO_2 in NaCl solutions to compute the rate of absorption of CO_2 by NaOH solutions at concentrations in excess of 2 N. The values of K required for this purpose were calculated from Equation (3), assuming the activation energy to be 13,200. Our results are listed in Table 4. These results are represented by the dotted line in Fig. 2. The individual points are denoted by triangles. The agreement between the experimental and the computed curves is quite satisfactory.

In view of the high turbulence that is present in the tests at 1800 propeller rpm, we also wanted to ascertain whether the process could be represented by the following equation:

$$\frac{d\omega}{d\tau} = \beta_\sigma P \frac{KC + V_\sigma}{KC + V_\sigma + \beta_\sigma/H}, \qquad (6)$$

inasmuch as this equation is the same as Equation (2) when $\Delta\tau$, the time required for renewal of the surface layer, is small.

Comparing Equation (6) with Equation (2), we find, after resolving the exponential series down to terms of the first order inclusive, that:

$$K_\sigma = mV_\sigma K_c \Delta\tau = mV_\sigma K,$$

where $\underline{m}$ is $\sqrt{2}$ for a reaction between carbon dioxide and hydroxyl ions.

The values of the absorption rate, as computed from Equation (6), are listed in Table 4 and are shown by the samll crosses in Fig. 2. The good agreement between the values of the absorption rate as computed from Equation (6) with the experimental values indicates that it is possible to employ this equation to calculate the processes taking place under the hydrodynamic conditions prevailing in the propeller agitator at 1800 rpm.

The correctness of Equation (2) was also borne out by determination of β_σ from the results of the following experiments. The rate of absorption of the carbon dioxide was measured at 26.4° C for two concentrations of sodium hydroxide, 0.36 $\underline{N}$ and 1.55 $\underline{N}$. In order to ensure identical hydrodynamic conditions in the two tests, constant viscosity was achieved by preparing the 0.36 $\underline{N}$ solution in an aqueous solution of glycerol. This made it possible to eliminate the constant $\underline{K}$ in solving Equation (2) and to obtain β_σ as a function of V_σ. The second relationship between the constants β_σ and $\underline{V_\sigma}$ was provided by the rate of absorption in pure water, exponential terms being excluded because $\underline{C} = 0$. The determination of β_σ thus boiled down to solving a system of two equations with two unknowns.

For the solution with a concentration of 0.36$\underline{N}$ (and glycerol):

$$\frac{d\omega}{d\tau} = 0.110 = \frac{\frac{1}{2}\, 0.36 \left[1 - e^{-\left(0.925 - \frac{0.110}{\beta_\sigma}\right) 0.0307\, K}\right] + 0.0307 \cdot 0.925}{\frac{1}{V_\sigma} + \frac{0.0307}{\beta_\sigma}},$$

for the 1.55 $\underline{N}$ solution:

$$\frac{d\omega}{d\tau} = 0.166 = \frac{\frac{1}{2}\, 1.55 \left[1 - e^{-\left(0.925 - \frac{0.166}{\beta_\sigma}\right) 0.0307\, K}\right] + 0.024 \cdot 0.925}{\frac{1}{V_\sigma} + \frac{0.024}{\beta_\sigma}},$$

and for pure water:

$$\frac{d\omega}{d\tau} = 0.055 = \frac{0.0485 \cdot 0.943}{\frac{1}{V_\sigma} + \frac{0.0485}{\beta_\sigma}}.$$

Solving these equations yielded $\beta_\sigma \cong 0.24$.

This value of β_σ should be compared with the value of $\beta\sigma$ as determined from the dotted curve in Fig. 2, inasmuch as the dotted curve represents the process taking place when the solubility of carbon dioxide in sodium hydroxide and in sodium chloride is the same. The determination of β_σ by the present method was based upon the same assumption. Using the dotted curve, we find $\beta_\sigma \cong 0.26$ by

the same method as was previously used for the experimental curve.

The agreement of the values of β_σ as determined in two entirely different ways is further confirmation of Equation (2).

The experimental data secured at 1200 propeller rpm were likewise worked up by Equation (2). The values of β_σ, 0.100 mole/min. · atm, and of $\underline{V}_\sigma$, 0.165 liter/min, were determined by the method described previously. The values of $\underline{K}$ computed from Equation (3), the initial value of $\underline{K}$ being that found from the experimental data for 16.5°C, are listed in Table 5. The same table gives the absorption rates calculated from Equation (2).

TABLE 5

Calculated Rate of Absorption and Velocity Coefficient K

Concentration of NaOH solutions at the test temp., gram/equiv./l.	Solution temp., °C	Velocity coefficient $\underline{K}$, calculated from Equation (3)	Absorption rate, calculated from Equation (2)
0.1	14.2	17.7	0.0108
0.90	20.5	28.9	0.0345
1.60	26.9	46.4	0.0510
1.96	30.5	60.3	0.056
2.60	35.0	82.5	0.064
2.96	40.0	116.0	0.068
3.60	46.1	172.5	0.071
4.00	50.0	222.0	0.071
5.00	59.4	395.0	0.070

The experimental and calculated curves of the absorption rate are plotted in Fig. 3. Comparison of these curves indicates that here too the process may be represented by Equation (2). The somewhat greater discrepancy is due to the higher value of $\Delta\tau$ in this test. Equation (2) was derived upon the assumption that the solubility of the gas in the surface layer remains constant during the period of the latter's renewal. As $\Delta\tau$ increases, this assumption becomes more inaccurate.

Equation (2) enables us to compute the degree of neutralization of the surface layer by inserting the value of the absorption rate in the exponential expression. Computation yielded the following values of the degree of neutralization under various hydrodynamic conditions at a temperature of 16.5° and a 0.4$\underline{N}$ concentration of sodium hydroxide in the solution: 0.065 in the intensive-agitation apparatus at 800 rpm; 0.100 in the intensive-agitation apparatus at 400 rpm; 0.23 in the propeller agitator at 1800 rpm; and 0.46 in the propeller agitator at 1200 rpm.

SUMMARY

1. The absorption of carbon dioxide by solutions of sodium hydroxide in a propeller agitator at high rpm has confirmed the correctness of the equation for the kinetics of absorption

$$\frac{d\omega}{\sigma d\tau} = \frac{mc\left[1 - e^{\left(-P - \frac{d\omega}{\sigma d\tau}/\beta\right) HK_c\Delta\tau}\right] + HP}{\frac{1}{V_n} + \frac{H}{\beta}},$$

based on the concept of the transfer of a substance by mass flow.

2. The experimental data obtained in an investigation of the absorption process in the propeller agitator have been used to calculate the activation energy of the reaction between carbon dioxide and hydroxyl groups.

LITERATURE CITED

[1] M.Kh.Kishinevsky and A.V.Pamfilov, J.Appl.Chem. 22, 1183 (1949).

Received June 24, 1950.

A STUDY OF THE SEPARATION OF THE ISOMERS OF XYLENE BY ADSORPTION*

T. G. Plachenov and I. A. Kuzin

The adsorption method of separating substances of similar structure and properties is widely employed in laboratories and industry at the present time.

The introduction of adsorption methods into laboratory and industrial technology has been occasioned by the circumstance that in many instances it is impossible to separate natural or synthetic mixtures in any other way, or else their separation entails high losses of valuable substances.

Commercial xylene is an example of such a mixture. It is impossible to recover pure isomers of xylene from its industrial mixtures by means of rectification [1]. Rectification, at best, yields fractions that are enriched with one isomer or another, it being somewhat easier to secure fractions that are enriched with o-xylene.

Whenever pure isomers are required, they are prepared synthetically or are isolated from industrial xylene chemically.

It is difficult, in practice, to isolate the isomers of xylene from industrial xylene even by chemical methods [2,3,4,5]. Metaxylene produced by the Kizhner method [6] contains other isomers of xylene.

The cryoscopic method of recovering the isomers of xylene from their industrial mixtures is ineffective since it entails repeated crystallization at low temperatures and gives an extremely low yield of the pure isomers.

We have found only one paper in the literature dealing with a study of the separation of a mixture of ortho- and metaxylenes by adsorption [7]. The paper reports that it is impossible to achieve even partial separation of this mixture by the adsorption method. The author of the paper in question reached this conclusion on the basis of limited experimental data, however, and his conclusion is not very convincing.

The objective of the present research has been an exploration of the feasibility of separating the isomers of xylene by the adsorption method.

EXPERIMENTAL

In the first section of our research we made a study of the adsorption properties of porous adsorbents, testing vapors of xylene isomers and ethylbenzene and mixtures of the two. The following were used as porous adsorbents: BAU industrial charcoal; TUTs-10, a charcoal produced from peat in the laboratory; and industrial silica gel and ferrogel, prepared in the laboratory.

---

*This research was begun under the guidance of Prof. E. V. Alexeyev.

Table 1 contains data on the porosity of the charcoals we used in our research. The volume of the charcoal pores was determined by the Dubinin and Zaverina method, [8].

The xylene isomers were purified before their adsorptibility was tested; the ortho- and paraxylenes were refined by distillation and desiccation above calcium chloride, while the metaxylene was refined by sulfonation and hydrolysis with sulfuric acid by the Kizhner method [8], followed by treatment with dilute nitric acid to remove the traces of ortho- and paraxylenes. The boiling point, specific gravity, and refractive index were determined for all the purified isomers.

TABLE 1

Porosity of Charcoals

Adsorbent	$\bar{V}_\varepsilon$, cm^3/g	V_{ma}, cm^3/g	W_s, cm^3/g	V_{mi}, cm^3/g	V_p, cm^3/g
Laboratory charcoal TUTs-10	0.99	0.39	0.60	0.44	0.16
BAU	1.51	1.11	0.40	0.23	0.17

Note: V_ε is total pore volume; V_{ma} is the macropore volume; W_s is the overall volume of adsorbing space; V_{mi} is the micropore volume; and V_p is the transitional pore volume.

TABLE 2

Properties of Initial Xylene Isomers

Isomer	Boiling point at 760 mm Hg, °C	Specific gravity	Refractive index	Per cent impurities
Orthoxylene	143.4	0.8801	1.5011	1.2
Metaxylene	138.9	0.8640	1.4942	
Paraxylene	137.8	0.8620	1.4928	
Ethylbenzene ...	136.2	0.8651	1.4951	

The properties of the initial xylenes are listed in Table 2.

The isotherms of the adsorption of orthoxylene, metaxylene, and ethylbenzene vapors by activated charcoal and gels were plotted in a Dubinin thermostat device [8]. The temperature of the thermostat was kept at 20 ± 0.5° by means of a toluene thermoregulator.

The retentivity of the charcoals and gels at 20° was tested by passing air through a layer of adsorbent saturated with vapors of the xylene isomers for 4 hours at a rate of 1 liter/cm^2/min, the test being run at higher temperatures by passing carbon dioxide through the charcoal layer in the apparatus pictured diagramatically in Fig. 1.

The carbon dioxide flowed from the tank (1) through the reducing valve (2) to the buffer bottle (3) and then to the flow meter (4). From the flow meter the gas passed through a Tischenko bottle (5) to the porcelain tube (6), heated by a coil of nichrome wire. The temperature to which the carbon dioxide was heated was regulated by the rheostat (7). The gas, heated to 200°C, entered the Pyrex tube (8) containing charcoal saturated with xylene. The dynamic tube was heated to 250° by an external coil of nichrome wire. The temperature was controlled by the rheostat (7') and measured by the angle thermometer (9). The xylene vapor entrained by the carbon dioxide passed through the condensers (10) and then through

the worm condenser (12), chilled to -70° by a mixture of acetone and dry ice in a Dewar flask.(13). From the worm condenser (12) the stream of carbon dioxide passed through a tube containing charcoal (14) to effect final elimination of the xylene vapor. The condensate was collected in the receivers (11) and (11').

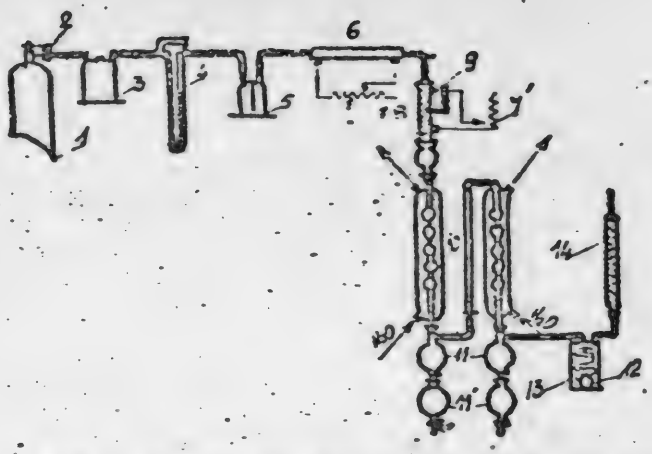

Fig. 1. Apparatus for investigating the retentivity of charcoals and gels.

1-Tank; 2-reducing valve; 3-buffer bottle; 4-flow meter; 5-Tishchenko bottle; 6-prcelain tube; 7 and 7'-rheostats; 8-Pyrex tube. 9-thermometer; 10-condensers; 11 and 11'-receivers; 12-worm condenser; 13-Dewar flask; 14 tube containing charcoal.

The adsorbent was saturated with xylene vapor in the apparatus illustrated in Fig. 2. Air from the line (1) entered a column filled with absorbent cotton (2) to free it from oil and other contaminations, after which it passed through a column filled with activated charcoal (3), in which its organic impurities and part of its moisture were eliminated. From the column (3) the air passed through an apparatus containing sulfuric acid (4), a buffer bottle (5), a tube containing silica gel impregnated with calcium chloride (6), where it was further desiccated, and a tube (7) filled with alumina gel. The quantity of dry air was measured by the flow meter (9). The air pressure in the system was regu-

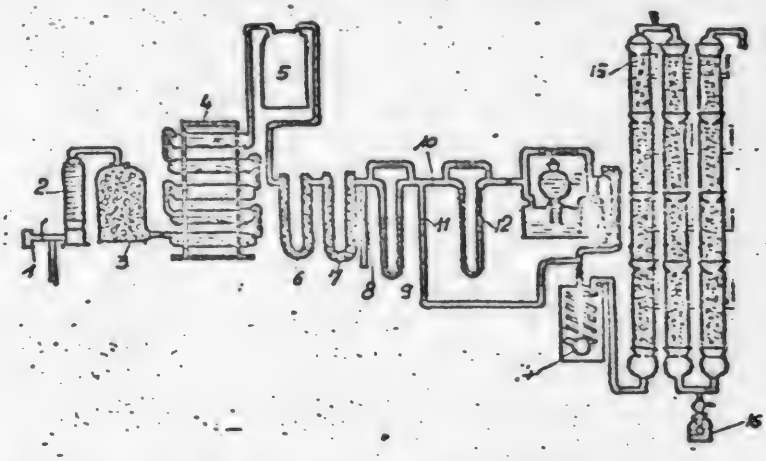

Fig. 2. Apparatus for saturating the absorbent with a xylene mixture.

1-Air line; 2-absorbent cotton column; 3-activated charcoal column; 4-H_2SO_4 apparatus; 5-buffer bottle; 6-tube containing silica gel; 7-tube containing alumina gel; 8-clamp; 9-flow meter; 10-stopcock; 11-stopcock; 12-flow meter. 13-gooseneck flask; 14-mixer; 15-adsorption tubes; 16-Drexel bottle.

lated by means of the clamp (8). After passing through the flow meter (9), the air was divided into two streams. One current of air passed through the stopcock (10) and the flow meter (12) into the gooseneck flask (13), containing the xylene

mixture, while the other air current passed through the stopcock (11) into the mixer (14). The air passing through the gooseneck flask containing the xylenes was saturated with xylene vapor, after which it passed on to the mixer. Thus we secured the requisite concentration in the mixer by passing the required amount of air through the gooseneck flask. From the mixer the air-vapor mixture passed into the adsorption tubes (15) filled with the adsorbent. Adsorption was continued until xylene began to emerge from the adsorbent layer. The passage of xylene was determined by a xylene reagent contained in the Drexel bottle (15). The xylene reagent used was sodium nitrite in concentrated sulfuric acid.

The Drexel bottle was inserted into the line when the last layer of adsorbent had been exhausted, as was readily noted by the adsorbent heating up as it became saturated. The adsorption tubes, made of Pyrex glass, 2.5 cm in diameter and 20 cm long, were connected together via ground-glass connections, so that the length of the layer could be varied. There was a glass screen at the bottom of each tube, on which the adsorbent was poured. Angle thermometers, with scales reading from 20 to 300°, were mounted halfway up the wall of each tube to measure the temperature when the xylene was desorbed from the adsorbent. The top of each tube was covered with asbestos and wound with a coil of nichrome wire to heat the packing during desorption.

The experiments with binary and ternary mixtures were run with the length of the adsorbent layer kept constant at 80 cm. When a 4-component mixture was investigated, the length of the adsorbent layer was varied from 80 to 240 cm.

In saturating the adsorbents with the mixtures, we had to secure a constant proportion of the constituents in the mixture when evaporating the liquid with air.

The usual gooseneck flask was not employed in evaporating mixtures of xylene isomers, inasmuch as the low-boiling fraction is the first to vaporize, followed by the mixture, and lastly, the high-boiling fraction. To secure uniform composition of the mixtures we made use of a Khramov gooseneck flask [10]. Use of this flask ensured uniform concentration of the constituents of the mixture.

The distribution of the xylene isomers along the length of the adsorbent layer during sorption of their mixtures was determined by desorption of the xylene from the adsorbent in layers and by chemical analysis of the xylenes desorbed from each layer.

The composition of the condensate was determined by the Leitman method (11), involving nitration ot the xylenes to nitro derivatives and analysis of the latter; the experimental error involved in this procedure totaled 0.5 to 1.0% in the determination of each isomer.

The results of determining the adsorption activity of the charcoals, silica gel, and ferrogel for vapors of o-xylene, m-xylene, p-xylene, and ethylbenzene are given in Fig. 3, where the vapor concentration is plotted along the axis of abscissas in mg per liter, and the adsorption of the vapor along the axis of ordinates in per cent.

The change in retentivity at 20° with the structure of the adsorbent is shown graphically in Fig. 4.

Table 3 lists the results of a study of the retentivity of TUTs-10 charcoal for metaxylene vapor at high temperatures.

We see from Fig. 3 that the extent of adsorption of the xylene isomers and of ethylbenzene may be arranged in the following order for all the adsorbents investigated: orthoxylene > metaxylene > paraxylene > ethylbenzene.

The retentivity of the adsorbents depends upon the structure of the adsorbent

as may be seen in Fig. 4: TUTs-10 charcoal retains 67-68% of the originally adsorbed orthoxylene and 61-62% of the original ethylbenzene, while the BAU charcoal retains 56-57% of the orthoxylene and 55-56% of the ethylbenzene. As may be seen from Table 1, this difference in the retentivity of the charcoals is due to the fact that the overall volume of the adsorbing space in the TUTs-10 charcoal contains 26.6% transitional pores and 73.4% micropores, while the overall volume of the adsorbing space in the BAU

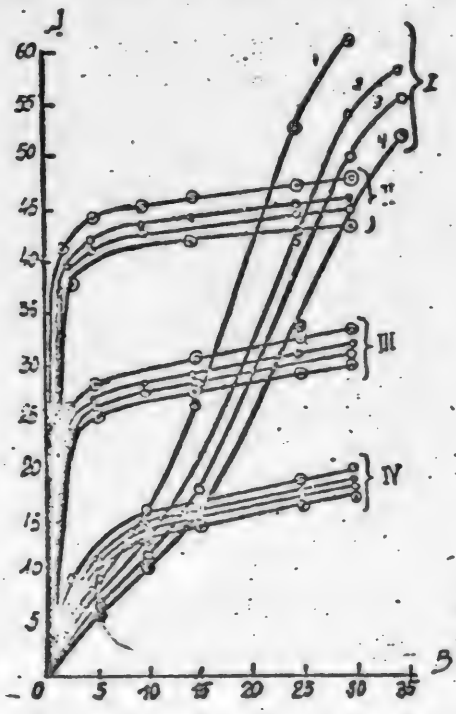

Fig. 3. Results of determining the adsorption activity of charcoals, silica gel, and ferrogel for vapors of o-xylene, m-xylene, p-xylene, and ethylbenzene.*

A-Adsorption of the vapor; B-vapor concentration, mg/liter. I-Silica gel; II-TUTs-10; III-BAU; IV-ferrogel; 1-ortho xylene; 2-metaxylene, 3-paraxylene; 4-ethylbenzene.

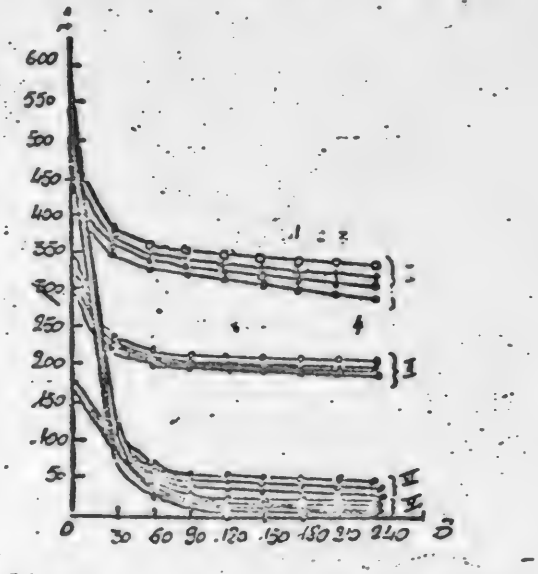

Fig. 4. Change in retentivity at 20° as a function of the structure of the adsorbent.

A-Retentivity of various adsorbents, mg/gram B-time, minutes. I-TUTs-10; II-BAU, III-ferrogel, IV-silica gel. 1-orthoxylene; 2-metaxylene; 3-paraxylene; 4-ethylbenzene.

charcoal contains 42.5% of transitional pores and 57.5% of micropores.

The results of our tests of the desportion of metaxylene from TUTs-10 charcoal at high temperature (Table 3) indicate that the retentivity of the charcoal drops to 7-8.5% by weight of the charcoal at a temperature of 200-250°. Increasing the desorption time from 15 to 30 minutes results in a slight decrease in the retentivity, so that the 200-250° must be regarded as the optimum temperature for desorbing the isomers of xylene by carbon dioxide.

The adsorbed metaxylene is completely desorbed when the charcoal is resaturated with metaxylene, the retentivity of the charcoal remaining unchanged.

The data obtained in our study of the adsorption properties of charcoals and gels for the vapors of orthoxylene, metaxylene, paraxylene, and ethylbenzene would lead one to expect that it would be possible to separate mixtures of xylene isomers by the method of adsorption on porous adsorbents with a large micropore volume.

*The order in which the curves are arranged in each curve group is the same in Figs. 3 and 4.

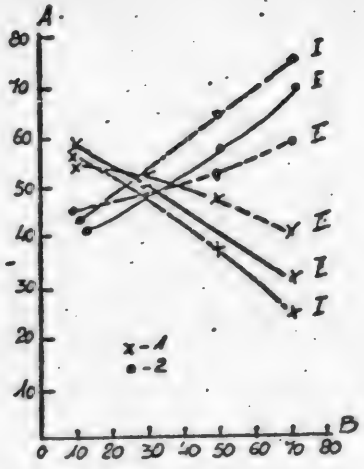

Fig. 5. Change in the composition of the mixture as a function of the length of the charcoal layer.

A-% composition of the mixture; B-length of the charcoal layer, cm. I-Silica gel; II-TUTs-10; III-BAU. 1-metaxylene; 2-ethylbenzene.

TABLE 3

The Retentivity of TUTs-10 Charcoal for Metaxylene Vapor

Time, min.	Desorption temp., °C	Residual xylene, % by weight of the adsorbed xylene	Residual xylene, % by weight of the charcoal
0	–	100	45.2
15	100	46.2	20.9
30	100	38.5	17.5
0	–	100	44.8
15	150	34.5	15.4
30	150	26.6	11.9
60	150	20.8	9.3
0	–	100	44.4
15	250	16.0	7.1
30	250	15.0	6.6
15	200	19.5	8.5
15	300	14.2	6.4

TABLE 4

Change in the Composition of a Desorbed Mixture as a Function of the Length of the Adsorbent Layer

C_o = 15 mg/liter metaxylene + 15 mg/liter ethylbenzene, $\underline{V}$ = 0.5 liter/min/cm^2. Weight of desorbed mixture = 5 grams.

Adsorbent	Layer No.	Analysis data: Yield of trinitrometaxylene, grams	Yield of trinitroethylbenzene, grams	Melting point of trinitrometaxylene, °C
TUTs-10.....	1	5.655	3.36	181.6
	2	4.875	4.00	181.3
	3	4.095	4.786	181.8
	4	3.022	5.692	181.4
BAU	1	5.362	3.712	181.5
	2	5.070	3.960	181.2
	3	4.680	4.290	181.1
	4	4.012	4.901	181.2
Silicagel...	1	5.580	3.547	181.7
	2	4.690	4.285	181.6
	3	3.510	5.280	181.6
	4	2.437	6.137	181.8

To shed more light on this question, we made a study of the adsorption separation of the following artificially prepared mixtures: metaxylene + ethylbenzene; orthoxylene + metaxylene; metaxylene + paraxylene; and orthoxylene + metaxylene + paraxylene.

The adsorption and desorption of a mixture of metaxylene and ethylbenzene was investigated, using TUTs-10 and BAU charcoals and silica gel.

The results of analysis of a desorbed mixture of metaxylene and ethylbenzene are listed in Table 4, the change in the composition of the mixture as a function of the length of the adsorption layer being shown graphically in Fig. 5.

When we examine the distribution of adsorption and the composition of the mixture along the TUTs-10, BAU, and silica gel layers, we note that the mixture is enriched with metaxylene in the first layers of all the adsorbents, the final layers being enriched with ethylbenzene. The adsorption of metaxylene in the first layer is 3% higher for TUTs-10 than for BAU. The mixture in the fourth layer is enriched with 10% more ethylbenzene in the TUTs-10 charcoal than in the BAU. The composition of the mixture in the first layers of the silica gel is the same as for the TUTs-10 charcoal, but in the fourth layer the mixture was enriched with 25% of the initial percentage of ethylbenzene, this figure being 6% higher than that for the TUTs-10 charcoal. This redistribution of the constituents along the length of the silica gel layer is due to the fact that half of the silica gel layer is operating at low concentrations, and at these concentrations the ethylbenzene is better displaced by the metaxylene.

When we compare the amounts adsorbed on the TUTs-10 charcoal and the silica gel, we readily see that the amount of xylene adsorbed by the first two layers of charcoal was close to the maximum value, the last two layers having adsorbed 75-80% of their equilibrium capacity at the given concentration, while the silica gel absorbed 80% in the first layer, 60% in the second, 29% in the third, and 12% in the fourth. Hence, silica gel may be utilized for separating mixtures of xylene isomers in the vapor phase, but this requires large quantities of silica gel.

Our experimental data lead us to conclude that finely porous, highly active charcoal should be employed for separating binary, ternary, and quaternary mixtures. We used TUTs-10 charcoal for this purpose.

The TUTs-10 charcoal was employed in ascertaining the effect of the following factors upon the degree of separation of binary mixtures of metaxylene

TABLE 5

Change in the Composition of a Desorbed Mixture as a Function of the Length of the Charcoal Layer

$V = 0.5$ liter/min/cm^2; $t = 20°$. TUTs-10 Charcoal. Weight of the Desorbed Mixture = 5 grams

Concentration, mg/liter	Layer No.	Analysis data		
		Yield of trinitrometaxylene, grams	Yield of trinitroethylbenzene, grams	M.p. of trinitrometaxylene, °C
1.0	1	6.045	3.138	181.6
	2	5.073	3.965	181.3
	3	3.705	5.165	181.3
	4	2.340	6.187	181.4
30	1	5.655	3.365	181.6
	2	4.875	4.09	181.3
	3	4.045	4.786	181.8
	4	3.022	5.692	181.4

TABLE 6

Change in the Composition of a Desorbed Mixture as a Function of the Length of the Charcoal Layer and of the Rate of Air Flow.

V = 0.5 liter/min/cm². t = 20°. TUTs-10 Charcoal. Weight of desorbed Mixture: 5 g. C_o = 15 mg/liter of metaxylene + 15 mg/l. ethylbenzene.

Rate of air flow l./min/cm²	Layer No.	Per cent composition of desorbed mixture		Analysis data		
		Meta-xylene	Ethyl-benzene	Yield of trinitrometaxylene, grams	Yield of trinitroethylbenzene, grams	M.p. of trinitrometaxylene, °C
0.25	1	59	41	5.753	3.383	181.8
	2	53	47	1.163	3.913	181.7
	3	45	55	4.388	4.537	181.6
	4	30	70	2.925	5.775	181.6
0.5	1	58	42	5.670	3.352	181.7
	2	51	49	4.972	4.042	181.6
	3	41	59	3.997	4.867	181.6
	4	31	69	3.023	5.695	181.4
1.0	1	57	43	5.557	3.547	181.4
	2	50	50	4.876	4.100	181.4
	3	42	58	4.089	4.788	181.6
	4	32	68	3.120	5.610	181.9

TABLE 7

Change in the Composition of a Desorbed Mixture as a Function of the Length of the Charcoal Layer and of the Initial Composition of the Mixture

V = 0.5 liter/min/cm²; t = 20°. TUTs-10 Charcoal. Weight of Desorbed Mixture = 5 grams.

Per cent composition of mixture	Layer No.	Per cent composition of desorbed mixture		Analysis data		
		Meta-xylene	Ethyl-benzene	Yield of trinitrometaxylene, grams	Yield of trinitroethylbenzene, grams	M.p. of trinitrometaxylene, °C
94% metaxylene + 6% ethylbenzene	1	98	2	9.559	0.165	181.6
	2	96	4	9.361	0.330	181.5
	3	93	7	9.063	0.577	181.4
	4	88	12	8.580	0.990	181.7
84% metaxylene + 16% ethylbenzene	1	92	8	8.970	0.660	181.6
	2	86	14	8.385	1.155	181.6
	3	82	18	7.995	1.485	181.5
	4	69	31	6.722	2.553	181.4
50% metaxylene + 50% ethylbenzene	1	58	42	5.655	3.365	181.6
	2	50	50	4.875	4.09	181.3
	3	42	58	4.095	4.786	181.8
	4	31	69	3.022	5.692	181.4
4% metaxylene + 96% ethylbenzene	1	5.8	94.2	0.565	7.785	–
	2	4.9	95.1	0.481	7.837	–
	3	3.8	96.2	0.385	7.940	–
	4	2.7	97.3	0.263	8.020	–
2% metaxylene + 98% ethylbenzene	1	2.7	97.3	0.263	8.023	–
	2	1.8	98.2	0.175	8.090	–
	3	0.8	99.2	0.078	8.167	–
	4	0.4	99.6	0.040	8.180	–

and ethylbenzene: 1) the initial concentrations in the vapor of the given mixture; 2) the rate of air flow; and 3) the quantitative proportions of the isomers in the mixture.

The results of these tests are listed in Tables 5, 6, and 7 and plotted in Fig. 6.

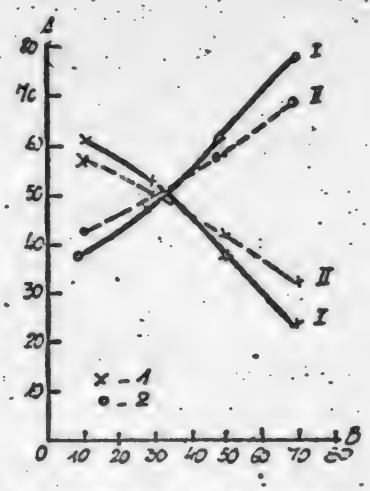

Fig. 6. Change in the composition of a mixture of metaxylene and ethyl benzene as a function of the length of the charcoal layer.

A-% composition of the mixture: B-length of the charcoal layer, cm. Concentration of the air-vapor mixture: I-1.0 mg/liter; II-30.0 mg/liter; 1-Metaxylene; 2-ethylbenzene.

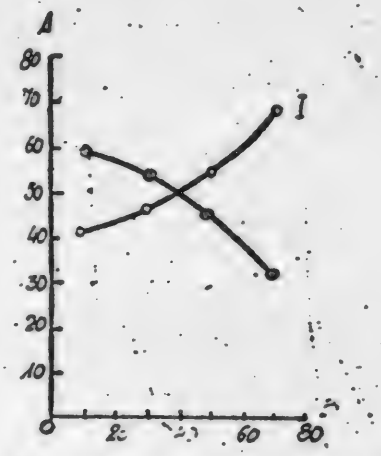

Fig. 7. Change in the composition of a mixture of metaxylene and orthoxylene as a function of the length of the TUTs-10 charcoal layer.

A-% composition of the mixture; B-length of the charcoal layer, cm. I-Metaxylene; II-orthoxylene.

The data shown in Table 5 and in Fig. 6 indicate that the displacement of ethylbenzene by metaxylene depends upon the initial concentration of the air-vapor mixture. At 1.0 mg/liter, the fourth layer was enriched with 26% of ethylbenzene, while the respective figure for 30 mg/liter was only 19%.

Our experiments have shown that the mixture is enriched with more metaxylene in the first layer and with ethylbenzene in the last layer when the concentration is 1 mg/liter, i.e., before the onset of capillary condensation, but saturation sets in very slowly under these conditions. It took 123 hours for the 80-cm charcoal layer to be saturated to the emergence point at a concentration of 1 mg/liter. At 30 mg/liter the saturation of the same layer was complete within 6.5 hours.

The test results listed in Table 6 demonstrate that in the fourth layer the mixture is enriched with as much as 70% ethylbenzene at an air-flow rate of 0.25 liter/min/cm^2, and with up to 68% at a rate of 1 liter/min/cm^2. The percentage of metaxylene in the initial layers varied by 1-2%, depending upon the rate of air flow. We may, therefore, conclude that the rate of air flow has no effect upon the displacement of ethylbenzene by metaxylene during the saturation of the charcoal.

The data in Table 7 indicate that metaxylene is sorbed better than ethylbenzene at all of its concentrations in the binary mixture, concentrating in the

TABLE 8

Change in the Composition of the Desorbed Mixture as a Function of the Length of the Charcoal Layer and of the Initial Composition of the Mixture

V = 0.5 liter/min/cm^2; t = 20°; TUTs-10 Charcoal. Weight of Desorbed Mixture: 5 g

Percentage composition of mixture	Layer No	Analysis data		
		Yield of trinitro-orthoxylene, grams	Yield of trinitro-metaxylene, grams	M.p. of trinitrometaxylene, °C
50% orthoxylene + 50% metaxylene	1	4.720	4.001	181.5
	2	4.270	4.573	181.6
	3	3.600	5.360	181.4
	4	2.580	6.630	181.5
10% orthoxylene + 90% metaxylene	1	1.200	8.283	181.5
	2	0.960	8.580	181.5
	3	0.720	8.872	181.5
	4	0.500	9.165	181.6

first layer of the charcoal, while the ethylbenzene is displaced to the last layer. The higher the percentage of metaxylene in the initial mixture, the greater its ability to displace the ethylbenzene.

The process involved in separating a mixture of orthoxylene and metaxylene was investigated with TUTs-10 charcoal at a concentration of 30 mg-liter and a specific rate of flow of 0.5/min/cm^2. The results of analysis of the desorbed mixture are listed in Table 8, the change in the composition of the mixture being plotted as a function of the length of the layer in Fig. 7.

Our study of the adsorption of mixtures of orthoxylene and metaxylene confirmed our previous results on the adsorption of the individual isomers of xylene and of binary mixtures of metaxylene and ethylbenzene. As our tests indicated, orthoxylene is adsorbed better than metaxylene in the individual state; this relationship being preserved when mixtures of the two are adsorbed. Orthoxylene is concentrated in the initial layers, the metaxylene, as the less readily adsorbed constituent, being forced back into the final layers. When a mixture containing 50% orthoxylene and 50% metaxylene was adsorbed, the two constituents were distributed as follows along the length of the adsorbent layer: the concentration of orthoxylene rose to 59% in the first layer, while that of metaxylene rose to 68% in the last layer. These figures demonstrate that in a mixture orthoxylene is adsorbed better than either metaxylene or ethylbenzene.

A mixture of meta- and paraxylenes represents the mixture of xylene isomers that is hardest to separate, inasmuch as these isomers have physicochemical properties that are nearly identical. The difference between the boiling points of meta- and paraxylenes is only 1°C, for instance, while their vapor pressures at 20°C differ by only 0.5 mm Hg. To ascertain the feasibility of separating a mixture of this sort, we ran tests of its adsorption of TUTs-10 charcoal. The results of our tests of the adsorption and desorption of a mixture of meta- and paraxylenes are listed in Table 9 and plotted in Fig. 8.

When a mixture containing 84% metaxylene and 16% paraxylene is adsorbed, the isomers are redistributed along the adsorbent layer. At the front end of the layer the mixture contains as much as 89% metaxylene, while it contains up to 21% of paraxylene in the last layer. These experimental results indicate that a mixture of meta- and paraxylenes can be enriched on activated charcoal, whereas such a mixture cannot be separated practicably by rectification into a column with an

TABLE 9

Change in the Composition of the Desorbed Mixture as a Function of the Length of the Charcoal Layer and of the Initial Composition of the Mixture

V = 0.5 liter/min/cm^2; t = 20°; C_0 = 30 mg/liter. TUTs-10 Charcoal. Weight of the Desorbed Mixture = 5 grams

Composition of mixture	Layer No.	Analysis data: Yield of trinitro-meta- and paraxylenes, grams	Analysis data: Melting point of trinitrometa- and paraxylenes, °C	Analysis data: Eutectic point, °C
94% metaxylene + 6% paraxylene	1	9.685	180.1	–
	2	9.672	180.1	120.1
	3	9.646	179.0	120.5
	4	9.595	178.0	121.0
84% metaxylene + 16% paraxylene	1	9.570	177.0	121.8
	2	9.556	176.2	122.1
	3	9.496	173.5	123.3
	4	9.430	171.4	124.0

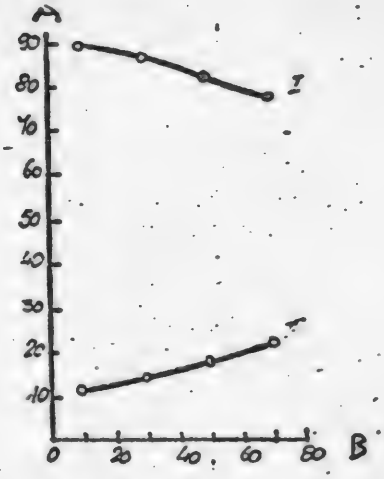

Fig. 8. Change in the composition of a mixture of metaxylene and paraxylene as a function of the length of the charcoal layer.

A-% composition of the mixture; B-length of the charcoal layer, cm. I-metxylene; II-paraxylene.

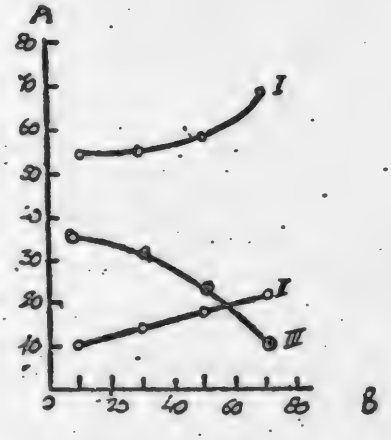

Fig. 9. Change in the composition of a ternary mixture of the isomers of xylene as a function of the length of the charcoal layer.

A-% composition of the mixture; B-length of the charcoal layer, cm. I-metaxylene; II-paraxylene, III-orhtoxylene.

efficiency of 50 theoretical trays.

To check our experimental results on the sorption of binary mixtures of xylene isomers and ethylbenzene, we ran tests on the sorption of ternary mixtures, artificially prepared from pure isomers of xylene.

The results of analysis of the desorbed mixture are listed in Table 10, the change in the composition of the desorbed mixture with the length of the charcoal layer being shown graphically in Fig. 9.

TABLE 10

Change in the Composition of a Desorbed Mixture as a Function of the Length of the Charcoal Layer and of the Initial Composition of the Mixture

V = 0.5 liter/min/cm^2; t = 20°; C_o = 30 mg/liter. TUTs-10 Charcoal.

% composition of mixture	Layer no.	% composition of the desorbed mixture by weight.			Analysis Data				
		ortho xylene	meta xylene	para xylene	g of xylene mixture used for	Yield of trinitro-orthoxylene (g)	Yield of trinitrometa- and para-xylenes, g	M.p. of trinitrometa- and para-xylenes, °C	Eutectic point °C
27% orthoxylene + 57% metaxylene + 16% paraxylene	1	35	55	10	5	2.800	6.137	175.8	122.3
	2	31	55	14	5	2.480	6.447	174.2	123.2
	3	23	59	18	5	1.330	7.112	172.8	123.9
	4	10	69	21	5	0.800	8.344	172.4	124.1
10% orthoxylene + 84% metaxylene + 6% paraxylene	1	15	81	3	5	1.240	8.129	180.7	–
	2	12	83	5	5	0.984	8.350	181.1	120.0
	3	9	84	7	5	0.728	8.732	179.1	–
	4	6	85	9	5	0.353	8.984	177.4	121.5

In the adsorption of ternary mixtures of xylene isomers the front layer is enriched with orthoxylene, the final layer being enriched with paraxylene.

We were unable, however, to isolate a single one of the isomers in the pure state in a single-pass adsorption of binary and ternary mixtures. It must be assumed that the individual isomers can be isolated from xylene mixtures by means of a multistage process of adsorption and desorption on porous adsorbents.

SUMMARY

Studies of the adsorption properties of charcoals, silica gel, and ferrogel for the vapors of the xylene isomers and of ethylbenzene as well as an investigation of the effect of the relative concentrations of the xylene isomers in the air-vapor mixture and of the rate of flow upon the degree of separation of binary and ternary mixtures, have shown that a mixture of orthoxylene and metaxylene may be separated by the adsorption method.

LITERATURE CITED

[1] M.I.Rosengart, Prog.Chem. 17, 2, 204 (1948).

[2] Yakobson, Ber., 10, 1014 (1887).

[3] M.I.Konovalov, J.Russ.Chem.Soc. 37, 531 (1905).

[4] N.M.Kizhner. Researches in Organic Chemistry. USSR Acad.Sci. Press (1937).

[5] Petterson, Millon, and Somerville, J.Chem.Soc., London, 125, 2488 (1924).

[6] V.I.Isagulyants. Synthetic Perfumes. (1936).

[7] B.Amphoux, Ann. Chem. 19, 1 (1944).

[8] M.M.Dubinin. Jubilee Symp. USSR Acad. Sci. I, 562 (1947).

[9] M.M.Dubinin. The Physicochemical Foundations of Sorption Technology. 2nd ed. State Chemical Press (1935).

[10] E.V.Aleksaevsky. General Course of the Chemistry of Corrosion Protection, I. Theoretical Chemistry Press, United Scientific and Technical Press (1935).

[11] Ya.I.Leitman, Trans. Leningrad Inst. Colloid Chem. Technology, 7 (1939).

Received October 1, 1950.

BLANK
PAGE

MEASURING THE CHANGES IN THE SPECIFIC SURFACE OF HIGHLY DISPERSED MATERIALS BY THE TORSION-BALANCE METHOD

A. I. Avgustinik and V. D. Dzhansis

Inasmuch as the reactions in many finely dispersed systems begin and develop at the surface of the reacting substances, it is highly important to be able to estimate the specific surface and to plot a continuous curve of particle distribution according to size [1].

The usual methods employed in the technology of the silicates: screening, settling in water and taking samples, by the Sabinin and Robinson method, the pipet methods and air separation, are of limited effectiveness and do not enable us to plot a "distribution curve" indicating the relationship between particle size and the percentages of particles, especially in the region of extremely fine fractions, below 0.5 μ.

For the same reason, it is impossible to make use of these methods to make even an approximate calculation of the specific surface, which grows ever more rapidly as the particle size diminishes.

TABLE 1

Specific Surface (M^2/Gram) of Chasovyari Clay as a Function of Particle Size

Particle radius (μ)	0.05	0.025	0.005
Specific surface, m^2/gram	3.8	7.1	15.0.

The specific surface (S) of Prosyanovsk kaolin, for example, is 5.7 m^2/gram for particles with radii of 30 to 0.05μ , rising to 6.4 m^2/gram for particles with radii of 30μ to 0.025μ , and being as high as 9.9 m^2/gram for particles with radii of 30 to 0.005 μ.

The increase in the magnitude of S is particularly apparent as we begin to allow for the increasingly small dimensions of particles of such lamellar material as Chasovyar clay (Table 1).

The value of the specific surface is governed chiefly by the presence of particles less than 0.1μ in diameter.

In our subsequent calculations of S, we took a radius of 0.005μ (50 A) as the limiting particle size because photographs of the clays under the electron microscope did not indicate the presence of any perceptible quantity of particles of that size. It may be noted that particles of this size (50 A) are readily visible in the microphotographs. The resolving power of an electron microscope would enable us to see even smaller particles if they were actually present in perceptible amounts in the clays. We have examined photographs of this sort in the papers by Eitel and Schusterius [2], Marchall, Chumbert and assoc. [3], and Ardenu, Endel, and Gofmann [4].

The methods of determining S from the air penetrability, which can be used

for homogeneous particles of rolled form (cement), does not yield reproducible results when applied to a heterogeneous mixture of particles most of which are flaky in form (clay and many ceramic materials) [5].

The methods based upon the adsorption of vapors, gases, or any indicators by a disperse medium often require complicated apparatus or high vacuum and yield results that differ considerably for the same materials.

The methods of determining the specific surface of clays from the change in the concentration of the sorbed medium or from the heat of adsorption do not yield comparable results owing to the fact that the amount of medium absorbed or the heat evolved is governed by the nature of the sorbed substance as well as by that of the sorbing substance. It is impossible, therefore, to assert that the bentonite reading for the sorption of, say, octane, 70 m^2/gram, is a better value of the specific surface than that obtained from the sorption of water vapor, 290 m^2/gram. From the adsorption of Ca^{++} and Ba^{++} ions by electrodialyzed bentonite, Chernikova has computed its surface as 1300-1390 m^2/gram, [6].

As a rule adsorption methods make it possible to estimate the overall specific surface as the outer surface of the particles plus the surface of the pores within the particles.

For some technical purposes, however, such as studying the caking of particles where they touch, it is not so much the total surface, (inclusive of the pores within the particles), as the outer surface that is of importance. For this purpose methods enabling us to determine or to compare the external specific surfaces of particles would be more desirable.

Methods that allow for the surface of the particle pores would be of special importance for sorption processes, for investigations of the cleavage or the synthesis of organic molecules by means of inorganic contact agents, and for reactions that take place in the gas phase.

It is evident that these two different groups of processes should be considered separately, in each case using the appropriate methods for determining the specific surfaces of highly disperse particles.

Inasmuch as disperse silicate materials are processed (ground) in water until they are clinkered, it is well to retain water as the phase in which the dimensions of the particles in clays, ceramic masses, slips, and sludges are measured.

The method of measurement is accordingly sedimentation, using Stoke's law. Inasmuch as balances are among the most precise instruments at our disposal, it is advisable to use a variant of this method, employing balances.

The Figurovsky method, in which a thin glass pointer acts as a spring, also serving as a balance beam with unequal arms is very popular; at the end of this point there is hung a minute glass cup holding the settling suspension in a liquid medium [7]. The deflection of the end of the glass pointer as the weight of the cup increases is read off by means of a microscope.

In our investigations of finely ground inorganic suspensions, we utilized the Figurovsky glass spring, though we abandoned it later, working out what we considered to be a more convenient method employing a torsion balance (made by the Kiev factory) ordinarily used in measuring the surface tension of liquids. This variant of the balance method (Fig. 1) is convenient for several reasons: it enables one to plot a continuous sedimentation curve; it does not tire the eyes, since it does not require readings by means of a microscope; it yields reproducible results; and it makes it possible to keep the settling height practically constant.

The deflection of the balance beam up and down is of the order of ± 0.5 mm, owing to the attachment of two stops 9 where the beam emerges (Fig. 1). The sedimentation pan 2 is made of nickel-plated copper (or brass) foil 0.1 mm thick, 24-27 mm in diameter, and with a rim 1.5 mm high. Its weight in water is 340-400 mg, together with the lacquered copper wire 0.1 mm in diameter.

We used several such balances, with a capacity of 1 gram, in making parallel sedimentation tests.

Sedimentation took place in a glass cylinder 3, 60-80 mm in diameter. The settling height, reckoned from the level of the suspension to the bottom of the pan, was constant, usually amounting to 12.5 cm.

The suspension of the cylinder was stirred by the stirring rod 4 made of sheet rubber with notches cut into it, attached to a glass rod.

The determinations were made as follows. The stop 7 was released, and the pointer was set at the zero point 10 by means of the adjusting screw at the back of the balance. The stop was relocked and the cylinder 3 containing freshly distilled water with the stirrer 4 immersed in it was placed under the hook 8 of the beam. Pan 2 was carefully lowered into the water in the cylinder so as to avoid collected

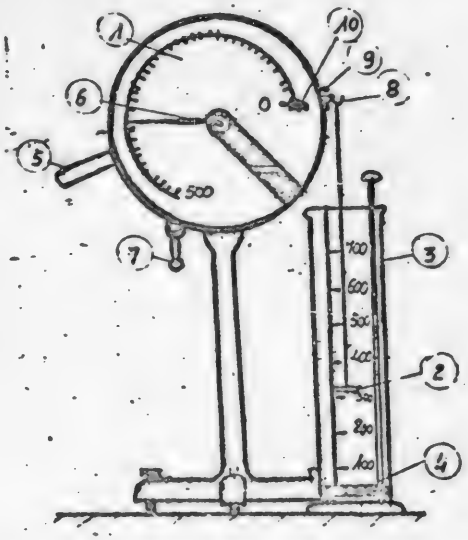

Fig. 1. Apparatus for studying finely ground inorganic substances.

1-Scale of the torsion balance; 2-sedimentation pan; 3-glass cylinder; 4-stirrer; 5-lever; 6-pointer; 7-stop; 8-hook; 9-stop plates; 10-null position of the pointer.

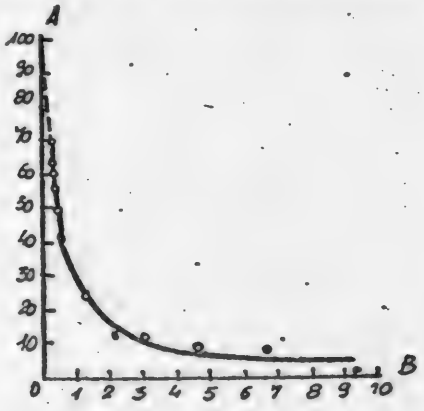

Fig. 2. Sedimentation curve for Prosyanovsk kaolin.

A-Q,% gain in weight; B-r, particle radius in μ.

bubbles of air on it, and the loop in the pan wire was slipped over the hook 8. The stop 7 was released and the weight of the pan in water was measured by moving pointer 6 (counterclockwise) by means of lever 5 until the pointer reached a position of equilibrium, 10. This position was taken as the null reading for subsequent settling of the suspension. The stop was relocked, the pan 2 was lifted out, and a previously prepared suspension of the material under test in water was placed in the cylinder.

The pan was lowered into the water again, taking care to avoid its entraining air bubbles and holding the pan wire in one hand to keep the pan 1-1.5 cm below

the level of the liquid. Then the suspension in the cylinder was stirred up by slowly moving the stirrer up and down with the other hand, the stirrer was lowered to the bottom of the cylinder the pan was gradually lowered in the cylinder, and the wire loop was slipped over the hook 8.

As this latter operation was performed a stopwatch was started. The first reading of the increase in weight was made after 10-15 seconds had elapsed, subsequent readings being made at the same intervals of time during the first half hour, which enabled us to compare the results of repeated sedimentations.

It is best to repeat the sedimentation after half an hour has passed, rinsing the pan out in the cylinder and again stirring up the suspension. The results must coincide. If the two results agree, suspension may be continued. The time required for settling depends upon the dispersion of the material. Some kaolins settle completely within 24 hours, while some clays are not completely settled after 4-5 days.

It is best to set the practical limit of sedimentation time in such a way as to make the last reading correspond to a particle radius of 0.1μ. Sedimentation of particles of Oglanlino bentonite, the specific gravity of which is 2.62, with a radius of 0.22μ, required 200 hours, while 256 hours were required for a radius of 0.1μ.

Sedimentation of particles of Prosyanovsk kaolin, with a specific gravity of 2.601 and a radius of 0.27 μ required 140 hours, the time required for a radius of 0.11 μ being 256 hours.

It is easy to extrapolate from these values to 100% sedimentation of the material. The curve "gain in weight (Q) versus particle radius (r)" is shown in Fig. 2.

Experiment has demonstrated the feasibility of securing identical sedimentation curves at room temperature, provided the temperature of the distilled water is kept constant.

The weight of the pan and the readings of the balance must be checked systematically.

We prepared samples by taking 1.2-1.3 grams of material, in terms of absolute dry weight. This amount of material was dispersed in a small quantity of water (8-10 ml); if the material contained large particles, it was passed through a No. 100 screen (10,000 openings per cm^2) and washed, the material that passed through the screen being used, while the residue left on the screen was allowed for separately.

From Stokes' law we get

$$r^2 = \frac{H\eta}{kz\Delta Dg}, \qquad (1)$$

where r is the particle radius in μ, on the assumption that the settling particle is spherical; H is the sedimentation height in cm; z is the sedimentation time in seconds; k is a proportionality factor, equaling 2/9; g is the acceleration due to gravity, 981 cm/sec^2; η is the viscosity of the water, 0.01 g/cm/sec at 19-20°C; and ΔD is the difference between the specific gravities of the settling substance and the water, equaling 1.6 in this case.

Inasmuch as the values of η, k, ΔD, and g are practically constant under the conditions of this experiment, the coefficient K may be used in Equation (1) instead of these factors, yielding

$$r = K\sqrt{\frac{H}{z}}. \qquad (2)$$

Equation (2) enables us to set up a relationship between the equivalent

radius r_i of the particles settling in time z_i and the total weight G_i of the precipitate during this period.

Plotting the $\%Q - r$ curve also requires that we know the sedimentation limit, i.e., the limiting increase in weight, $G_{max.}$, of the balance pan that is theoretically possible if all the suspension were to settle out.

We can find this quantity by starting out with the volume of the suspension above the pan and its concentration:

$$Q_{max.} = v \frac{g}{V} \frac{\Delta D}{D_{sol.}}, \qquad (3)$$

where $v = \frac{\pi d^2 H}{4}$ is the volume of the suspension above the pan, 75 ml according to our data; g is the acceleration due to gravity, 981 cm/sec^2; V is the volume of suspension in the cylinder, 700 ml in our experiments; ΔD is the difference between the specific gravity of the solid substance, $D_{sol.}$ and that of the medium (water); d is the diameter of the cup; and H is the sedimentation height in cm.

We must also make a correction for the involvement of particles of different size; according to theory [8] this is expressed by the equation

$$q = p - z \frac{\Delta p}{\Delta z}, \qquad (4)$$

where p is the weight of the precipitate in mg at a time z; and Δp is the change (gain) in weight during the time Δz.

$Q\%$ is determined from the equation

$$\Delta Q\% = \frac{\Delta q \cdot 100}{G_{max.}}. \qquad (5)$$

The specific surface of particles with a weight of Δq and a mean radius of $r_{ave.}$ is found from

$$\Delta S = \frac{3\Delta q}{D_{sol.} r_{ave}}, \qquad (6)$$

where Δq is expressed in grams and $r_{ave.}$ is given in centimeters.

We made the following assumption to allow for the specific surface of those particles that practically always remain in suspension because of their extremely minute size.

We assume that the theoretically possible settling of all the particles ought to take place in such a way as to make all subsequent readings lie along a prolongation of the $Q - r$ curve. In other words, we interpolate the intermediate points between the last observation and the terminal one, which we know, for 100% sedimentation of the suspension, taking the interpolated section to be linear, which a permissible supposition if we consider the observed curve (Fig. 3), and endeavoring to connect the final observed points to the point representing 100%. It may be noted that on the scale

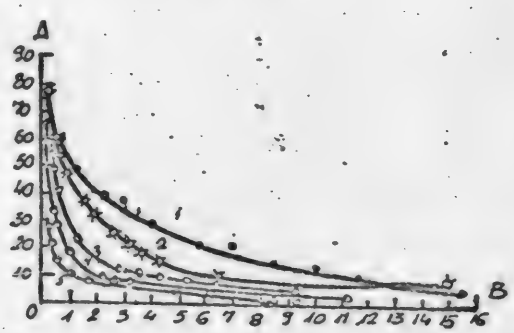

Fig. 3. Settling curves for various clay materials.

A-% gain in weight of Q; B-mean radius of particles, $r_{ave.}$ in μ. 1-Borovishi clay; 2-Glukhovetsk kaolin; 3-Prosyanovsk kaolin; 4-Chasovyari clay; 5-Oglanlino bentonite.

TABLE 2

Calculation of the Specific Surface of Prosyanovsk Kaolin

Z, (min)	ΔZ (sec)	p (mg)	Δp (mg)	r (μ)	q (mg)	Δq, (mg)	ΔQ (%)	Q (%)	$r_{ave.}$ (μ)	ΔS (cm^2)
5	300	5.0	5.0	10.7	0	–	–	–	–	–
10	600	8.5	3.5	7.7	1.5	1.5	1.9	1.9	9.2	1.9
20	600	10.0	1.5	5.5	7.0	5.5	7.0	8.9	6.6	9.6
50	1800	13.5	3.5	3.5	7.6	0.6	0.8	9.7	4.5	1.6
110	3300	17.5	4.0	2.3	9.5	1.9	2.5	12.2	2.9	7.5
170	3600	21.5	4.0	1.9	10.2	0.7	0.9	13.1	2.1	3.3
1235	63900	38.0	16.5	0.7	18.9	8.7	11.1	24.2	1.3	77.0
2990	105300	46.0	8.0	0.45	32.4	13.5	17.3	41.5	0.6	258.0
4130	68400	49.0	3.0	0.38	38.1	5.7	7.3	48.8	0.42	156.0
5570	86400	51.0	2.0	0.33	43.3	5.2	6.6	55.4	0.35	171.0
7010	86400	52.0	1.0	0.29	47.2	3.9	5.0	60.4	0.31	145.0
8450	186400	54.0	2.0	0.27	48.5	1.3	1.6	62.0	0.28	53.0
15360	414600	54.5	0.5	0.11	53.4	4.9	6.28	68.3	0.19	236.0
									Total	1181.0
						11.8	15.1	83.4	0.1	1356.0
						5.46	7.0	90.4	0.05	1257.0
						5.15	6.6	97.0	0.025	2365.0
						1.56	2.0	99.0	0.0125	1432.0
						0.78	1.0	100.0	0.005	1793.0
							Sum	ΣΔS	–	9384

Interpolated

employed, the closer the $Q - r$ curve is to the Q axis, the closer the final section of the curve will approach a straight line. This is especially advantageous when dealing with clays of high dispersion and high specific surface (such as bentonite), since it reduces the possible error in determining the specific gravity due to departures from linearity along the terminal section of the $Q - r$ curve.

We attempted to determine the possible magnitude of the departure of the specific surface from that prevailing when the terminal section of the $Q - r$ curve is assumed to be linear by means of test calculations for conceivable changes in the shape of this terminal section. We obtained a discrepancy of ± 15%. We therefore believe that the assumption of the linearity of the terminal section of the curve involves a possible error of no more than 15% in the specific surface from the value that might have been determined by the particle sedimentation method if the latter had not been disturbed by Brownian movements and the test could have been prolonged for dozens of days.

We therefore plotted the $Q - r$ curve (Fig. 2) from our observed points, connecting the last point A to the point representing 100% by a straight line.

By way of example, we cite a calculation of the specific surface of Prosyanovsk Kaolin, with a sp. gr. of 2.601, the sample of which weighed 1190 mg, in terms of dry weight.

Our observations were processed in accordance with the equations given above, all the data being listed in Table 2.

The data in the last six lines of the table were obtained by interpolation.

The specific surface of Prosyanovsk kaolin is found to be

$$S = \frac{\Sigma \Delta S}{G_{max.}} = \frac{9022 \cdot 10^{-4}}{78 \cdot 10^{-3}} =$$

$$= 11.5 \text{ m}^2/\text{gram}.$$

TABLE 3

Specific Surfaces of Argillaceous Materials

Material	Specific surface, m^2/gram
Glukhovetsk kaolin	10.8
Prosyanovsk kaolin	11.5
Borovichi clay	12.2
Chasovyari clay	15.0
Oglanlino bentonite	28.6

The values of the specific surface have been computed for several materials by the method set forth (Table 3).

SUMMARY

1. A new variant of the gravimetric method of determining the specific surface of highly disperse materials, employing a torsion balance, yields results that are satisfactorily reproducible.

2. This method may be used to evaluate the specific surfaces of various argillaceous materials.

LITERATURE CITED

[1] A.I.Avgustinik. Physical Chemistry, 275-277 (1947).

[2] V.Eitel and K.Shusterius, Naturwissenschaften, 28, 19, 300-303 (1940).

[3] Marchall, Chumbert, Soil Sci., 54, 1, 149-158 (1942).

[4] M.Ardenu, K.Endel, and J.Gofmann, Ber. deut. keram. Ges., 21, 6, 209-227 (1940).

[5] V.F.Zhuravlev and M.M.Sychev, J.Appl. Chem. 20, 3, 172-178 (1947).

[6] T.N.Chernikova Colloid J. 9, 1, 29-33 (1947).

[7] N.A.Figurovsky. Contemporary Methods of Sedimentation Analysis of Suspensions and Emulsions, 15-16 (1939).

Received July 14, 1950.

BLANK
PAGE

A SUSPENDED LAYER OF PARTICLES OF DIFFERENT SHAPES*

N. I. Smirnov and Li De En

Chair of Synthetic Rubber Technology, Lensoviet Institute of Technology, Leningrad

We have previously made a study of the hydrodynamics of a suspended layer in the region of turbulent flow [1], using spherical particles. In actual processes that make use of the phenomenon of the suspended layer, however, the particles are not always spherical. More often than not the shape of the particles is irregular. There arises the necessity, therefore, of making a study of the effect of particle form upon the hydrodynamics of a suspended layer. We asserted that in the region of turbulent flow the criterial equation for the hydrodynamics of a suspended layer of spherical particles:

$$Eu = 8.58\ Re^{-2.2}\ Ar\ G_1^{0.5} G_2^{0.33} G_3^{0.33}\ , \qquad (1)$$

will hold good for particles of other shapes as well, provided the equation coefficient of 8.58 is changed as necessary to accord with the shape of the particles. In other words, we assumed that the coefficient in Equation (1) is governed chiefly by the particle shape. With this as a basis, we ran tests on suspended layers of cylindrical, cubic, and irregular particles. The results of these tests were processed from Equation (1), it being our aim to find the specific coefficient in this equation for each particle shape in order to endeavor to relate the value of the coefficients thus found with the particle shape.

EXPERIMENTAL

We ran the experiments in a glass column 24.5 mm in internal diameter, described in a previous report [1]. The experimental conditions were the same as those prevailing for our tests with spherical particles. We observed the suspended layer in water, kerosene, air, and carbon dioxide. The latter materials have been described previously [2].

We prepared the cylindrical particles by cutting up aluminum wire 1.136 mm in diameter into lengths of a certain size, using a gage. The cubic particles were crystals of table salt, produced by the slow evaporation of a saturated aqueous solution of the salt. We used quartz sand as particles of irregular shape. All the particles were screened, certain fractions being taken of each. The dimensions of the cylindrical and cubic particles were measured by a micrometer to within 0.001 mm. A total of 100 particles of each fraction was counted out for measurement.

The size of the particles in each fraction was taken as the arithmetical mean of the dimensions of the particles measured. We took the maximum dimension

* Report VI of a series on the motion of a body within a medium.

of the cylindrical particles as the controling dimension for calculating their criteria. In our tests the height of the aluminum cylinders was greater than their diameter in the two fractions selected, so that the cylinder height was taken as the controlling dimension.

We determined the mean size of the sand particles used in our calculations from the mean size of the openings in the screen through which the given fraction passed. The density of the particles of different materials was measured in a pycnometer at 20°. These densities were later used in our calculations without any correction for the test temperature. The dispensing with temperature corrections introduced a certain, though extremely minute, error into our calculations of the Archimedes number. The characteristics of all the particles employed in our tests are listed in Table 1.

TABLE 1

Characteristics of Particles

Particle form	Particle material	Density, kg/m³	Measured size, 10^{-3} m	Deviations from mean size	
				Maximum deviation, %	Deviation, %
Cylinder	Aluminum	2655.2	2.264	Up to ± 5 From ± 5 to ± 10 From ±10 to ± 12	62 36 2
Ditto	Ditto	Ditto	1.482	Up to ± 5 From ± 5 to ± 10 From ±10 to ± 13	60 36 4
Cube	Table salt	2160.0	1.376	Up to ± 5 From ± 5 to ± 10 From ±10 to ± 15 From ±15 to ± 18	39 35 21 5
Ditto	Ditto	Ditto	0.983	Up to ± 5 From ± 5 to ± 10 From ±10 to ± 13	61 31 8
Ditto	Ditto	Ditto	0.807	Up to ± 5 From ± 5 to ± 10 From ±10 to ± 15 From ±15 to ± 20	54 30 14 2
Irregular	Sand	2636.0	1.350	Passes through screens from No. 16 to No. 25	
Ditto	Ditto	Ditto	0.675	Passes through screens from No. 64 to No. 100	
Ditto	Ditto	Ditto	0.570	Passes through screens from No. 100 to No. 121	

A total of 192 tests were run with cylindrical particles under various conditions, 185 tests being run with cubic particles and 233 tests with irregular particles. We decided not to cite the conditions and results of all these tests in the present report, owing to the bulkiness of the material. A random selection

TABLE 2

Tests of Particles of Different Forms

Test No.	Temp. °C	Measured particle size 10^{-3}m.	Density of the medium kg/m^3	Viscosity of the medium, 10^{-4} kg/sec/m^2	Loss of head, kg/m^2	Velocity of the medium 10^{-2} m/sec.	Initial layer height, 10^{-2}m	Height of suspended layer 10^{-2}m	Euler's criterion		Discrepancy, %
									Observed	Computed	
1	2	3	4	5	6	7	8	9	10	11	12
Aluminum cylinders in water											
1	5.8	2.264	1000.0	1.512	78.30	3.848	6	10	518.70	559.35	+ 7.8
2	5.8	2.264	1000.0	1.512	91.00	8.280	6	22	130.23	134.35	+ 3.2
3	5.8	2.264	1000.0	1.512	99.30	9.735	6	30	102.79	99.08	- 3.2
4	6.2	2.264	1000.0	1.493	91.50	3.339	8	12	805.10	887.80	+10.2
5	6.2	2.264	1000.0	1.493	98.60	7.494	8	24	172.39	189.04	+ 9.7
6	6.2	2.264	1000.0	1.493	107.80	9.290	8	36	125.40	134.82	+ 7.5
7	6.2	2.264	1000.0	1.493	113.30	2.971	10	14	1315.70	1346.10	+ 2.3
8	6.2	2.264	1000.0	1.493	118.20	5.747	10	22	351.14	354.40	+ 0.8
9	6.2	2.264	1000.0	1.493	132.80	8.427	10	38	183.47	178.06	- 2.9
10	5.8	1.482	1000.0	1.512	78.50	3.657	6	10	575.86	573.86	- 0.3
11	5.8	1.482	1000.0	1.512	85.00	7.587	6	22	144.82	149.84	+ 3.4
12	5.8	1.482	1000.0	1.512	91.50	9.371	6	34	102.20	108.58	+ 6.2
13	6.0	1.482	1000.0	1.502	92.50	2.996	8	12	1010.60	1034.50	+ 2.4
14	6.0	1.482	1000.0	1.502	103.80	6.683	8	24	227.98	222.28	- 2.5
15	6.0	1.482	1000.0	1.502	109.10	8.460	8	36	149.53	152.24	+ 1.8
16	6.0	1.482	1000.0	1.502	107.00	2.645	10	14	1728.00	1799.30	+ 4.1
17	6.0	1.482	1000.0	1.502	121.00	5.939	10	26	336.57	319.66	- 5.0
18	6.0	1.482	1000.0	1.502	124.90	7.289	10	34	230.10	222.24	- 3.4
Aluminum cylinders in kerosene											
19	17.6	2.264	938.5	1.750	86.81	5.071	6	12	353.90	370.60	+ 4.7
20	17.6	2.264	938.5	1.750	103.24	8.715	6	24	142.06	142.17	0.0
21	17.6	2.264	938.5	1.750	115.25	10.154	6	32	116.84	111.67	- 4.4
22	–	2.264	938.5	1.750	114.03	3.869	8	14	778.10	785.14	+ 0.9
23	17.6	2.264	938.5	1.750	121.54	7.788	8	26	209.41	210.10	+ 0.6
24	17.6	2.264	938.5	1.750	127.64	9.031	8	34	165.87	162.24	- 2.2
25	17.6	2.264	938.5	1.750	135.61	3.483	10	16	1168.70	1115.60	- 4.5
26	17.6	2.264	938.5	1.750	140.03	6.217	10	24	378.64	353.47	- 6.7
27	17.6	2.264	938.5	1.750	147.82	8.540	10	36	211.85	201.25	- 5.0
Aluminum cylinders in air											
28	19.5	2.264	1.207	0.0184	82.37	78.443	4	5	1106.60	1076.80	- 2.7
29	19.5	2.264	1.207	0.0184	110.90	74.367	6	7	1631.50	1613.20	- 1.1
30	19.5	2.264	1.207	0.0184	138.90	76.831	8	9.2	1912.40	1736.30	- 9.2
31	19.5	2.264	1.207	0.0184	162.37	81.270	10	11.5	1996.40	1953.80	- 2.1
32	19.5	1.482	1.207	0.0184	75.70	65.250	4	5	1450.00	1542.30	+ 6.3
33	19.5	1.482	1.207	0.0184	109.70	72.235	6	7.2	1708.70	1594.00	- 6.7
34	19.5	1.482	1.207	0.0184	147.20	72.103	8	9.5	2207.30	1928.30	-12.6
35	19.5	1.482	1.207	0.0184	164.26	77.075	10	11.7	2236.20	1909.20	-14.6
Aluminum cylinder in carbon dioxide											
36	19.0	2.264	1.790	0.0151	104.32	51.190	6	7	2173.00	2131.60	- 1.5

TABLE 2 (continued)

1	2	3	4	5	6	7	8	9	10	11	12
					Aluminum cylinders in carbon dioxide						
37	18.5	2.264	1.794	0.0150	121.20	58.960	8	9.5	1889.70	1864.70	- 1.3
38	18.2	2.264	1.796	0.0150	164.23	59.317	10	11	2549.60	2147.10	-15.8
39	18.2	1.482	1.796	0.0150	88.97	59.836	6	7	1327.80	1342.20	+ 1.1
40	18.0	1.482	1.832	0.0150	118.13	62.637	8	9.5	1597.50	1471.40	- 7.9
					Table salt in kerosene						
41	19.0	1.376	938.3	1.705	57.10	3.347	6	12	532.30	561.82	+ 5.5
42	19.0	1.376	938.3	1.705	64.27	5.945	6	24	190.14	200.48	+ 5.4
43	19.0	1.376	938.3	1.705	66.62	6.716	6	32	154.47	168.40	+ 9.0
44	20.6	1.376	938.1	1.656	67.73	3.922	8	18	460.30	496.40	+ 7.9
45	20.6	1.376	938.1	1.656	71.29	5.442	8	26	269.80	273.10	+ 1.3
46	20.6	1.376	938.1	1.656	74.39	6.541	8	34	181.82	198.27	+ 9.0
47	20.5	1.376	938.1	1.659	78.04	2.179	10	16	1719.20	1706.40	- 0.7
48	20.5	1.376	938.1	1.659	82.73	4.012	10	24	537.63	506.13	- 5.8
49	20.5	1.376	938.1	1.659	86.96	5.644	10	36	285.46	296.95	+ 4.0
50	19.3	0.983	938.2	1.676	55.17	2.604	6	12	850.80	877.90	+ 3.2
51	19.3	0.983	938.2	1.676	60.14	4.912	6	24	260.57	269.43	+ 3.6
52	19.3	0.983	938.2	1.676	63.33	5.659	6	32	206.76	220.68	+ 6.7
53	19.3	0.983	938.2	1.676	68.12	2.155	8	14	1534.30	1579.20	+ 2.9
54	19.3	0.983	938.2	1.676	72.34	3.824	8	22	517.28	507.85	- 1.8
55	19.3	0.983	938.2	1.676	76.19	5.151	8	34	300.23	305.45	+ 1.7
56	19.2	0.983	938.2	1.699	83.78	1.763	10	16	2820.00	2718.30	- 3.6
57	19.2	0.983	938.2	1.699	88.85	3.300	10	24	852.50	778.72	- 8.6
58	19.2	0.983	938.2	1.699	92.23	4.574	10	36	460.00	436.26	- 5.2
59	18.5	0.807	938.3	1.721	61.46	1.830	6	12	1919.80	2136.90	+11.3
60	18.5	0.807	938.3	1.721	65.48	3.697	6	24	504.53	552.90	+ 9.5
61	18.7	0.807	938.3	1.715	68.03	4.305	6	32	383.84	443.04	+15.4
62	18.5	0.807	938.3	1.721	64.47	1.965	8	14	1745.40	1792.80	+ 2.5
63	18.5	0.807	938.3	1.721	69.72	2.830	8	22	910.40	934.45	+ 2.6
64	18.5	0.807	938.3	1.721	81.73	3.989	8	34	536.96	507.65	- 5.8
65	19.0	0.807	938.3	1.705	78.58	1.494	10	16	3676.40	3709.00	+ 0.9
66	19.0	0.807	938.3	1.705	82.75	2.363	10	24	1549.30	1537.60	- 2.0
67	19.0	0.807	938.3	1.705	86.41	3.451	10	36	757.06	765.25	+ 0.1
					Table salt in air						
68	18.4	1.376	1.227	0.0184	56.90	61.320	4	5	1209.90	1260.20	+ 4.2
69	18.0	1.376	1.229	0.0183	73.90	61.540	6	7.2	1557.60	1610.40	+ 3.4
70	19.5	1.376	1.207	0.0184	94.10	64.454	8	9.5	1841.00	1839.70	- 0.2
71	19.5	1.376	1.207	0.0184	113.40	69.415	10	11.7	1912.80	1781.90	- 6.8
72	19.2	0.807	1.224	0.0184	50.30	47.990	4	5	1750.40	1839.10	+ 5.1
73	19.4	0.807	1.223	0.0184	69.10	46.868	6	7	2523.40	2488.60	- 1.3
74	19.4	0.807	1.223	0.0184	98.30	45.583	8	9	3883.20	3168.20	-18.0
75	19.0	0.807	1.225	0.0184	113.40	48.015	10	11	3939.00	3244.20	-17.6
					Table salt in carbon dioxide						
76	18.0	1.376	1.798	0.0150	64.48	55.360	6	7.2	1148.80	1236.00	+ 1.6
77	18.0	1.376	1.798	0.0150	85.20	61.284	8	9.7	1224.40	1186.00	- 3.1
78	18.0	1.376	1.798	0.0150	111.08	58.623	10	12	1723.30	1529.20	-11.2
79	18.2	0.807	1.796	0.0150	60.72	43.508	6	7.7	1752.20	1905.60	+ 8.7
80	18.0	0.807	1.798	0.0150	82.37	44.503	8	9.5	2265.00	2234.00	- 1.3
81	19.0	0.807	1.790	0.0150	98.38	47.690	10	12	2571.40	2066.40	-12.8

TABLE 2 (Continued)

1	2	3	4	5	6	7	8	9	10	11	12
					Sand in water						
82	8.0	1.350	999.9	1.414	71.90	3.085	6	12	741.40	865.05	+16.7
83	8.0	1.350	999.9	1.414	81.30	5.783	6	24	238.55	273.53	+14.6
84	8.0	1.350	999.9	1.414	84.20	6.611	6	32	189.00	224.22	+18.6
85	8.0	1.350	999.9	1.414	88.60	2.602	8	14	1283.60	1457.20	+13.5
86	8.0	1.350	999.9	1.414	96.40	5.332	8	26	345.06	367.90	+ 6.7
87	8.0	1.350	999.9	1.414	98.90	5.945	8	34	277.64	318.30	+14.6
88	8.0	1.350	999.9	1.414	109.60	2.122	10	16	2387.60	2589.00	+ 8.4
89	8.0	1.350	999.9	1.414	119.50	3.567	10	28	921.60	988.00	+ 7.2
90	8.0	1.350	999.9	1.414	121.00	5.527	10	36	388.69	409.94	+ 5.5
91	9.0	0.675	999.8	1.373	68.20	3.072	6	12	693.00	706.50	+ 1.9
92	9.0	0.675	999.8	1.373	73.20	4.145	6	20	408.54	432.48	+ 4.9
93	9.0	0.675	999.9	1.373	76.80	5.089	6	32	284.33	321.46	+13.1
94	8.8	0.675	999.9	1.381	88.80	1.818	8	14	2634.60	2606.00	- 1.1
95	8.8	0.675	999.9	1.381	91.20	3.498	8	22	731.05	718.15	- 1.7
96	8.8	0.675	999.9	1.381	96.00	4.758	8	34	416.00	422.16	+ 1.5
97	8.8	0.675	999.9	1.381	105.00	1.747	10	16	3377.10	3238.00	- 4.1
98	8.8	0.675	999.9	1.381	109.50	3.019	10	24	1179.00	1101.20	- 6.6
99	8.8	0.675	999.9	1.381	111.70	4.182	10	36	626.75	615.43	- 1.8
100	9.0	0.570	999.8	1.373	68.80	1.546	6	12	2761.30	3042.90	+10.2
101	9.0	0.570	999.8	1.373	73.00	3.429	6	24	694.50	664.54	- 4.3
102	9.0	0.570	999.8	1.373	74.50	4.042	6	32	436.98	509.04	+16.5
103	9.0	0.570	999.8	1.373	104.00	1.143	10	16	7635.50	7771.00	+ 1.8
104	9.0	0.570	999.8	1.373	105.40	2.272	10	24	1957.60	2049.50	+ 4.7
105	9.0	0.570	999.8	1.373	107.50	3.390	10	36	869.90	924.10	+ 3.0
					Sand in kerosene						
106	19.2	1.350	938.2	1.699	83.78	3.603	6	12	675.00	718.90	+ 6.5
107	19.2	1.350	938.2	1.699	86.51	5.690	6	20	279.40	311.90	+11.6
108	19.2	1.350	938.2	1.699	92.42	7.408	6	32	176.10	204.14	+15.9
109	18.4	1.350	938.3	1.724	130.33	2.154	10	16	2935.60	2840.50	- 3.3
110	18.7	1.350	938.3	1.715	138.87	5.629	10	36	458.20	461.44	+ 0.7
111	18.7	1.350	938.3	1.715	87.72	2.248	6	12	1814.90	1650.10	- 8.8
112	19.8	0.675	938.1	1.680	91.96	4.421	6	24	491.80	469.54	- 4.5
113	19.8	0.675	938.1	1.680	93.34	4.993	6	32	391.46	395.38	+ 1.0
114	19.3	0.675	938.2	1.676	126.85	1.453	10	16	6277.30	5636.40	-10.2
115	19.3	0.675	938.2	1.676	132.44	3.285	10	28	1283.50	1121.00	-12.6
116	19.3	0.675	938.2	1.676	135.10	4.012	10	36	877.75	785.40	-10.5
117	20.0	0.570	938.1	1.673	83.02	1.998	6	12	3012.00	2961.00	- 1.7
118	20.0	0.570	938.1	1.673	85.93	2.985	6	20	1008.90	1014.70	+ 0.5
119	20.0	0.570	938.1	1.673	88.18	4.066	6	32	557.90	601.30	+ 7.7
120	20.0	0.570	938.1	1.673	107.42	1.298	8	14	6667.00	6272.50	- 5.9
121	20.0	0.570	938.1	1.673	112.10	2.891	8	26	1402.40	1297.50	- 7.5
122	20.0	0.570	938.1	1.673	114.26	3.537	8	34	955.10	910.90	- 4.6
123	19.5	0.570	938.2	1.689	131.07	1.489	10	20	6179.00	5420.50	-12.2
124	19.5	0.570	938.2	1.689	134.54	2.425	10	28	2283.80	2131.80	- 6.6
125	19.5	0.570	938.2	1.689	138.53	6.132	10	36	1487.50	1300.90	-12.5
					Sand in air						
126	19.0	1.350	1.225	0.0184	72.90	53.580	4	5	2035.30	2253.00	+16.9
127	19.0	1.350	1.225	0.0184	101.67	51.555	6	7	3065.50	3619.40	+ 3.4
128	19.0	1.350	1.225	0.0184	130.38	53.176	8	9.2	3692.50	3532.80	- 4.3
129	19.0	1.350	1.225	0.0184	161.90	56.250	10	11.5	4097.20	3613.00	-11.8

TABLE 2 (continued

1	2	3	4	5	6	7	8	9	10	11	12
					Sand in air						
130	19.4	0.675	1.223	0.0184	63.64	46.768	4	5	2330.30	2468.00	+ 5.9
131	19.4	0.675	1.223	0.0184	96.49	44.615	6	7.2	3888.40	3599.60	- 7.4
132	19.2	0.675	1.224	0.0184	127.09	47.180	8	9.2	4639.50	3714.00	-19.9
					Sand in carbon dioxide						
133	19.5	1.350	1.785	0.0151	98.40	43.370	6	7	2874.70	2793.00	- 2.6
134	18.5	1.350	1.794	0.0150	129.44	47.082	8	9.2	3193.40	2798.00	-12.4
135	18.5	1.350	1.794	0.0150	157.68	29.654	10	11.5	3497.70	2887.30	-17.4
136	17.5	0.675	1.807	0.0150	58.84	38.090	4	5	2202.20	2325.30	+ 5.5
137	17.5	0.675	1.807	0.0150	92.73	44.489	6	7	2550.00	2123.40	-16.7

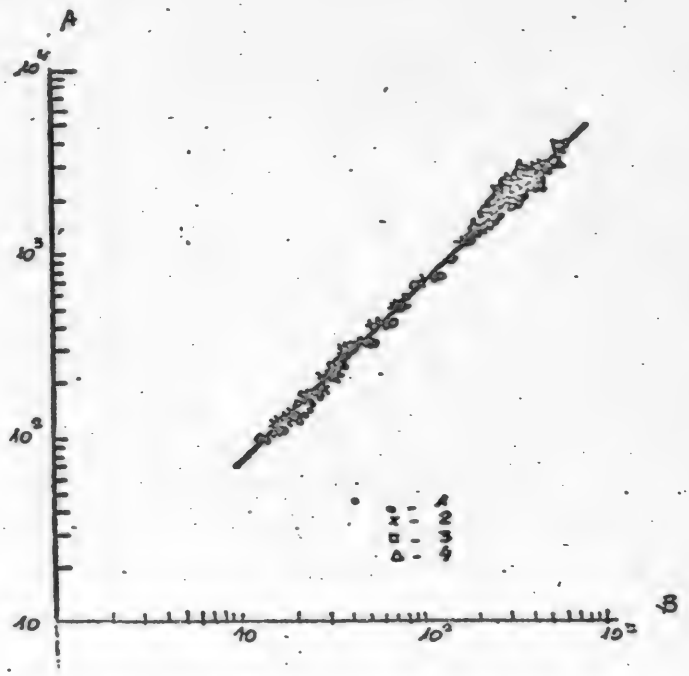

Fig. 1. Results of tests using cylindrical particles.

A-Eu; B-$Re^{0.2}$ Ar $G_1^{0.8}$ $G_2^{0.33}$ $G_3^{0.33}$

1-Aluminum cylinders in water; 2-aluminum cylinders in kerosene; 3-aluminum cylinders in air; 4-aluminum cylinders in carbon dioxide.

of some of the tests is given in Table 2; it covers, however the whole range of conditions used in our investigations.

Working up all our experimental data in the form of the function represented by Equation (1), we found that the criterial equation of the hydrodynamics of a suspension layer took on the form of:

$$Eu = 7.15\ Re^{-2.2}\ Ar\ G_1^{0.5} G_2^{0.33} G_3^{0.33} \quad (2)$$

for cylindrical particles 2.264 mm high;

$$Eu = 7.45\ Re^{-2.2}\ Ar\ G_1^{0.5} G_2^{0.33} G_3^{0.33} \quad (3)$$

for cylindrical particles 1.482 mm high;

$$Eu = 7.10\ Re^{-2.2}\ Ar\ G_1^{0.5} G_2^{0.33} G_3^{0.33} \quad (4)$$

for cubic particles; and

$$Eu = 7.75\ Re^{-2.2}\ Ar\ G_1^{0.5} G_2^{0.33} G_3^{0.33} \quad (5)$$

for irregular particles.

The last column in Table 2 gives the discrepancies between the values of Euler's criterion computed from this equation and the actual observed values. In by far most of the tests the agreement between the computed and the observed values is fully satisfactory. The accuracy of the derived equations is shown most strikingly in Figs. 1, 2, and 3, in which the results of all the tests we have run are plotted.

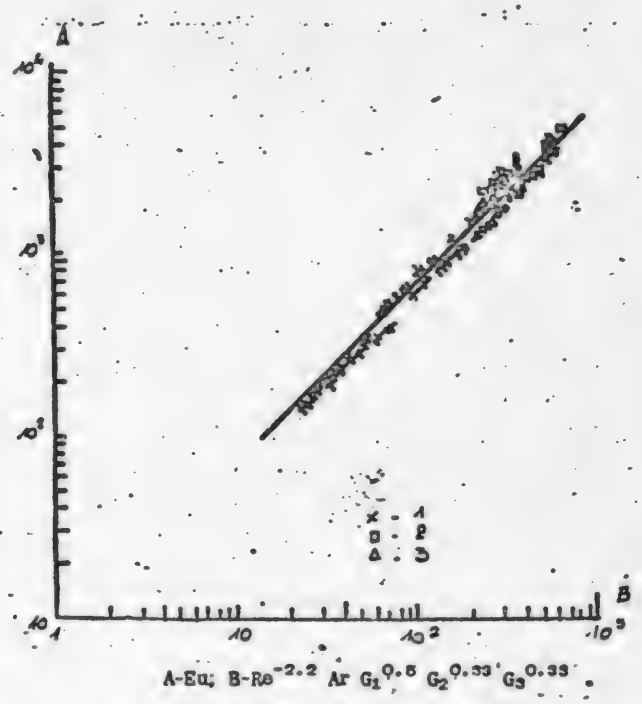

Fig. 2. Results of tests using cubic particles.

1-Cubes of table salt in kerosene; 2-cubes of table salt in air; 3-cubes of table salt in carbon dioxide.

EVALUATION OF RESULTS

Inspection of Equations (1), (2), (3), (4), and (5) leads us to conclude that differences in the shape of the particles constituting a layer suspended in a current affect only the magnitude of the coefficient of the hydrodynamic criterial equation. Hence, in the most general case, for particles of any shape, the criterial

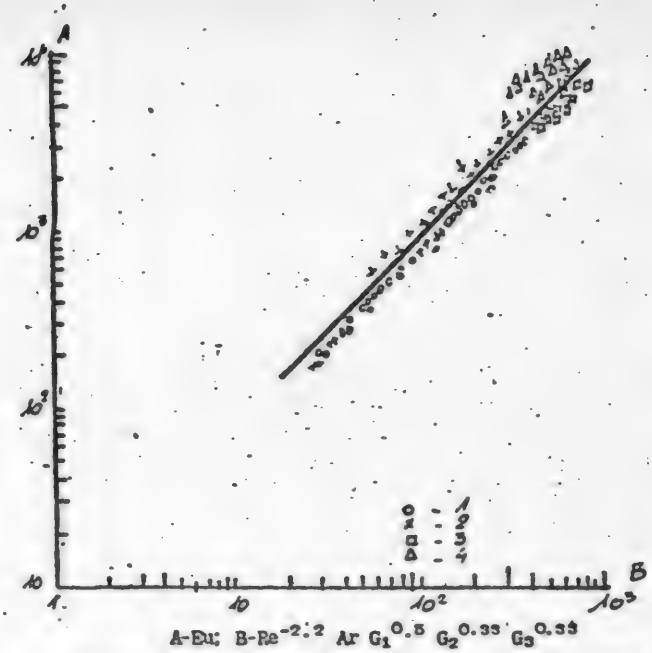

A-Eu; B-$Re^{-2.2}$ Ar $G_1^{0.5}$ $G_2^{0.33}$ $G_3^{0.33}$

Fig. 3. Results of tests with particles of irregular shape.

1-Sand in water; 2-sand in kerosene; 3-sand in air; 4-sand in carbon dioxide.

equation for the hydrodynamics of a suspended layer must take the form of

$$Eu = C\underline{f}\, Re^{-2.2}\, Ar\, G_1^{0.5} G_2^{0.33} G_3^{0.33}, \qquad (6)$$

where C is a constant for all coefficients, and $\underline{f}$ is a criterion or simplex for the form of the suspended solid particles.

As we know, bodies of like volume but different shapes possess surfaces of different magnitude. That is why we made an attempt to relate the value of the criterion or simplex $\underline{f}$ to the surface of the respective particles, in order to obtain an idea of the nature of this $\underline{f}$. Inasmuch as a sphere possesses the smallest surface of all forms having a given volume, we decided to set $\underline{f}$ equal to 1 for the sphere. Then $\underline{f}$ may be computed in two ways for the other forms. The first method is purely theoretical, based upon the equation:

$$\underline{f} = \frac{F_s}{F_p}, \qquad (7)$$

where F_p is the surface of a particle of the shape under test, and F_s is the surface of a spherical particle of equal volume. The second method is based upon our experimental data. Indeed, we ought to be able to find the value of $\underline{f}$ by dividing the value of the coefficient in Equations (2), (3), (4), and (5) by the value of the same coefficient in Equation (1). The values of the simplex $\underline{f}$ as computed in both ways for particles of different shapes is given in Table 3.

The satisfactory agreement of the values of this simplex for different shapes, as computed from the theoretical equation with its values as found from the experimental data is first of all, further confirmation of the reliability of the criterial equations we have derived for the hydrodynamics of a suspended layer in the region of turbulent flow, i.e., of Equations (1), (2), (3), (4), and (5), as well as

TABLE 3

Values of the Simplex $\underline{f}$ for Particles of Different Shapes

Particle shape	Value of $\underline{f}$	
	From Equation (7)	From Experimental data
Sphere	1.000	1.000
Cylinder 2.266 mm high	0.832	0.833
1.482 mm high	0.868	0.868
Cube	0.806	0.827
Irregular	–	0.903

confirming the postulates that underlay our derivation of these equations in one of our preceding reports [2]. Moreover, this agreement entitles us to write Equation (6) in the following definitive form:

$$Eu = 8.58\ \underline{f}\ Re^{-2.2}\ Ar\ G_1^{0.5} G_2^{2.33} G_3^{0.33}\ . \qquad (6a)$$

SUMMARY

The definitive form of the criterial equation for the hydrodynamics of a suspended layer for particles of any shape in the region of turbulent flow shows that the value of the shape simplex may be computed from the simple ratio of the surface of a sphere whose volume is the same as that of the suspended particle to the surface of that particle.

LITERATURE CITED

[1] N.I.Smirnov and Li De En, J. Appl. Chem. 24, No. 1 (1951).*

[2] N.I.Smirnov and Li De En, J. Appl. Chem. 24, No. 4, 383 (1951).**

Received October 18, 1950.

---

*See CB translation p. 65 ff.

**See CB translation p. 419 ff.

BLANK
PAGE

BRIEF COMMUNICATIONS

THE ACTION OF A SOLUTION OF FERRIC SULFATE UPON IRON SULFIDE*

I. N. Kuzminykh and E. L. Yakhontova

Mendeleev Institute of Chemical Technology, Moscow, Awarded the Order of Lenin

In our previous reports we have set forth data on the rate of reaction between zinc sulfide and a solution of ferric sulfate [1], as well as the results of our tests of wet leaching zinc out of a mixture of various sulfides [2]. The effect of various factors: temperature, solution composition, concentration of the suspension, and duration, upon the progress of this heterogeneous process has been described.

We set forth the results of analogous experiments with iron sulfide, FeS, below.

Like other compounds of the MeS type, iron sulfide can react quantitatively with an aqueous solution of ferric sulfate as follows:

$$FeS + Fe_2(SO_4)_3 \rightarrow FeSO_4 + S.$$

There are no figures on the kinetics of this heterogeneous process in the literature.

EXPERIMENTAL

We ran tests with two samples of commercial iron sulfide, prepared from pyrites. One of them (Sample I) was prepared from a finely pulverized pyrites concentrate, containing 48.4% sulfur and 42.2% iron. This was done by heating the pyrites to 750-800° in a medium free from oxygen (in an atmosphere of steam); this resulted in the conversion of the FeS_2 into FeS. Part of the FeS reacted with the steam, yielding a product containing 84.4% FeS (30% sulfur).

The other sample of iron sulfide was secured from a VKhZ type furnace (from the third level, down from the top) in one of our sulfuric-acid plants, in which flotation pyrites is roasted. It contained 20.5% sulfidic sulfur which was combined with iron as chemical analysis demonstrated. Sample II contained 56.4% FeS, the remainder consisting of SiO_2, silicates, and iron oxides.

The tests were run in a vessel fitted with a stirrer, into which a batch of the sulfide (10-48 grams) was placed together with 100 ml of an acidulated aqueous solution of $Fe_2(SO_4)_3$. In all our tests the suspension was stirred in the same way. A constant temperature (50-100°) was maintained throughout each test by the application of heat. The solution was analyzed for $Fe^{\cdot\cdot}$, $Fe^{\cdot\cdot\cdot}$, and H_2SO_4 before and after each run; in some of the tests the solid residue was analyzed for elementary sulfur. Calculation of the balance-sheet of these tests showed that the reaction between the FeS and the $Fe_2(SO_4)_3$ followed the equation given above in so far as its stoichiometry was concerned.

*Report III of a series on the action of ferric sulfate upon sulfides.

The results of each test were evaluated according to the progress of the reaction. There were two indexes of this progress: first the change in the composition of the solution – the loss of Fe^{+++} and the rise in Fe^{++} during the test; and second, the change in the composition of the solid phase – the conversion of the sulfidic sulfur into elementary sulfur. The graphs reproduced below show the progress of the reaction by means of the accumulation of elementary sulfur during the run (in grams per liter of solution).

Tests run at various temperatures (50 to 100°) have shown that the amount of reacted FeS rises some 25% per 10° of temperature rise in both samples, all other conditions being equal. This is evidence that the rate of the given heterogeneous process is governed by the diffusion factor, as was the case in the tests with other sulfides, i.e., by the phenomena of diffusion into the stationary film of liquid that surrounds each solid particle.

Tests were run to determine the influence of the solution composition upon the process velocity, in which the percentages of Fe^{++}, Fe^{+++}, and free H_2SO_4 in the solution were varied, while all other conditions were kept the same. The experimental data on the effect of the concentration of Fe^{+++} in the solution upon the progress of the reaction are reproduced in Fig. 1 as three curves, Curves 1 and 2 referring to Sample I and Curve 3 referring to Sample II. All these tests

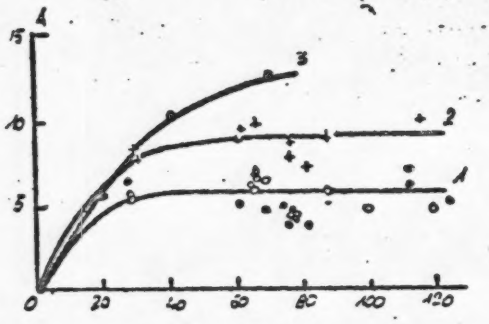

Fig. 1. Effect of the concentration of Fe^{+++} in the solution upon the rate of the reaction between FeS and $Fe_2(SO_4)_3$. Temperature: 100°. Acidity of the solution: 20-25 g H_2SO_4 per liter.

A-Accumulation of elementary sulfur in the solid phase, g/liter; B-Fe^{++} concentration in the initial solution, g/liter. Curves 1 and 2: Sample I; Curve 3: Sample II. Test duration and suspension concentration: 1-30 minutes at 100 g/liter; 2-15 minutes 250 g/liter; 3-60 minutes at 160 g/liter.

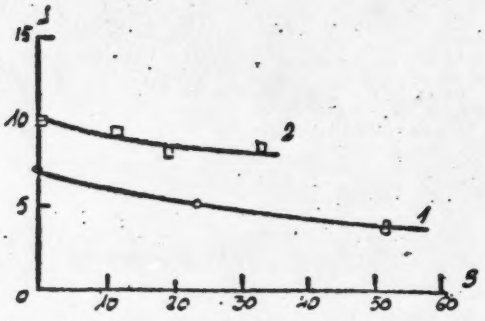

Fig. 2. Effect of the concentration of $FeSO_4$ in the solution upon the rate of the reaction between FeS and $Fe_2(SO_4)_3$. Temperature 100°. Acidity of the solution: 20 g H_2SO_4 per liter.

A-Accumulation of elementary sulfur in the solid phase, g/liter; B-Fe^{++} concentration in the initial solution, g/liter. Curve 1-Sample I; Curve 2-Sample II. Test duration and suspension concentration: 1-20 minutes and 29 g/liter; 2-60 minutes and 34-44 g/liter.

were run at 100°, with a solution acidity of 20-25 g/liter. The tests represented by Curve 1 lasted 0.5 hour at a suspension concentration of 100 g/liter; Curve 2 lasted 15 minutes at 250 g/liter; and Curve 3 lasted 1 hour at 160 g/liter. The initial concentration of Fe^{+++} in the solution varied from 20 to 120 g/liter (with no Fe^{++} present).

Figure 1 shows that increasing the solution concentration up to a certain point results in accelerating the reaction of FeS with Fe^{+++}, after which this factor ceases to influence the velocity of the process in question. This limit occurs sooner or later, depending upon the other experimental conditions: it occurs at

30 g of Fe^{+++} per liter in Curve 1, at 60 g/liter in Curve 2, and at still higher concentrations of Fe^{+++} in the solution in Curve 3. This depends upon how great is the excess of Fe^{+++} above the FeS entering into reaction during the test. The higher the content of FeS per unit volume of solution and the longer the run, the more Fe^{+++} enters into reaction and the smaller the excess of Fe^{+++} present in the solution. Accordingly, the limiting concentration of Fe^{+++} will be higher in the solution in which any further increase in the Fe^{+++} concentration ceases to affect the process velocity.

The variation of the process in question with the percentage of $FeSO_4$ in the solution is shown in Fig. 2. The tests were run at 100°, with an acidity of 20 g H_2SO_4 per liter. The lower curve refers to Sample I, the test of which lasted 20 minutes; the upper curve refers to an hour-long test of Sample II. The suspension concentrations were 150 and 160 g/liter, respectively. The Fe^{+++} concentrations in the initial solutions were 29 and 34-44 g/liter, respectively. The variable factor was the initial concentration of Fe^{++} (ranging from 0 to 51 g/liter).

These tests indicated that increasing the concentration of Fe^{++} in the solution, all other conditions being equal, involves a perceptible retardation of the heterogeneous process under study. As noted above, this process is governed by the diffusion phenomena taking place in the liquid film surrounding each solid particle. It must be supposed that as the concentration of $FeSO_4$ is raised the viscosity of the solution is changed, resulting in an impairment of the conditions for diffusion in the film. From the thermodynamic standpoint, it is impossible for $FeSO_4$ to have slowed down the reaction as a reaction product.

The effect of the solution acidity upon the rate of conversion of the FeS was investigated at 100° in the range of 20-59 g H_2SO_4 per liter, using Sample I (Fig. 3). The suspension concentration was 250 g/liter; the initial Fe^{+++} content was 65 g/liter; and the tests lasted 15 minutes. The shape of the curve is evidence of the retardation of the process as the solution acidity is increased.

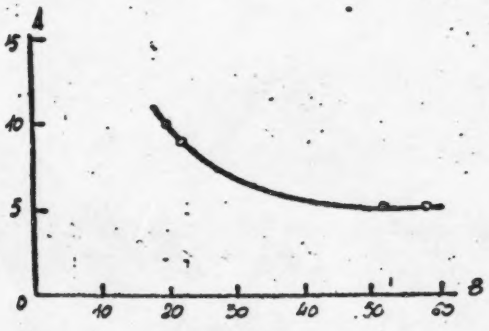

Fig. 3. Effect of the solution acidity upon the rate at which FeS is converted (Sample I). Temperature: 100°. Suspension concentration: 250 g/liter.
A-Accumulation of elementary sulfur, g/liter; B-solution acidity, H_2SO_4 /liter.

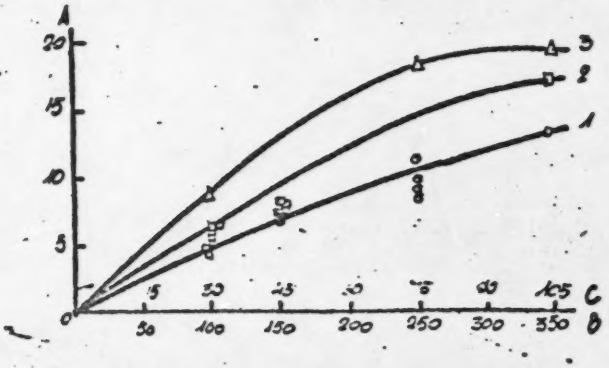

Fig. 4. Effect of the suspension concentration upon the process of treating FeS (Sample I). Temperature: 100°. Fe^{++} in the initial solutions: 61-67 g/liter; H_2SO_4: 20 g/liter
A-Accumulation of elementary sulfur in the solid phase, g/liter, B-suspension concentration, g/liter, C-sulfidic sulfur, g/liter. Length of tests, in minutes: 1-15, 2-30; 3-60.

The tests represented by the three curves in Fig. 4 show the effect of the suspension concentration upon the course of the processing of FeS (Sample I). There are two scales laid off along the axis of abscissas: the